Master of Science in Energy and Nuclear Engineering
Politecnico di Torino - Department of Energy (DENERG)
Academic Year 2017-2018

Master of Science Thesis

Two-phase flow models coupled with developed steam-water table look-up method for 1D fast transient flows in Europlexus

Academic supervisor
Prof. Cristina BERTANI, PhD [a]

Student
Alessandro PANTANO (s223636)

Company supervisors
Philippe LAFON, PhD [b]
Marco DE LORENZO, PhD [b]

[a] Politecnico di Torino, DENERG
[b] EDF R&D, IMSIA UMR EDF-CNRS-CEA-ENSTA

Acknowledgements

This work is the final step of my study career, which allowed me to be part of an exciting Double Degree Program between Politecnico di Torino and Grenoble INP-Phelma. All the hurdles and the difficult moments I faced in these years would be so hard without the help of some people that I want to acknowledge.

I would start to say thanks to all the people that helped me during these months in Politecnico and at EDF, R&D Saclay. In particular, a big *"merci"* is devoted to Philippe, that trusted me and on my skills of engineer, person and man. Thanks also to the professor Bertani for the precious suggestions given for this work.
I would like to say thanks also to Marco, my second supervisor. Thanks to him I enhanced all the skills of problem solving I got during these six months and all the knowledge about the physics of the models I worked on. It was a pleasure to share moments of hard work and pure friendship.

I would like to say thanks to my Sicilian friends. Even if the distance sometimes is a problem, they supported me with strong affection, also from one part of the Europe to the other extreme. In particular, thanks to Federica, Mariajosé and Peppe.

A special thanks is also devoted to all the friends that I met during my Double Degree in France, in particular, *merci* to Alexis, Yahya and Anne-Cecile for helping me with french language and for giving me interesting notions of french and tunisian cultures.

I would like to thank also my friends in Turin, that helped in difficult moments of my life, inside and outside the Politecnico. Among them I would like to thank especially Riccardo, Marialuisa and Andrea and all the other classmates that helped me during these years.

If I overcame all the difficulties is also because of the support of all the other friends of Collegio Einaudi, that I want to thank for all the amazing moment spent in two years of "hard" study. Among them I want to express my gratitude to Vincenzo V., Alberto G., Matteo C., Michele, Chiara G. and Daniele M. for all the beautiful moments spent together.

More than a "thank" is devoted to Fred, Giusy and Mattia. They were with me in the bad moments of my life and enjoyed with me all the good ones. *Grazie di cuore Carusi!*

If I am here and I had this great opportunity to study in Politecnico is thanks to my family, which supported me psychologically and economically: *Grazie Mamma, Grazie Papà*. To my brother, that I want to encourage to never stop to fight, despite the negative moments of the life. Thanks also to those members of my family that dreamed to be here today, but they are surely watching over me from the top of the sky.

Last but the first for importance, the girl who assisted me during this long path, with her patience and simplicity.
Her love was my most important motivation to do my best everyday, and to do my best for her.

A Chiara

Abstract

The physics of the two-phase flow models involved on fast transient phenomena has a predominant importance in nuclear studies and in other industrial fields, where fluid-structure interaction occurs.
Focusing only in the aspect concerning the fluid, in this work we give some comparisons between two-phase flow models for fast transients, in order to understand the main theoretical differences and the related physical aspects due to the different thermodynamic non-equilibria involved. In the presented models, an EoS as a function of specific volume (v) and specific internal energy (e) of the fluid is always needed in order to close the system of the governing flow equations, based on a conservation law.
According to this specific need, it has been decided to tabulate the physical magnitudes, such as pressure, temperature and speed of sound, in a (v, e) domain and pick them during the simulation, when they are required. To do that, a proper algorithm has been developed. This one uses a bicubic interpolation of the EoS provided by IAPWS-IF97, creating a tabulation, that is fully coupled with the proposed models.
A version of the steam-water look-up tables, already available and used for the simplest models, have been also extended to cover metastable vapor applications. To accomplish this goal, the construction of the spinodal curve on the vapor side has been performed, in order to find the limit of the admissible mechanical states. Then, the new domain in (v, e) has been constructed, widening the range of applicability of the new steam-water tables.
The developed look-up table procedure is consequently valid to be coupled with simpler model, as HEM and HRM, as well as for the forthcoming Six-equation model, not available at that moment. Its use is compared to the iterative method, so called "model EAU", already existing on EUROPLEXUS code, in order to show a *direct* and *accurate* way to calculate the thermodynamic properties.
Finally, the new Steam Water Look-up Tables, already validated, are tested using the Homogeneous Equilibrium Model (HEM) and the Homogeneous Relaxation Model (HRM) on EUROPLEXUS code for some industrial application cases.

Keywords: steam-water tables; table look-up method; metastable vapor; spinodal curve; depressurisations.

Lo studio dei modelli di deflusso bifase per fenomeni di transitori rapidi ha una notevole importanza, nel campo nucleare così come in ogni ambito industriale dove si osservano fenomeni rilevanti dal punto di vista dell'interazione fluido-struttura.
Focalizzandosi solamente sull'aspetto del deflusso bifase, e tralasciando gli aspetti di interazione con la struttura, questo lavoro fornisce importanti aspetti di paragone tra i vari modelli per transitori rapidi. L'obiettivo è quello di capire le principali differenze teoriche, legate ai modelli e gli aspetti fisici, corrispondenti ai principali disequilibri termodinamici introdotti.
Tutti i modelli proposti hanno bisogno di essere accoppiati ad una Equazione di Stato in funzione del volume specifico (v) e dell'energia interna (e) del fluido, in modo tale da chiudere il sistema di equazioni espresso in forma delle leggi di conservazione di massa, energia e quantità di moto del sistema.

Secondo questo specifico bisogno, le grandezze fisiche di interesse, come pressione, temperatura e velocità del suono, sono state tabulate in un dominio (v, e) e prelevate da esso durante il calcolo. Per fare ciò è stato elaborato un algoritmo specifico atto a svolgere questa funzione. Quest'ultimo usa un'interpolazione bicubica delle Equazioni di Stato fornite dalla IAPWS-IF97, creando una tabulazione completamente accoppiata ai modelli proposti.
Le tabelle dell'acqua, già disponibili e usate in accoppiamento con modelli più semplici, sono state estese in modo tale da essere accoppiate a modelli più complessi, inglobanti stati termodinamici di vapore metastabile. Per fare ciò è necessaria la costruzione della curva spinodale del vapore, che corrisponde al limite di stabilità meccanica degli stati termodinamici. Di conseguenza, il nuovo dominio in (v, e) risulta essere definito, ampliando il range di applicazioni delle tabelle dell'acqua.
*Le nuove tabelle dell'acqua e del vapore sono quindi pronte per essere accoppiate a modelli più semplici, come HEM e HRM, o più complessi come il Sei-equazioni, non ancora pronto ad essere utilizzato in tale momento. L'uso di tale tabulazione è stato paragonato ad un modello fisicamente equivalente, ma che adotta una procedura iterativa, chiamato "modello EAU", già disponibile all'interno del codice EUROPLEXUS. In questo modo si dimostra l'*efficacia *di un metodo* diretto *per il calcolo delle proprietà termodinamiche, rispetto ad uno equivalente, ma che adotta una procedura iterativa.*
In conclusione, le nuove tabelle dell'acqua e del vapore, sono testate su alcuni casi industriali, in accoppiamento con i modelli bifase per transitori rapidi quali "Homogeneous Equilibrium Model"(HEM) e "Homogeneous Relaxation Model"(HRM), sempre all'interno del codice di calcolo EUROPLEXUS.

Contents

List of Figures

If not otherwise specified, figures are original.

List of Tables

If not otherwise specified, tables are original.

Nomenclature

E	specific total energy	$\frac{kJ}{kg}$
e	specific internal energy	$\frac{kJ}{kg}$
h	specific enthalpy	$\frac{kJ}{kg}$
e_{trip_L}	internal energy of the liquid at triple point	$\frac{kJ}{kg}$
e_{trip_R}	internal energy of the vapor at triple point	$\frac{kJ}{kg}$
e_{crit}	internal energy at critical point	$\frac{kJ}{kg}$
g	Gibbs free energy	$\frac{kJ}{kg}$
f	Helmholtz free energy	$\frac{kJ}{kg}$
c	speed of sound	$\frac{m}{s}$
T	temperature	K
T_{trip}	temperature at the triple point	K
p	pressure	MPa
p_{trip}	pressure at triple point	MPa
u	velocity	$\frac{m}{s}$
v	specific volume	$\frac{m^3}{kg}$
x	flow quality	$-$
x_{stat}	static quality	$-$
x_{eq}	thermodynamic quality	$-$
α_v	void fraction	$-$
Θ	characteristic time to reach the equilibrium condition	s
C_v	specific heat capacity at constant volume	$\frac{kJ}{kgK}$
$\mathbf{F}_x$	partial derivative of a vector "$\mathbf{F}$" with respect to the x variable	$-$
u_x	partial derivative of "u" with respect to the x variable	$-$

The reported units of measure have been generally considered, unless otherwise specified.

Acronyms

CFD	Computational Fluid-Dynamics
EoS	Equation(s) of State
HEM	Homogeneous Equilibrium Model
HRM	Homogeneous Relaxation Model
LOCA	Loss Of Coolant Accident
EDF	Électricité de France
IAPWS	International Association for the Properties of Water and Steam
IF	Industrial Formulation
RIA	Reactivity Injection Accident
CFL	Courant–Friedrichs–Lewy number
PDE	Partial Differential Equation

Chapter 1

Introduction

This introduction exposes the context of this work, pointing out the importance of this research thesis on industrial applications related to two-phase flow modeling and fluid-structure interaction, mainly in nuclear industry.
At the beginning, an outline of the thesis is given in order to introduce the overall topic to the reader.

1.1 Outline of the thesis

This thesis has been structured in seven chapters. In Chapter 1 an introductory part is done in order to introduce the company where this thesis work took place, as well as the industrial context of the topic and the related practical industrial cases, showing the main problems to face.

In Chapter 2 the main needs are presented in terms of governing equations, showing the simplifications done in the models for fast transient phenomena. Then, the main differences between the two-phase flow models are presented in terms of different thermodynamic non-equilibrium introduced. The utility of the coupling with a look-up table method is also shown.

In Chapter 3, the metastable vapor extension performed on the tabulation is explained, starting from the construction of the spinodal curve, considered as the limit of the mechanical stability states and the boundary of the metastable vapor conditions.

Since the metastable vapor boundary has been determined, in Chapter 4 the subdivision of the domain for the new (v, e) tabulation is illustrated, according to the new physical boundaries. The introduction of the new vapor spinodal curve, in fact, changes the way to subdivide the (v, e) domain considered in the simulation.

Chapter 5 illustrates some maps of the physical magnitudes tabulated on the (v, e) domain. This is done in order to analyze the range of applicability of the steam-water look-up tables, but also their accuracy with respect to the exact solution provided by the EoS.

Then, some numerical simulation tests are perfomed using EUROPLEXUS code, with the modified tabulation, potentially useful for industrial application. Some results are hence shown and discussed in Chapter 6.

Finally, some conclusions and perspectives are proposed in Chapter 7.
At the end of the report a short list of videos can be found in attachment.

1.2 Introduction of the company

EDF (Électricité de France) is the main producer and provider of electricity in France and one of the most important in all over the world, with $584.7\,TWh$ of electricity produced only in 2016. It is also the company which produces the highest amount of renewable energy in all Europe with $28\,GW$ of installed power, with an overall $85.7\,\%$ carbon-free generation. This amount of power generated by renewable sources is supposed to be incremented to $50\,GW$ before the 2030.
The installed power is divided as shown in the table 1.1, according to the data reported at 2016.

Energy Source	Percentage on the power mix[%]	Contribution to EDF carbon emissions[%]
Coal	5.7	62.7
Gas and co-generation	8.4	35.5
Renewables (Including Hydro)	8.8	-
Nuclear	76.8	-
Other	0.3	1.8
TOT	100	100

Table 1.1: Table of electrical energy produced by EDF [1](Data related to the period April 2016 to March 2017).

EDF is partner of several companies in 30 different countries in the world, mainly Italy, Belgium and UK, and it is also the owner of a part of different companies which are involved in the production and distribution of energy in other countries. In the mix of installed power, the nuclear energy production is quite consistent: 58 reactors are installed in 19 power plants in France.
Even if the Nuclear energy production is declining in the last years, in EDF the improvement and the development devoted to this field does not stop. The spirit of research and the necessity to have a great amount of electricity, pushed the company to spend the 44% of the overall investment budget of 2016 for the nuclear power. However, the research in other new technologies devoted to different energy production fields has been boosted in the last 15-20 years.
Nuclear power is hence one of the most important energy sources and obviously cares of EDF studies. The reason is due to different aspects such as material properties under irradiation, reliability of the reactor materials, fluid-structure interaction. Being aware of these aspects, and in our particular case of the last one, EDF has a wide interest to develop its proper models and codes in order to study the physics of the phenomena that can affect the operation of its nuclear power plants and turbomachines. Their performances, in fact, are highly influenced by the thermodynamic state of the water and by the possible presence of the liquid phase in a vapor mixture.
In order to focus on this branch of study, EDF uses the EUROPLEXUS code, a simulation software which is dedicated to the fast transient phenomena involving fluid-structure interaction.
In this general context, my thesis has been carried out at EDF R&D Saclay, from February 20^{th} to August 18^{th} of 2017 in the department ERMES (ElectRotechnique et Mécanique des Structures), ex

AMA (Analyses en Mécanique Avancée).
In this department an intense activity of research and development on the structure mechanics is performed, in order to contribute to the improvement of the performances and to the duration of the components in a nuclear power plant.
Typical study cases performed in order to assess the characteristics described before, are scenarios concerning the fast phase change of the water inside the reactors, when accidental conditions occur. These studies are based on numerical simulation, since in most of the cases there are not many experimental data available.

In this particular branch of the nuclear safety, where disequilibrium conditions are taken into account in the two-phase mixture, a fast and robust tool, which is the steam-water table with look-up method is described. This tool is definitely proposed in order to guarantee a direct and precise calculation of properties such as pressure, temperature and speed of sound as a function of (v, e), and used in EUROPLEXUS code. To conclude, this work is part of the R&D project FAST, which has the goal to improve some development tools for fast dynamic application, to be used for nuclear safety concerns.

In this specific environment I carried out my internship, which allowed me to go in depth of the knowledge of these phenomena, and to elaborate this final work of my master thesis.

1.3 Industrial context

Nuclear energy is one of the main non fossil fuel technologies providing a considerable amount of electricity production in all over the world, due to its characteristic high power density. However, the few remarkable accidents, occurred in the past of the nuclear energy, influenced a lot the necessity to increase the care of the related safety systems in nuclear power plants.
Nevertheless, in case of a hypothetical accident, it is of primary importance to forecast the consequences that it can entail to the components of the power plant.
Therefore, a study in depth of the fluid-structure interaction has been carried out in these years, focusing on numerical analysis in cases where two-phase fast transient flows are involved. All the phenomena that will be described are studied with EUROPLEXUS[2], a code which uses an algorithm based on a fully fluid-structure coupling.
However, in this thesis only the fluid aspect has been considered in the development performed, without involving the effects on the surrounding mechanical structure.
In nuclear safety, in fact, it is very important to have a wide knowledge of the fluid properties, that can change according to the specific transient, hence the use of high accuracy CFD software is recommended.
About the main industrial cases linked to the present context it is duty-bound to mention cases like Reactivity Injection Accident (RIA), Steam explosion, water-hammer and fast depressurizations. The four mentioned cases constitute just some examples of the multitude of two-phase flow industrial cases. Even if these three are among the most studied cases in the development of two-phase flow models on EUROPLEXUS, in this thesis a particular attention has been devoted just to the cases like fast depressurization and steam explosion described in Chapter 6.

1.3.1 RIA and Steam Explosion

The Reactivity Injection Accident (RIA) is associated, in nuclear fields, to a sudden reactivity increase in the nuclear core. This phenomenon leads, as the ultimate effect, to the fast increase of the temperature linked to the rise of the amount of energy provided by neutrons fission. That energy triggers the evaporation of the fluid, generating a shock wave that increases the inner pressure. Another nuclear accident who leads to the same final consequence is the steam explosion. This severe accident is hypothetically happening during a core melting, in absence of a proper cooling.
If the fuel is not cooled down, it tends to increase its temperature, due to the heat released by fission products, hence to melt. When the molten fuel, so called corium, interacts with water it induces a violent evaporation of the water itself, triggering a huge explosive phenomenon.
During the explosion, the liquid water receives a high amount of thermal energy, which contributes to a fast phase transition. The liquid becomes vapor, increasing abruptly its volume and generating a pressure rise and a consequent formation of a shock wave, propagating into the vessel and damaging the surrounding structures.
These consequences described for both the phenomena are of crucial importance for the structure mechanics of the nuclear components, because it is essential to estimate in a precise way the value of the maximum pressure peak reached. In fact, the final goal is to work properly on the design of the materials employed in the construction and on their mechanical strength, which strongly depends on the maximum mechanical constraint undergone by the component.

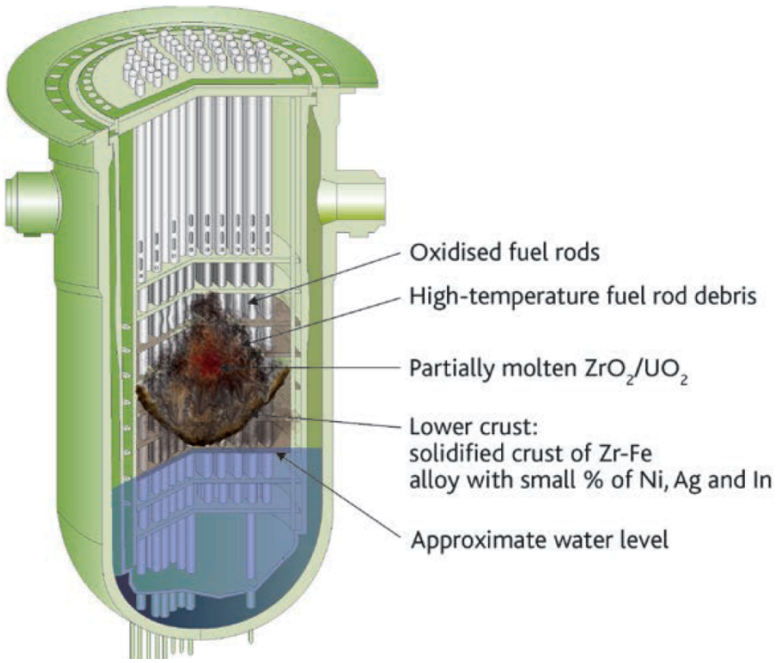

Figure 1.1: Picture taken from [3]. Steam explosion representation: the molten fuel (corium) interacts with water generating a violent steam explosion.

1.3.2 Water-hammer

The water-hammer is a typical phenomena occurring when a valve is brutally shut. This action generates a pressure wave going back and forth along the pipe and its amplitude is proportional to the initial pressure of the liquid at the moment when the valve is shut.
This phenomenon, concerning more whatever kind of pipelines than strictly the nuclear field, is one of the most studied case in fast transient fluid dynamics for different reasons.
The most important one is due to the increase of pressure that can damage the pipe and propagate along it towards a wave. The pressure increase is proportional to the difference of velocity, according to the Joukowsky equation

$$\Delta p = \rho c \Delta u. \tag{1.1}$$

Since the product ρc in the Eq. (1.1) is almost constant for a liquid, the pressure peak is strongly dependent on the velocity variation due to the valve shut. Moreover, for higher initial velocities, there is a risk of cavitation. In fact, the generation of local steam bubbles, at the moment when they collapse, provokes local pressure waves that could damage the mechanical structure.
All these phenomena can be mainly prevented avoiding the rapid shut of the valve, and consequently the pressure wave generated in correspondence of it. Nevertheless, it is very important to study the effect of this phenomenon and its direct consequences on the materials, due to the wide number of concerned industrial applications. For further information on water-hammer physics see [4].

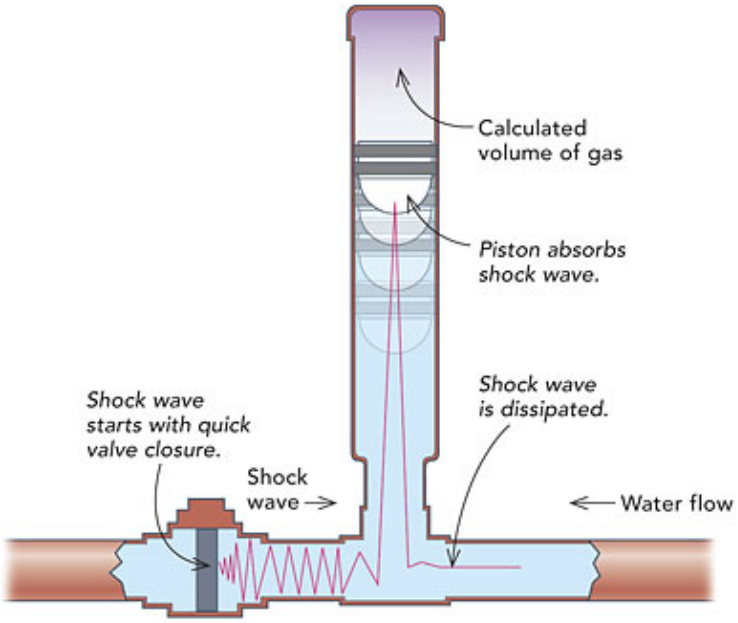

Figure 1.2: Picture taken from [5]. Water-hammer representation: the sudden closure of the valve generate a shock wave and a related pressure peak that can damage the mechanical structure.

1.3.3 Fast depressurisations

The fast depressurisation of a pipe, is a phenomenon which implies a decrease of the pressure value inside the pipe or a circuit. It may recall some characteristics of the LOCA accident, of primary

importance in nuclear field. This accident consists in a rupture of a pipe in the primary circuit, which starts emptying from the location where the break occurs.
Different effects of LOCA accident can be produced according to the pipe break size generated. Of course, the wider the break, the stronger and faster the depressurisation will be. The hypothetical large-break LOCA, for example is a double-ended guillotine or 200% break, so the loss of coolant occurs from both the complete sections of the pipe where the rupture is generated.
The consequent pressure decrease causes a fast evaporation of the liquid water, while the high pressure difference between the zones of the vessel can cause serious damages at the components, as shown in figure 1.3.
In fact, the mechanical wave, generated by the strong pressure difference between the primary circuit and the external pressure, impacts the internals, damaging the vessel and its internals.
For these reasons, on this specific accident it is focused most of the time spent on the design of the nuclear safety system, hence, a proper knowledge of the phenomenon has a wide importance for the next step of the design of a nuclear power plant.

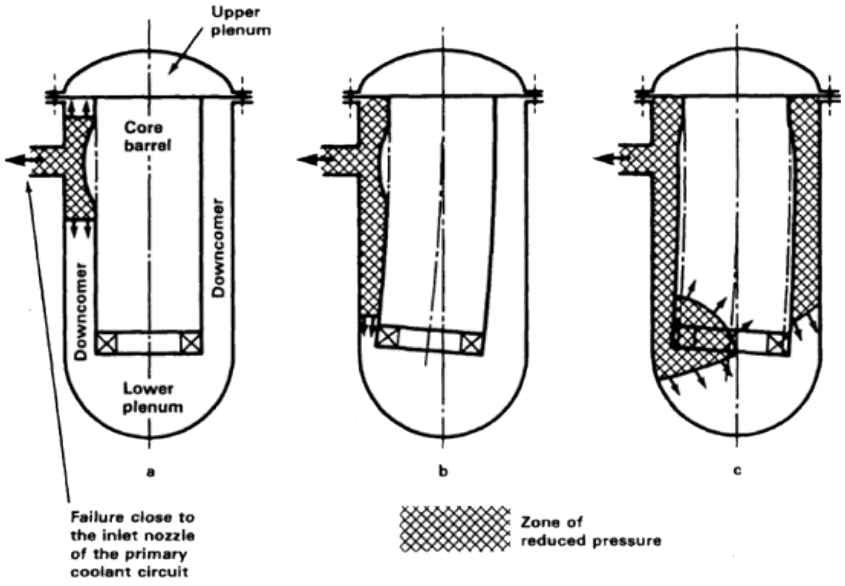

Figure 1.3: Picture taken from [6]. LOCA representation: the loss of coolant due to a sudden breach close to the nozzle generates a strong depressurisation, that propagates to the components inside the vessel.

Chapter 2

Homogeneous two-phase flow models and adequate EoS

The aim of this section is to provide the mathematical and physical fundamentals for the comprehension of the two-phase flow models presented here and developed on EUROPLEXUS code.
First of all it is necessary to specify that all of these models deal with compressible flows. This is because in all the applications where the water phase transition occurs, the density varies on 1-2 orders of magnitude, so the fluid can not be considered as incompressible.
Then, after this consideration, the governing equations for the two-phase flows are illustrated, explaining the differences between the models in the hierarchy proposed.
Further, the choice of an accurate EoS of the type $p = p(v, e)$ is taken, in order to close the systems of equations for each model.

2.1 Governing equations

Fast dynamic flow and CFD codes deal with mechanical phenomena occurring in a very short range of time, often lower than $1s$. To face these kinds of problems, the expression of the variables used in the constitutive equations has to be expressed in a conservative form (see section 2.1.1.1), in order to take into account the formation of sudden shocks, when present in the flow. Due to the rapid nature of the transient, the simplifications of adiabatic and inviscid flow can be made according to [7]. In our application we deal with two-phase flows in 1D horizontal geometries, hence gravity forces can be neglected. For these listed reasons, the Euler equations can be used to describe the physics of the problem.

2.1.1 The Euler Equations

The Euler equations is a non-linear, time-dependent hyperbolic system of equations, which governs the dynamic of compressible flows at high pressures, where body forces, viscous stresses and heat exchange are neglected. For the definition of hyperbolic the reader is referred to the section 2.2.1.
Considering a fluid in a 3D geometry, it is possible to apply the fundamental laws of conservation of mass, Newton's second law and conservation of energy as shown in the following system of equations

$$\begin{cases} \partial_t \rho + \partial_x(\rho u) + \partial_y(\rho v) + \partial_z(\rho w) = 0, \\ \partial_t(\rho u) + \partial_x(\rho u^2 + p) + \partial_y(\rho uv) + \partial_z(\rho uw) = 0, \\ \partial_t(\rho v) + \partial_x(\rho uv) + \partial_y(\rho v^2 + p) + \partial_z(\rho vw) = 0, \\ \partial_t(\rho w) + \partial_x(\rho uw) + \partial_y(\rho vw) + \partial_z(\rho w^2 + p) = 0, \\ \partial_t(\rho E) + \partial_x[(\rho E + p)u] + \partial_y[(\rho E + p)v] + \partial_z[(\rho E + p)w] = 0, \end{cases} \tag{2.1}$$

where (x, y, z) are the spatial 3D coordinates, $\rho(x, y, z)$ is the density of the fluid, $p(x, y, z)$ is the pressure, while the energy E in the system of Eq. (2.1) is the total specific energy, which includes the specific energy and the kinetic contribution. The magnitudes $u(x, y, z)$, $v(x, y, z)$, $w(x, y, z)$ are respectively the x-, y- and z- components of the velocity vector.
The system of Eq. (2.1) can be expressed in a more compact notation as

$$\mathbf{U_t} + \mathbf{F}(\mathbf{U})_\mathbf{x} + \mathbf{G}(\mathbf{U})_\mathbf{y} + \mathbf{H}(\mathbf{U})_\mathbf{z} = 0, \tag{2.2}$$

where the vectors $\mathbf{U}, \mathbf{F}, \mathbf{G}, \mathbf{H}$ are

$$\mathbf{U} = \begin{bmatrix} \rho \\ \rho u \\ \rho v \\ \rho w \\ \rho E \end{bmatrix}; \qquad \mathbf{F} = \begin{bmatrix} \rho u \\ \rho u^2 + p \\ \rho uv \\ \rho uw \\ \rho u(\rho E + p) \end{bmatrix}; \qquad \mathbf{G} = \begin{bmatrix} \rho v \\ \rho uv \\ \rho v^2 + p \\ \rho vw \\ \rho v(\rho E + p) \end{bmatrix}; \qquad \mathbf{H} = \begin{bmatrix} \rho w \\ \rho uw \\ \rho vw \\ \rho w^2 + p \\ \rho w(\rho E + p) \end{bmatrix}.$$

Even if the Eq. (2.2) is a system of equations applicable to 3D fluid flows, this work focus only on 1D fast transient flows, so in this particular branch of applications, the considered compact form of the Euler equations will be

$$\mathbf{U_t} + \mathbf{F}(\mathbf{U})_\mathbf{z} = 0, \tag{2.3}$$

where

$$\mathbf{U} = \begin{bmatrix} \rho \\ \rho u \\ \rho E \end{bmatrix}; \qquad \mathbf{F} = \begin{bmatrix} \rho u \\ \rho u^2 + p \\ u(\rho E + p) \end{bmatrix}.$$

Furthermore, in the following notation it has been decided to consider as z the horizontal axes where the fluid flows, in order to do not confuse the reader with x, which is the flow quality.

2.1.1.1 Importance of Conservative Formulation

The Euler equations, as mentioned at the beginning of the section 2.1 are expressed in a conservative form. It literally means that the derivatives in the equations are not expanded. For instance, taking into account the Eq. (2.3), its derivatives would be expanded as

$$\begin{cases} \rho_t + u\rho_z + u_z\rho = 0, \\ \rho_t u + u_t\rho_t + p_z + \rho_z u^2 + uu_z\rho = 0, \\ \rho_t E + E_t\rho + u_z(\rho E + p) + u(\rho_z E + E_z\rho + p_z) = 0. \end{cases} \tag{2.4}$$

Making some rearrangements on the system of Eq. (2.4), and substituting the first mass conservation equation in the second momentum conservation one, it reads

$$u_t + \frac{p_z}{\rho} + uu_z = 0. \tag{2.5}$$

Similarly to the momentum conservation, also the energy conservation equation can be rearranged, using the mass conservation and the Eq. (2.5). It reads

$$E_t + u_z\frac{p}{\rho} + u(E_z + \frac{p_z}{\rho}) = 0. \tag{2.6}$$

The expanded derivative of the Euler equations, expressed in a non-conservative formulation are

$$\begin{cases} \rho_t + u\rho_z + u_z\rho = 0, \\ u_t + \frac{p_z}{\rho} + uu_z = 0, \\ E_t + u_z\frac{p}{\rho} + u(E_z + \frac{p_z}{\rho}) = 0. \end{cases} \tag{2.7}$$

If we would discretize this formulation, we would obtain a different discrete form with respect to the conservative formulation (see section 2.2). In [8], it is demonstrated that for a specific conservation law, the conservative and non-conservative formulations lead to have two different wave solutions (see section 2.2.1), with a consequent wrong solution given by the non-conservative formulation. Therefore, the application of a conservative formulation is mandatory in applications like the ones presented in this work, where we refer to fast transient two-phase flow phenomena.

2.2 Numerical scheme

Systems of conservation law equations expressed in a differential form, such as the one in Eq. 2.3 are usually solved using a Finite Volume Method scheme. In the applications shown in this work, performed using the EUROPLEXUS code, the 1D geometry is discretized in uniform volumes or cells, as the ones in figure 2.1. Every cell has a center value in each node, that represents the mean value of each small volume i, making up the whole domain.

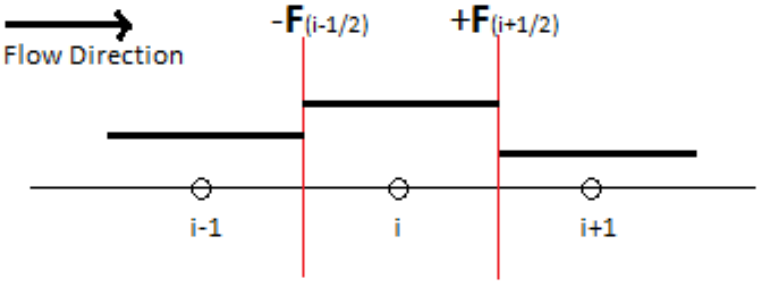

Figure 2.1: Figure describing a Finite Volume Scheme in a 1D domain. The cell i transfers mass, momentum and energy through its left and right interfaces.

Let us consider now the Eq. (2.3) in its discretized vector form, that reads

$$\frac{\mathbf{U_i^{n+1}} - \mathbf{U_i^n}}{\Delta t} = -\frac{\mathbf{F^n_{i+\frac{1}{2}}} - \mathbf{F^n_{i-\frac{1}{2}}}}{\Delta x}, \tag{2.8}$$

hence

$$\mathbf{U_i^{n+1}} = \mathbf{U_i^n} - \frac{\Delta t}{\Delta x}(\mathbf{F^n_{i+\frac{1}{2}}} - \mathbf{F^n_{i-\frac{1}{2}}}). \tag{2.9}$$

The Central Difference Scheme (CDS) is the most used one for the discretization of the partial differential equations in a finite volume approach. Nevertheless the Eq. (2.9) is the discretized form for the Eq. (2.3), expressed according the Upwind Difference Scheme (UDS).
It is important to remember that an UDS is a first order accurate type scheme, while the CDS is a second order one (see [9]). Moreover, the UDS is not intrinsically stable, but its stability depends on the Courant-Friedrichs-Lewy (CFL) number

$$CFL = \Delta t \frac{c_{max}}{\Delta x} \leq 1, \tag{2.10}$$

where c_{max} is the maximum speed wave to be determined (see section 2.2.1).

Despite its intrinsic drawbacks, the UDS is used in the discretization of the partial differential equations on the EUROPLEXUS code, forcing us to adopt very small values of Δt in order to ensure the stability of the model.
The main reason of its application is due to the fact that, adopting the UDS we take into account the direction of the flow during the discretization process, hence also the direction of the wave propagation. The symmetrical CDS do not take care about it, neglecting all the information linked to the wave propagation (see [8]).

Since the condition of the vector $\mathbf{U}$ is well known at the time t^n, the solution of the problem, that corresponds to the determination of the fluxes at the cell interfaces, is linked to the one of a Riemann problem.

2.2.1 Riemann problem

The Riemann problem is a Cauchy problem for conservation laws, namely an initial value problem which solution corresponds to a number of waves equal to the number of equations belonging to the system. The problem can be mathematically summarized as follows

$$\begin{cases} \mathbf{U}_t + \mathbf{F}(\mathbf{U})_x = 0, & -\infty < x < \infty, t > 0, \\ \mathbf{U}(x,0) = \begin{cases} \mathbf{U}_L, & x < x_{i-\frac{1}{2}} \\ \mathbf{U}_R, & x > x_{i+\frac{1}{2}} \end{cases} \end{cases} \tag{2.11}$$

where the $\mathbf{U}_L$ and $\mathbf{U}_R$ are the values of the $\mathbf{U}$ vector respectively on the left and on the right of the interface, for each i_{th} cell, in figure 2.1. Taking into account the Eq. (2.3), we can rewrite it in its quasi-linear form that reads

$$\mathbf{U_t} + \mathbf{A}(\mathbf{U})\mathbf{U_z} = 0, \tag{2.12}$$

where $\mathbf{A}(\mathbf{U})$ is the Jacobian matrix of the $\mathbf{F}(\mathbf{U})$:

$$\mathbf{A}(\mathbf{U}) = \frac{\partial \mathbf{F}}{\partial \mathbf{U}} = \begin{pmatrix} \frac{\partial f_1}{\partial u_1} & \frac{\partial f_1}{\partial u_2} & \frac{\partial f_1}{\partial u_3} \\ \frac{\partial f_2}{\partial u_1} & \frac{\partial f_2}{\partial u_2} & \frac{\partial f_2}{\partial u_3} \\ \frac{\partial f_3}{\partial u_1} & \frac{\partial f_3}{\partial u_2} & \frac{\partial f_3}{\partial u_3} \end{pmatrix}. \tag{2.13}$$

Considering the matrix $\mathbf{A}(\mathbf{U})$, the system of Eq. (2.3) is said hyperbolic if the matrix $\mathbf{A}(\mathbf{U})$ has real eigenvalues, calculated as

$$|\mathbf{A}(\mathbf{U}) - \lambda \mathbf{I}| = det(\mathbf{A}(\mathbf{U}) - \lambda \mathbf{I}) = 0, \tag{2.14}$$

where $\mathbf{I}$ is the identity matrix.

Physically speaking, the eigenvalues $\lambda_1, \lambda_2, \lambda_3$ of the matrix $\mathbf{A}(\mathbf{U})$ are the speed of the propagation waves, that transport the physical information within the fluid.
The determination of the speed of propagation is very important also for the definition of the fluxes at the interfaces of the i_{th} cell in the Eq. (2.9). To approximate these values, the HLLC-Riemann solver has been adopted from [10]

$$\mathbf{F}_{i+\frac{1}{2}}^{HLLC,n} = \begin{cases} \mathbf{F}_l & if\ S_l > 0 \\ \mathbf{F}_l^* = \mathbf{F}_l + S_l\left(\mathbf{U}_l^* - \mathbf{U}_l\right) & if\ S_l \leq 0 < S^* \\ \mathbf{F}_r^* = \mathbf{F}_r + S_r\left(\mathbf{U}_r^* - \mathbf{U}_r\right) & if\ S^* \leq 0 < S_r \\ \mathbf{F}_r & if\ S_r \leq 0, \end{cases} \tag{2.15}$$

where S_l, S^* and S_r are respectively the three speeds of the waves, determined by [11] as

$$S_l = min(u_l - c_l; u_r - c_r), \qquad S_r = max(u_l + c_l; u_r + c_r) \tag{2.16}$$

and the middle wave propagating speed, according to [8]

$$S^* = u^* = \frac{p_r - p_l + \rho_l u_l(S_l - u_l) - \rho_r u_r(S_r - u_r)}{\rho_l(S_l - u_l) - \rho_r(S_r - u_r)}. \tag{2.17}$$

In this way the fluxes across the interfaces $\mathbf{F}_{i+\frac{1}{2}}$ and $\mathbf{F}_{i-\frac{1}{2}}$ are computed for each i_{th} cell of the domain, at each time-step n, hence a solution for the starting vector Eq. (2.3) can be found.

2.3 Models Hierarchy

In many fast transient phenomena the presence of non-equilibrium between the two phases occurs. In order to understand the behavior of the fluid in these thermodynamic states, different models have been elaborated to include one or more non-equilibrium phenomena. The presented hierarchy starts from a simple equilibrium condition model, where pressure, temperature and chemical potential are the same for the two phases, at the same velocity. Then, further equations are introduced and added

to the simpler model in order to consider a specific non-equilibrium.
In principle, a wider number of equations leads to a greater degree of freedom in some parameters constituting the model. On the other hand, having a greater number of equations, it is possible to better understand the physics behind the phenomena and look at them in depth, taking into account some peculiarities caused by the disequilibrium between the phases.
Considering a short range of time as the order of ms, an important and common factor between the different models presented in the hierarchy is that the heat losses and frictions are neglected, as well as the gravity forces, and body forces effects.
This simplification is done because they could not have an effective influence on the interpretation of the phenomena, as explained in [7]. Being aware of these considerations, the two-phase flow models are hence described below, listed according to their degree of complexity. Starting from the condition of complete thermodynamic equilibrium, a hierarchy of models has been set up according to the progressive non-equilibrium considered in a second moment.

2.3.1 Homogeneous Equilibrium Model

Although some non-equilibrium between the two phases of water often occurs in a fast transients flow, it is mandatory to describe the key features that characterize the condition of perfect thermodynamic equilibrium between the phases. This condition is not only the starting point and a fundamental brick of the scale of complexity introduced in the hierarchy, but also a quite used model in several industrial calculations.
The Homogeneous Equilibrium Model (HEM) is simply derived by the Euler equations in 1D geometry, in the cases where one dimention is preponderant with respect to the other two. It is quite adaptable to simulate bubbly flows, or all the regimes where the volume flow rate of the liquid phase is elevated, hence with a low vapor content. For further details on two-phase flows regimes, see [12].
The idea to consider the full equilibrium between the two phases, really appropriate in a stable mixture, is the easiest one to perform for different reasons, listed below.

- A lower number of equations implies a simpler mathematical model to be solved.
- No other degree of freedom is present, hence the model is independent on the specific considered case. If a thermodynamic non-equilibrium exists between the phases, in fact, it implies the involvement of an equation more, consequently another degree of freedom to be introduced, often dependent on the specific physical case.
- Low computational cost and faster procedure due to the direct research of the properties through the steam-water look-up table method.

Taking into account the simplification done in section 2.1.1, a 1D-Euler system of equations (e.g. HEM[13]) is set as a partial differential equations system such as:

$$\begin{cases} \partial_t \rho + \partial_z(\rho u) = 0, \\ \partial_t(\rho u) + \partial_z(\rho u^2 + p) = 0, \\ \partial_t(\rho E) + \partial_z[(\rho E + p)u] = 0, \end{cases} \tag{2.18}$$

where E is the specific total energy:

$$E = e + \frac{u^2}{2}. \tag{2.19}$$

The variables of the system (2.18) can be considered in the vectorial form $\mathbf{U}$ expressed as follows :

$$\mathbf{U} = \begin{bmatrix} \rho \\ \rho u \\ \rho E \end{bmatrix};$$

Hence, the system can be consequently rewritten in its compact conservative form as

$$\partial_t \mathbf{U} + \partial_z(\mathbf{F}(\mathbf{U})) = 0, \tag{2.20}$$

where

$$\mathbf{F} = \begin{bmatrix} \rho u \\ \rho u^2 + p \\ u(\rho E + p) \end{bmatrix}.$$

Nevertheless, the system of Eq. (2.18) is not closed, since there are three equations and four physical unknowns (p, u, v, e), where $v = 1/\rho$ is the specific volume of the thermodynamic state. Assuming, in fact the complete equilibrium between the two phases, the specific energy and the specific volume of each thermodynamic state are determined as

$$\begin{aligned} e &= x e_v(p) + (1-x) e_l(p), \\ v &= x v_v(p) + (1-x) v_l(p), \end{aligned} \tag{2.21}$$

where e_v and v_v are respectively the specific internal energy and specific volume for the saturated vapor at pressure p. While e_l and v_l are the specific internal energy and the specific volume for the saturated liquid at the same pressure.
The parameter x is known as the flow quality

$$x = \frac{mass\, flow\, rate\, of\, vapor}{total\, mass\, flow\, rate}. \tag{2.22}$$

It is important to precise that when there is no slip between the two phases, so $u_l = u_v = u$ in case of HEM, the flow quality is coincident with the static quality

$$x = x_{stat} = \frac{mass\, of\, vapor}{total\, mass}. \tag{2.23}$$

In this specific case, the thermal equilibrium between the phases occurs, according to the HEM definition, hence the flow quality is equal to the thermodynamic quality

$$x = x_{eq} = \frac{h - h_l}{h_v - h_l}, \tag{2.24}$$

where h is the specific enthalpy of the thermodynamic state and h_k, with $k = l, v$, is the specific enthalpy of the phase.

Therefore, as shown in Eq. (2.21), an additional equation, or better an EoS is needed in order to close the system, such as

$$p = p(v, e). \tag{2.25}$$

The Eq. (2.25), provides a correlation for the pressure as a function of the specific volume and the internal energy of the fluid, given by the solution of the system of Eq. (2.18). For the determination of the pressure as a function of (v, e), several definitions such in [14] and [15] have been elaborated for academical purposes.
However, for more accurate applications in industrial context, other EoS determined by semi-empirical experiences are used. The main problem due to the use of this type of EoS, which uses a greater number of coefficients (see [16]), is hence its elevated cost.
If the pressure is directly found by the equation of state, an iterative procedure is required, because the equation of state provided can not be cast as $p(v, e)$. Having to deal with iterative procedure, as in the case of use of "model EAU", the results will be sometimes influenced by an oscillating behavior (see section 6.2).
To avoid this issue, a direct tabulation is necessary in order to be coupled with the system of Eq. (2.18), without any form of iteration. The HEM, which stems from this coupling, appears finally as a simple model, but also robust and able to deal with whatever two-phase flow case, because not dependent on other physical degrees of freedom.
Obviously, the tabulation has been done in the proper way to guarantee the efficiency and the accuracy of the model described.
Finally, if this simple and basic model presents the characteristics to deal with possible industrial applications, on the other hand, the complete equilibrium between the two phases does not allow the model to accomplish the perfect interpretation of the physics in many fast transient case.

2.3.2 Homogeneous Relaxation Model

As mentioned in the previous section, during fast transients, metastable states normally appear, hence there is the necessity to take into account the thermal or chemical non-equilibrium.
For example, in a rapid depressurisation, the pressure decreases very fast in the initial subcooled liquid. The immediate consequence, proved by experimental measurements, is that the liquid phase stands at temperature higher than its saturation value at the correspondent pressure. Therefore, metastable liquid is generated.
For further details concerning depressurisation phenomena and related experimental data see [17].

In order to take into account the different temperature between liquid and vapor mixture, the HRM presents the two phases in thermal disequilibrium condition, shown as follows:

$$\begin{aligned} p_l &= p_v = p, \\ T_l \neq T_v &= T_{sat}(p), \\ g_l &= g_v = g, \\ u_l &= u_v = u. \end{aligned} \tag{2.26}$$

The system of Eq. (2.27) is composed by the same three partial differential equations which belong to the HEM. Furthermore, the thermal equilibrium constraint between the two-phases is relaxed by the presence of the supplementary first equation, as it is shown in the system that reads:

$$\begin{cases} \partial_t(\alpha_v\rho_v) + \partial_z(\alpha_v\rho_v u) = \Gamma_{l\to v}, \\ \partial_t\rho + \partial_z(\rho u) = 0, \\ \partial_t(\rho u) + \partial_z(\rho u^2 + p) = 0, \\ \partial_t(\rho E) + \partial_z[(\rho E + p)u] = 0. \end{cases} \tag{2.27}$$

In fact, physically speaking, this equation expresses the variation of the vapor mass fraction. In case of non-equilibrium conditions, there is a mass transfer from the metastable liquid to the saturated vapor through the process of vaporization.
The mass transfer is modeled by a source term $\Gamma_{l\to v}$, on the right hand side of the Eq. (2.27). In fact, $\Gamma_{l\to v}$ quantifies the liquid transferred to the vapor phase during the vaporization, as illustrated below in the Eq. (2.28),

$$\Gamma_{l\to v} = -\rho\frac{x - x_{eq}}{\Theta}, \tag{2.28}$$

where the flow quality x does not correspond to the thermodynamic quality x_{eq}, reached in equilibrium conditions between the two phases.
However, as explained in the previous section 2.3.1, the flow quality x can be considered, for this specific case, equal to the static quality

$$x = x_{stat} = \frac{mass\,of\,vapor}{total\,mass} = \frac{\alpha_v\rho_v}{\rho}, \tag{2.29}$$

where, if we consider the cross section of the pipe,

$$\alpha_v = \frac{area\,of\,the\,cross\,section\,occupied\,by\,vapor}{total\,cross\,section\,area}. \tag{2.30}$$

The characteristic time Θ expressed in Eq. (2.28) is always positive and describes thus the way x tends to x_{eq}. If $\Theta \to 0^+$, the HRM would tend to the HEM, hence x would tend to the thermodynamic quality in equilibrium conditions x_{eq}.
Therefore, the Θ parameter is the degree of freedom introduced by this model. Its value highly influences the interpretation of the physics and the different results. For this reason, its choice has to be done in an accurate way and taking into account the specific case to analyze.
However, when it is possible, Θ is obviously related to a validation procedure through the empirical results. For further details about Θ parameter and for its different formulations see [18].

The HRM is a model that allows to take into account the disequilibrium between liquid and vapor phases, as expressed in the system (2.26).
Due to this constraint, the thermodynamic state in terms of (v, e) is hence defined as

$$\begin{aligned} e &= xe_v(p) + (1-x)e_l(p,T_l), \\ v &= xv_v(p) + (1-x)v_l(p,T_l), \end{aligned} \tag{2.31}$$

If the consideration of the thermal non-equilibrium is an advantage for the HRM, on the other hand, this model is more computationally expensive. In fact, the method to compute the physical magnitudes is strictly iterative in case of two-phase flow conditions.
Furthermore, the iterative procedure is the main issue entailed by this model. This aspect is responsible of the increase of the computational time necessary for the research of the properties to pick in the two-phase domain.
Moreover, due to the iterative procedure, the HRM is presented as less robust compared with HEM.
To sum up, if the research of the pressure for the HRM is a function of (v, e, x) as it is written on the Eq. (2.32),

$$p_{HRM} \quad = \quad p(v, e, x), \tag{2.32}$$

for the simpler but more robust HEM model, the direct procedure to get the pressure is only a function of (v, e), as remarked in section 2.3.1.
In conclusion, if the HRM is able to consider the physics of the phenomena taking into account the thermal non-equilibrium between the two-phases, there are essentially three main drawbacks introduced with respect to the HEM:

- greater computational cost, due to the presence of the supplementary equation introduced and the iterative procedure;
- the model is less robust due to the presence of an iterative procedure;
- Θ is not a general parameter but depends on the specific application case.

2.3.3 Six-equation unique-velocity model

In some cases concerning two-phase fast transient flows, the two phases are considered in a complete thermodynamic non-equilibrium, involving a greater number of equations than the previously described HEM and HRM.
For example, it is the case of some thermodynamic states of the two-phase mixture in a steam turbine, where complete disequilibrium occurs. This related complexity of the model allows to deal with the physical phenomena in a more accurate way, extending the domain of study to other industrial applications where thermo-chemical and mechanical non-equilibria occur.
To sum up, on the thermodinamic point of view, the complete disequilibrium between the two phases consists in

$$\begin{aligned} p_l &\neq p_v, \\ T_l &\neq T_v, \\ g_l &\neq g_v, \\ u_l &= u_v. \end{aligned} \tag{2.33}$$

The assumption to have a velocity equilibrium between the two phases is not completely wrong, since we assume, as in the Eq. (2.34), that instantaneous relaxations are solved, as explained in [19]. Consequently to this condition of disequilibrium, other degrees of freedom have to be introduced in order to quantify and express the physical constraints on the mathematical point of view.
As a results, a six-equation model with single velocity is able to handle the complete thermodynamic disequilibrium through the system of equations as follows:

$$\begin{cases} \partial_t \alpha_1 + u\partial_z \alpha_1 = \frac{\alpha_1}{a\rho_1 \Theta^p}(p_1 - p_2) + \frac{\alpha_1}{a\rho_1}\frac{hA_{int}}{V}(T_1 - T_2) - \frac{1}{\rho_1}\left(1 - \alpha_1 \frac{i_p k_T - k_p i_T}{k_p j_T - j_p k_T}\right) G_{1\to 2}\frac{A_{int}}{V}, \\ \partial_t(\alpha_1\rho_1) + \partial_z(\alpha_1\rho_1 u) = -G_{1\to 2}\frac{A_{int}}{V}, \\ \partial_t(\alpha_2\rho_2) + \partial_z(\alpha_2\rho_2 u) = +G_{1\to 2}\frac{A_{int}}{V}, \\ \partial_t(\rho u) + \partial_z(\rho u^2 + \alpha_1 p_1 + \alpha_2 p_2) = 0, \\ \partial_t(\alpha_1\rho_1 E_1) + \partial_z[\alpha_1(\rho_1 E_1 + p_1)u] + \Sigma = -\frac{\alpha_1 p_{int}}{a\rho_1\Theta^p}(p_1 - p_2) + b_T\frac{hA_{int}}{V}(T_1 - T_2) - b_g G_{1\to 2}\frac{A_{int}}{V}, \\ \partial_t(\alpha_2\rho_2 E_2) + \partial_z[\alpha_2(\rho_2 E_2 + p_2)u] - \Sigma = +\frac{\alpha_1 p_{int}}{a\rho_1\Theta^p}(p_1 - p_2) - b_T\frac{hA_{int}}{V}(T_1 - T_2) + b_g G_{1\to 2}\frac{A_{int}}{V}, \end{cases} \tag{2.34}$$

where

$$b_T = \alpha_1\rho_1\left[\frac{p_{int}}{a\rho_1^2}\left(\frac{\Gamma_1}{\alpha_1} + \frac{\Gamma_2}{\alpha_2}\right) - \frac{1}{\alpha_1\rho_1}\right], \tag{2.35}$$

$$b_g = \alpha_1\rho_1\frac{j_p i_T - i_p j_T}{k_p j_T - j_p k_T} \tag{2.36}$$

and

$$a = \rho_1\Gamma_1\left[\frac{p_{int}}{{\rho_1}^2} - \left(\frac{\partial e_1}{\partial\rho_1}\right)_{p_1}\right] + \rho_2\Gamma_2\frac{\alpha_1\rho_2}{\alpha_2\rho_1}\left[\frac{p_{int}}{{\rho_2}^2} - \left(\frac{\partial e_2}{\partial\rho_2}\right)_{p_2}\right], \tag{2.37}$$

with Γ_1 and Γ_2 the Grüneisen coefficients of the liquid and vapor phases, p_{int} the pressure at the interface between the two phases, Σ the energy exchange between the phases due to the forces exerted and Θ_p the characteristic time for the pressure relaxation.

The coefficients b_T and b_g allow respectively to keep constant the pressure gap between the phases during the temperature relaxation process and to keep constant the pressure and temperature gap during the chemical relaxation process.
The definition of the coefficients i_p, j_p, k_p, i_T, j_T, as well as k_T can be found in [19], where further details about the relaxation terms are given.

On the right hand side of the system of equation, the source terms take into account the effect of the thermodynamic disequilibrium between the two phases. These parameters differ basically in three types, according to the physical magnitude that contributes to the disequilibrium between the two phases:

- $\frac{\alpha_1 p_{int}}{a\rho_1\Theta^p}(p_1 - p_2)$ is a mechanical relaxation term, which relaxes the two phases towards a pressure equilibrium condition. Liquid and vapor, being at two different pressures, generate a work due to the force applied from the higher pressure phase to the lower one.
  This force let the higher pressure phase expand, leading the system to a pressure equilibrium.

- $b_T \frac{hA_{int}}{V}(T_1 - T_2)$ is a thermal relaxation term. Consequently to the temperature difference, a heat flux is generated between the two phases. The heat transfer, involving just the convection, occurs until the mixture is relaxed towards the equilibrium temperature.

- $b_g G_{1\to 2} \frac{A_{int}}{V}$ is a thermo-chemical relaxation term, proportional to the difference between the two Gibbs free energies of the two phases. The phase with the greater g will be the phase that will transfer the mass during this relaxation step, while the other one will receive it. Obviously, the mass transfer process will take place until the two energies will converge to an equilibrium value.

For other informations concerning the relaxation terms see [19] and [20].

Finally, the Six-equation single velocity model has the advantage to consider metastable states of the liquid and vapor phases, so more suitable than the HRM model to study fast transient industrial cases. Moreover, it is able to handle a double EoS in a direct form

$$p_v = p_v(v_v, e_v) \qquad p_l = p_l(v_l, e_l), \tag{2.38}$$

avoiding the iterative procedure typical of the HRM. On the other hand, the drawback to deal with six equations and the source terms that sometimes depend on the specific industrial case, make this model more computationally expensive, and not uniformly applicable.
In conclusion, even if they are not really concerned in this report, it was imperative to cite the existence of other models for two-phase flow.
These ones introduce more or fewer degrees of complexity than the Six-eq. model previously described, such as the 5-eq. model or the 7-eq. model, which involves also the velocity non-equilibrium between the phases. For further details about them consult, respectively, [21] and [22].

2.4 Goals and choice of EoS

What has been presented in section 2.3, by the system of Eq. (2.18) is actually one of the simplest models dealing with two-phase fast transient flows. Nevertheless, it is quite appropriate for several industrial applications, as described in [23].
However, there are many physical phenomena that imply the generation of metastable liquid or metastable vapor. According to the degree of disequilibrium which is necessary to take into account, a different model is used, as it was described in details in section 2.3.
Notwithstanding, all the models described have in common the strong need of an EoS of the form $p = p(v, e)$ or similar in order to close the system of equations.

In the past, different forms of EoS have been proposed such as in [14] and [15]. In this section we make a short description of possible types of EoS to use, remarking the characteristics of each one and pointing out the advantages and drawbacks.

2.4.1 Perfect gas EoS

In case of perfect gas the correspondence between p and v, e is straightforward, such as

$$p = (\gamma - 1)\rho e, \tag{2.39}$$

where γ is the ration between the specific heats at constant pressure and at constant volume.
The perfect gas EoS, can describe in some cases the thermodynamic conditions of a fluid at low pressures and high temperatures. Thus, with its very trivial expression, it is suitable for academical purposes.
Notwithstanding, for the reason that water is not a fluid that presents a linear variation of its properties along its domain of application, as a perfect gas, hence this simple model is not suitable for industrial cases.

2.4.2 Van der Waals EoS

Starting from the simplest perfect gas EoS, in the past there were some attempt to describe the real gas behavior, introducing other degrees of freedom, linked to the microscopic scale aspects.
In order to better describe the behavior of the fluid at higher pressures, the van der Waals EoS has been elaborated in the form

$$p = \frac{RT}{v - b} - \frac{a}{v^2}, \tag{2.40}$$

where $R = 8.314472 \frac{J}{molK}$ is the Gas constant; a is a parameter linked to the electrostatic attraction of the molecules; while b is the molar volume linked to the repulsive molecular forces.

Although the van der Waals EoS is more suitable than the perfect gas one, the range of application for compressible flows is limited and not applicable in case of two-phase conditions, because of large density variation.
Moreover, on the physical and mathematical point of view, dealing with Eq. (2.40) implies the effect to have a possible unphysical states where

$$\left(\frac{\partial p}{\partial v}\right)_T < 0. \tag{2.41}$$

For this reason, there could be some thermodynamic states overcoming the physical limit of the spinodal curve, which is not physically accepted in the model proposed in this work.

2.4.3 Stiffened Gas EoS

As previously specified, water is a fluid presenting stiff conditions. It practically means that for small pressure variation there could be large variation of other physical magnitudes such as the specific volume. This problem, which is not circumvented by the previous two kinds of EoS, is done by the Stiffened Gas model in the form presented by [24]:

$$p = (\gamma - 1)(e - q)\rho - \gamma P_\infty, \tag{2.42}$$

where γ, P_∞ and q are physical parameters to be empirically determined.
Therefore, the model of stiffened gas EoS is a linearization of the fluid behavior around a thermodynamic reference state. Even if it often leads to physical results, if the fluid condition is quite closed to the thermodynamic reference state, this EoS could give some large uncertainties for large pressure variations, or even unphysical results.
This issue could be set dividing the domain in zones with similar thermodynamic conditions, each one characterized by multiple reference states. However, this solution would lead to high discontinuities in the determination of the properties from one zone to another, with consequent low accuracy.
Moreover, dealing with the stiffened gas model presents other problems. Firstly, it is a pure linearization of the thermodynamic properties, hence the determination of all the first and second order derivatives would be problematic, for example to calculate the speed of sound, c (see [18]). Secondly, taking into account that the term γP_∞ stays constant, the pressure could become negative, which is not accepted for the use of the models proposed in this work and of industrial applications. For further details about it, see [25].

Taking into account all these aspects, we understand that the stiffened gas is a quite simple and relatively accurate model for academical purposes. However, it can not ensure a high accuracy, which is compulsory when we talk about industrial applications. Therefore, a more complex but accurate type of EoS is needed.

2.4.4 Empirical EoS

The exigence to deal with industrial applications involves the requirement of the highest accuracy as possible. The attempt to elaborate a model describing the thermodynamic behavior of the fluid, implies many drawbacks, such as discontinuities when the properties are determined or unphysical results.
To avoid these issues, described in the previous sections, a lot of experiments has been carried out in order to acquire data from physical tests and measurements.
Therefore, experimental and sophisticated EoS are needed in order to take into account the dependence of the fluid and to achieve adequate accuracy.

2.4.4.1 Water Properties: IAPWS Formulations

Water is one of the most used fluids in industrial applications, hence diverse studies have been carried out so far in order to extrapolate useful EoS formulations to be implemented. Dealing with these kinds of EoS implies a higher computational cost during the numerical simulation, as well as some cumbersome EoS definition.
In fact, the EoS derived by the empirical experiments are never cast in specific volume and internal specific energy, so an inversion is required for their use.

In this particular context, for what concerns the industrial applications of water and steam, the International Association for the Properties of Water and Steam, gave a great contribution in the study of the thermodynamic conditions of this fluid.
In fact, the empirical data collection, gathered during the years of research, allowed the determination of newer and more accurate properties with respect to the ones given by NBS/NRC (National Bureau of Standards of Nuclear Regulatory Commission) in [27].
These ones were published in the 80's and the thermodynamic properties are cast as a function of the

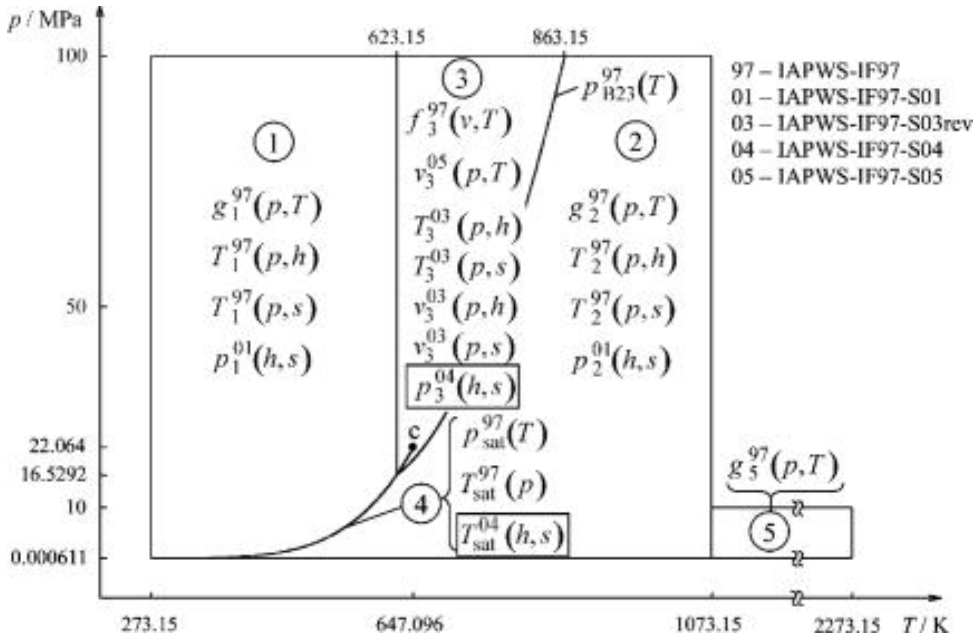

Figure 2.2: Picture taken from [26]. Regions of the Domain according to IAPWS in $(p-T)$ (Region 1: liquid domain; Region 2: vapor domain; Region 3: supercritical vapor domain; Region 4: saturation curve; Region 5: vapor at high temperature).

pressure and temperature of the state.

Even though this formulation was widely used in industrial applications, this work was reviewed by the IAPWS in order to ensure a higher precision, reducing the discontinuities of the properties. Still nowadays, for industrial applications concerning the water, the properties can be derived by two main formulations of EoS, both proposed by IAPWS, which are divided as follows:

- IAPWS-IF97[16] providing an EoS in $g(p,T)$ and $f(\rho,T)$, with specific definition of physical magnitudes of interest according to the region of validity as shown in figures 2.2 and 4.1. The thermodynamic domain is divided in five different regions and the equation of state is provided as $f(\rho,T)$ uniquely in region 3 and as $g(p,T)$ in the other regions. Therefore, the properties are cast as a function of (p,T) in all the regions, except for the region 3 ones in (ρ,T).
- IAPWS-95 Formulation[28] providing a unique EoS in $f(\rho,T)$, with an independent definition with respect to the location of the point on the thermodinamic domain.

Due to its unique equation of state, the IAPWS-95 Formulation appears more manageable. Nevertheless, the EoS provided by IAPWS-IF97 have been chosen in order to create the tabulation, for the reasons listed below:

1. special formulation for metastable vapor, thinking at the inclusion of possible metastable vapor states;
2. greater applicability in terms of temperature and pressure range[1]:

[1]The real range of validity of pressure in at high temperatures has been extended after to 50 MPa.

$$273.16\,K \leqslant T \leqslant 1073.15\,K \quad p \leqslant 100\,MPa;$$
$$1073.15\,K \leqslant T \leqslant 2273.15\,K \quad p \leqslant 10\,MPa;$$

3. greater adaptability for industrial applications, due to the lower number of terms in the polynomial making up the EoS.

Region of the tabulation	EoS	Limits of applicability [p and T]
1	$g = g(p,T)$	$p_{trip} < p < 16.529\,MPa, \quad T < T_{sat}(p)$
		$16.529\,MPa < p < 100\,MPa, \quad T < 623.15\,K$
2	$g = g(p,T)$	$p_{trip} < p < 16.529\,MPa, \quad T_{sat}(p) < T < 1073.15\,K$
		$16.529\,MPa < p < 100\,MPa, \quad T_{b_{23}} < T < 1073.15\,K$
3	$f = f(\rho,T)$	$16.529\,MPa < p < 100\,MPa, \quad 623.15\,K < T < T_{b_{23}}$
4	$p = p_{sat}(T)$	$p_{trip} < p < 22.064\,MPa$
5	$g = g(p,T)$	$p_{trip} < p < 10\,MPa \quad 1073.15\,K < T < 2273.15\,K$

Table 2.1: Properties of water according the the Industrial Formulation provided by the IAPWS. The $T_{b_{23}}$ boundary is computed using a special algorithm privided by IAPWS.

However, even if the IAPWS-IF97 has been used for the determination of the properties in all the tabulated domain, the IAPWS-95 Formulation has been also adopted during the procedure. In fact the construction of the vapor spinodal needs an EoS as a function of (ρ, T), as it will be explained more in details in the section 3.2.

2.5 Tabulation on $(\mathbf{v}, \mathbf{e})$ domain

As it has been mentioned in the previous sections, a fast and accurate method to correlate the pressure as a function of (v, e) should be found. Since the type of EoS has been chosen, it is more efficient to create a direct tabulation, constructed on the domain of the independent variables (v, e), and use it during the research of the point where (v, e) are given by a system of Eq. (2.18), for each time step. In this way the proper pressure, temperature, and speed of sound will be directly found as a function of the independent input variables (v, e).
Then, in this way any possible iterative procedure will be avoided, fastening the process of the research of the point. This method, called look-up table interpolation, is described in details in [29]. It ensures high accuracy and boosts the computational process.
The only trouble to deal with it is that the EoS used in the construction of the steam-water tables, as said in section 2.4.4.1, are defined in the form of

$$f = f(\rho, T), \tag{2.43}$$

in the case of the use of IAPWS-95 Formulation, where f is the Helmholtz free energy

$$f = e - Ts. \tag{2.44}$$

However, this formulation is very costly in terms of computational time, due to the number of terms contained in its polynomials. Therefore, for industrial applications a simpler form of the EoS is given by the IAPWS-IF97 and used in the form

$$f = f(p,T) \qquad or \qquad g = g(p,T), \tag{2.45}$$

where g is the Gibbs free energy

$$g = h - Ts. \tag{2.46}$$

These formulations are both provided by the IAPWS, respectively in [16] and [28]. Having to deal with a domain in (v,e), this problem should be circumvented in order to fasten the calculation. To do that, a residual function $\mathbf{F} = \mathbf{F}(p,T)$ such as the one in Eq. (2.47) can be defined. Matching the couple (v,e) given by the EoS and the one given by the Euler system in Eq. (2.18), it is possible to nullify the function and find the proper couple (p,T) with the following Newton-Raphson iteration:

$$\mathbf{F}(p,T) = \begin{pmatrix} e - e_{EoS}(p,T) \\ v - v_{EoS}(p,T) \end{pmatrix}. \tag{2.47}$$

In case of a model which does not use a look-up table method, a different iterative procedure is performed during the calculation in order to find the couple (p,T). However, this process leads to some inaccuracies of the results due to possible oscillations (see the section 6.2).
Then, once that the tabulation of the physical magnitudes on the (v,e) domain has been completed, the iterative procedure previously mentioned is avoided, hence its related oscillating behavior.
Therefore, the look-up table method allows to reach good results in terms of accuracy, reducing the computational cost during the determination of the properties. For this reason, this method seems to be suitable for industrial application cases.

Chapter 3

Metastable vapor extension

This chapter introduces one of the main innovative contributions of this work: the consideration of metastable vapor states and the construction of the vapor spinodal curve. In applications involving metastable vapor, it is compulsory to know the range of applicability and to bound these thermodynamic states in the tabulation performed in (v, e), already presented in [30]. Other similar contribution at this topic can be found in [31].

3.1 Introduction of the constraints

The knowledge of the vapor spinodal, which is the boundary of metastable vapor domain, is necessary to extend the tabulation in order to include these new thermodynamic states into the tabulation. At the beginning of this work, the approach was pretty similar to the one used to deduce the spinodal on the liquid side [18].
Considering the IAPWS-IF97, the properties of the region 3[16], which is slightly extensible to other regions, are expressed through an EoS of the type $f(\rho, T)$. Consequently, due to its independent variables $f(\rho, T)$, its use has been extrapolated over the boundaries of application. For the definition of all the thermodynamic states belonging to the spinodal curve, the mechanical stability constraint has been imposed as follows:

$$\left(\frac{dp}{dv}\right)_T = 0. \tag{3.1}$$

The Eq. (3.1) has been fixed for each isothermal curve, in order to find the trend given applying the properties of the region 3, provided by the IAPWS-IF97, down to very low temperatures states. Basically, even if an Eos in (ρ, T) is more suitable for this precise application, it is not possible to go too much below the temperature of $623\ K$ imposed by the region 3.
The properties of this region, in fact, can be easily extrapolated to other regions of the domain, as done for the liquid spinodal construction, but not so far from the temperature that bounds the properties of the region 3 itself.
In fact, it is of primary importance to keep in mind the range of physical magnitudes involved where the EoS, specified for each thermodynamic region, are applied. Reminding the example of the liquid spinodal construction, the extension is performed down to the temperature of $593\ K$, hence not so far from the threshold of $623\ K$ suggested by [16] for region 3 properties.
On the other hand, in the case of the construction of the vapor spinodal curve, it implies states with

very low temperature, down to $T = 273.16\ K$, which make the properties of region 3 not applicable.

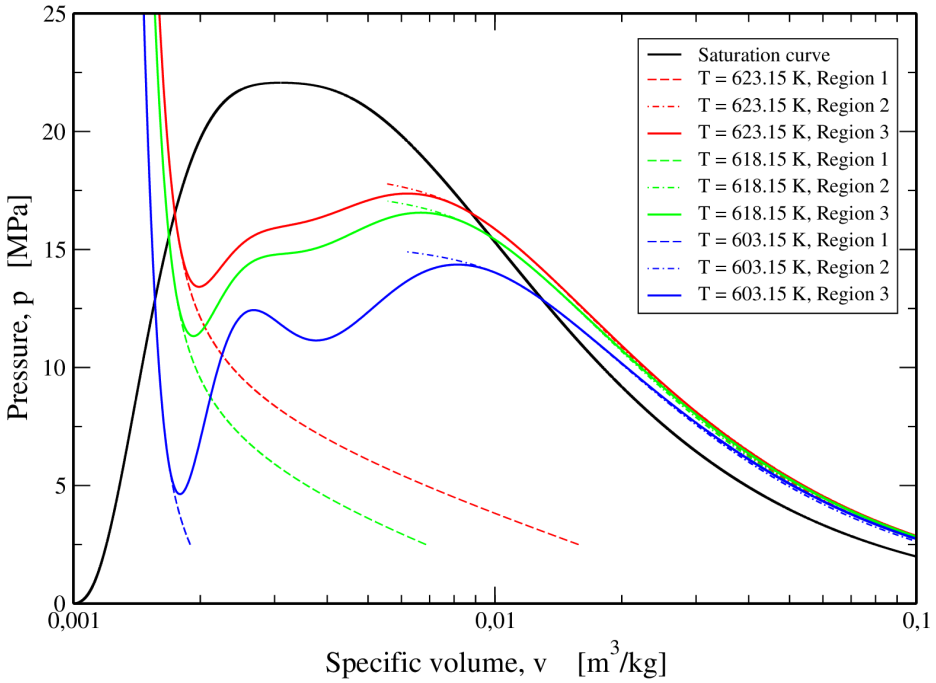

Figure 3.1: Figure taken by [18]. Attempt to extrapolate properties of the region 3 in metastable vapor domain. Down to temperatures not so lower than $623.15\,K$, this extrapolation gives however good results.

Therefore, the application of this procedure on the construction leads to unphysical results. Therefore, being aware of the considerations previously done, another way to compute the spinodal has been adopted, taking into account the IAPWS-95 Formulation.

3.2 The spinodal curve on the vapor side

Due to the problem previously mentioned, the use of the IAPWS-IF97 was recognized as cumbersome, so the IAPWS-95 Formulation has been adopted in order to construct the spinodal curve. The advantage of this formulation is to provide an equation of state as a function of density and temperature of the water, and completely independent on the region of the domain where the thermodynamic state is [28].
However, for reasons described in section 2.4.4.1, the IAPWS-IF97 has been used for the whole tabulation and for the reconstruction of the same curve. Before explaining how the vapor spinodal curve has been constructed, it is better do describe three key steps listed below, necessary to fix the limits of the same curve.

3.2.1 Definition of the thermodynamic limit states of the curve

- The point at lower specific volume is imposed fixing the critical point conditions at $p = 22,064\,MPa$ and $T = 647.096\,K$, which is the maximum in a (p, v) domain. In this point,

all the physical magnitudes are well known. Therefore, the upper point in figure 3.2 is set up.

- The point at greater specific volume is fixed as the point that satisfies the constraint of the mechanical stability of the spinodal curve, $\left(\frac{dp}{dv}\right)_T = 0$, with temperature $T = T_{trip} = 273.15\,K$.
- The maximum of the curve, in a (v, e) domain as in figure 4.2 is found through the golden section method [32]:
  - two thermodynamic states closed respectively to the critical and to the triple points are considered;
  - knowing the temperature T of the two states, the density in correspondence of the saturation is calculated, in order to use it as a guess value. Then, a Newton-Raphson iterative method is used for the residual function

$$\mathbf{F}(\rho) = \left(\frac{dp}{dv}\right)_T (\rho) = 0, \tag{3.2}$$

    in order to find the density of the state belonging to the spinodal. This procedure is applied for both the states within an iterative process. This one terminates only when the specific energies of the two points have the same value, having imposed a small tolerance at the beginning, hence the two states almost overlap .
    Therefore, the maximum of the curve in (v, e) domain is found. Knowing the position of the maximum, all the properties are calculated there and the construction can take place.

3.2.2 Construction of the curve

Since the limits of the curve are fixed, the construction is definitely performed in sequential steps as follows, for each specific thermodynamic state belonging to it.

- The constraint of the Eq. (3.1) has been coupled with the already known specific internal energy value, as follows in the residual function of Eq. (3.3)

$$\mathbf{F}(\rho, T) = \begin{pmatrix} e - e_{EoS}(\rho, T) \\ \left(\frac{dp}{dv}\right)_T (\rho, T) = 0 \end{pmatrix}. \tag{3.3}$$

- The IAPWS-95 Formulation has been used in a Newton-Raphson iterative method. The purpose is to find the values of density and temperature that nullify the first component of the residual function $\mathbf{F}(\rho, T)$ in Eq. (3.3) and guarantee the constraint of Eq (3.1).
- When the iteration terminates, density and temperature are already known, hence all the properties of the considered thermodynamic states are calculated through the IAPWS-95 Formulation.

This procedure, explained for one single thermodynamic state, is separately applied to all the states belonging to the vapor spinodal curve on the (v, e) domain: on the left side with respect to the maximum, it goes from the state with $p = p_{crit}$ until the maximum point of the curve. On the right side from right limit state at $T = T_{trip}$ until the maximum point.
The found spinodal curve has a double importance. Firstly, it represents the limit of the physical admissible states of the thermodynamics, secondly it is considered as one of the boundaries of the tabulation that will be performed. It is interesting to note that among the considered states there are some of them with very low temperatures belonging to the new admissible vapor domain. In fact, aiming to fix a clear boundary for the new tabulation, some points with temperature lower than 273.16 K have also been considered to complete the construction of the curve.

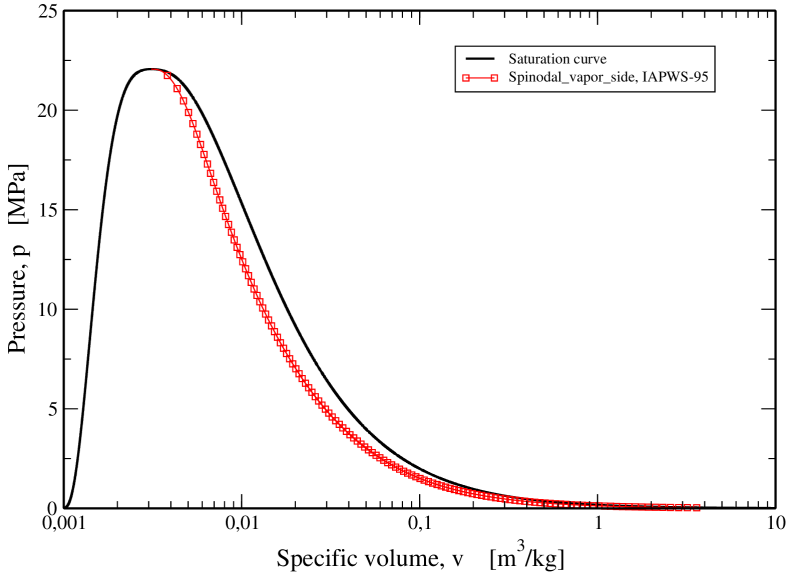

Figure 3.2: Spinodal curve in the (p, v) domain constructed using IAPWS-95 Formulation. The construction has been done down to the triple point temperature at 273.16 K.

3.3 Reconstruction using the IAPWS-IF97

Since the spinodal curve has been determined, a region containing the metastable vapor states can be tabulated in (v, e), as will be explained in details in Chapter 4. During this step, inside this region, pressure and temperature are found for each state belonging to the new portion of the tabulated domain.
Imagining these thermodynamic states delimited by the spinodal curve and the isobaric p_{trip} curve as a tabulated grid of thermodynamic ”points” or ”nodes”, as shown in figure 3.3, the properties of each node are hence calculated using the Newton-Rahpson iterative algorithm in the Eq. (2.47).

In this configuration, for each ”row” of this grid, correspondent to an iso-internal energy line, the pressure and the temperature are calculated, moving from the p_{trip} curve (right boundary) to the vapor spinodal one (left boundary). Within this ”grid construction” or tabulation of the domain, in each iso-e line, we move leftwards point by point reaching the vapor spinodal boundary.

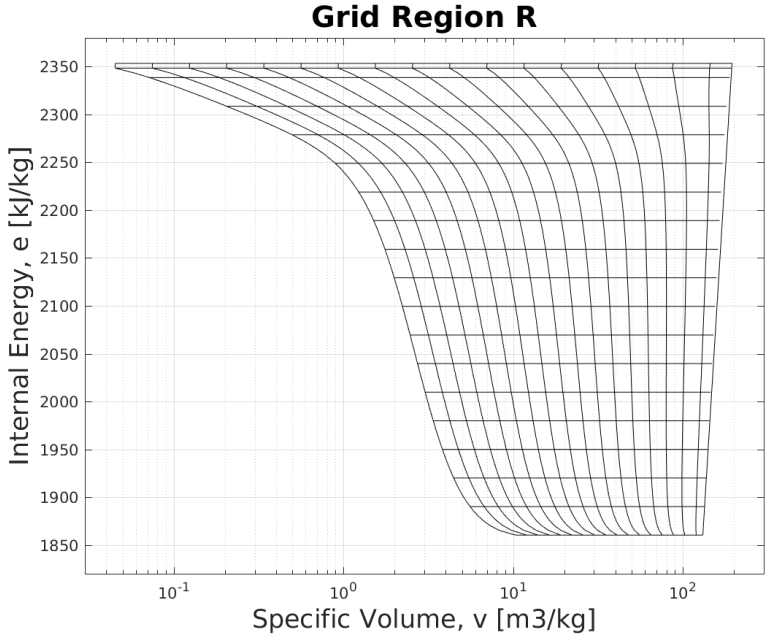

Figure 3.3: Representation of the grid of nodes making up the region including metastable vapor states. The algorithm used during the simulation counts 100 nodes of specific volume v and 200 nodes of specific internal energy e. In this picture the grid has been coarsened (20×20) with respect to the real one (100×200) in order to give an idea of its structure. The internal lines in figure are got through the spline-based interpolation. They join vertically the nodes of this grid, passing through each five nodes of all the iso-e of the real tabulation.

At that moment, we know already the couple (v, e) of the states belonging to the vapor spinodal curve. Then, a Newton-Raphson iterative method, such as in the Eq. (2.47) is used to recalculate the pressure and the temperature of the node, using the IAPWS-IF97. This method is applied for all the rows (iso-e lines) of the grid, hence a new spinodal curve can be recalculated. Finally, the results obtained have been compared with the previous ones related to the curve got through the IAPWS-95 Formulation, in figures 3.4 and 3.5.

During the extrapolation of the spinodal, it is important to keep in mind that the properties of region 3[16] can not be extrapolated wherever in the domain, but down to a certain temperature, as it has been already remarked.
Looking at the figure 3.4, the left side of the vapor spinodal has been extrapolated only using the properties of the region 3. This approach leads us to a wrong calculation of the physical magnitudes, since the properties of region 3 are done to be applied for temperature greater than $623\ K$[16]. However, the curve extrapolated by IAPWS-IF97 starts to get further from the one deduced by IAPWS-95 Formulation only for temperature much lower than the threshold imposed. This is a proof that the EoS provided by the region 3 are more flexible and adaptable to other regions.
On the other hand, they can not be extrapolated in a wide range of tolerance. Therefore, the use of the properties of the region 2 must be taken into account for temperature lower than $623\ K$. Keeping it in mind, the spinodal is completely extrapolated, as it is illustrated in figure 3.5.

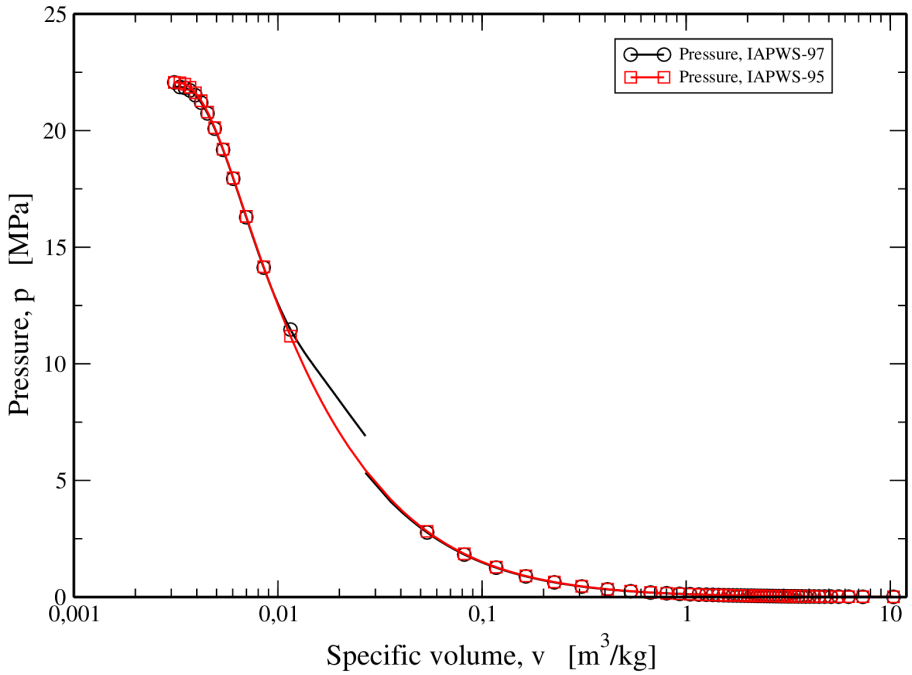

Figure 3.4: Wrong extrapolation of the boundary. The permanent use of the region 3 properties can not be extended for temperature lower than $623.15\ K$.

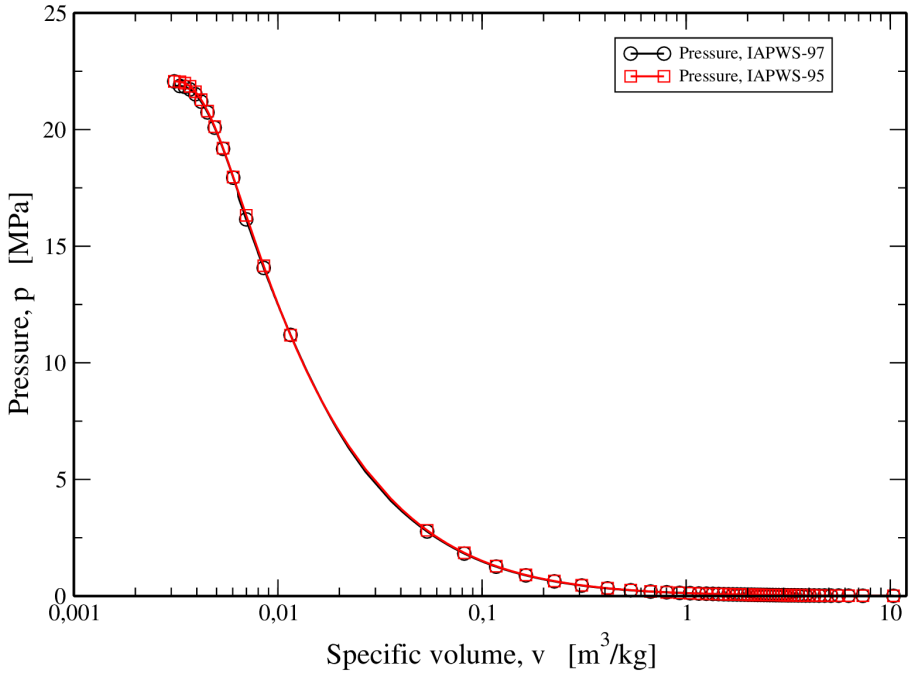

Figure 3.5: Good extrapolation of the boundary. This results show the right construction taking into account the proper application of the IAPWS-IF97 properties.

The results show it clearly overlapping to the original one, obtained using the IAPWS-95 Formulation. Also other magnitudes such as speed of sound and temperature of the vapor spinodal curve have been recalculated, with results shown respectively in figures 3.6 and 3.7. The two trends do not overlap as well as the one of the pressure, but they are quite conform.
In this way the tabulation can pursue, using only the IAPWS-IF97, while the IAPWS-95 Formulation is used just in the moment of the first construction of the spinodal curve in order to define the border of the domain. It is important to specify that the speed of sound definition on the spinodal curve is the isentropic one. For further details about its definition consult the Appendix B.

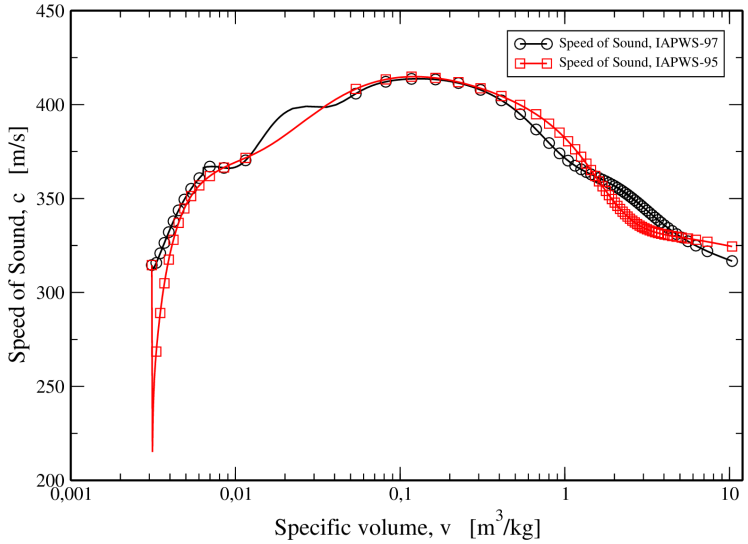

Figure 3.6: Speed of sound profile on the spinodal curve. The result obtained using the IAPWS-IF97 are quite similar to the ones provided by the IAPWS-95 Formulation.

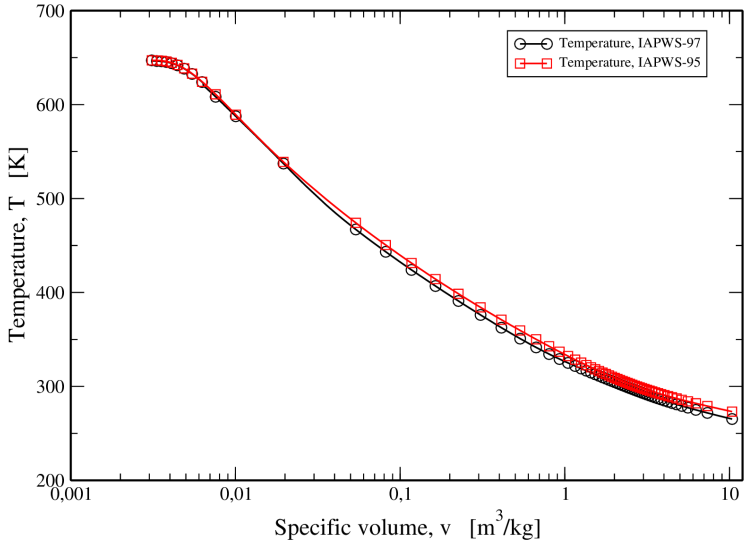

Figure 3.7: Temperature profile on the spinodal curve. The result obtained using the IAPWS-IF97 are quite similar to the ones provided by the IAPWS-95 Formulation.

Chapter 4

Grid regions and research of the (v, e) point

The inclusion of the vapor metastable states involves an obvious modification of the structure of the tabulation previously used in EUROPLEXUS code. Thus, new parts are hence added to the previous one. In this Chapter we give a more detailed illustration about the subdivision of the tabulation and the research of the point, showing the borders of each zone on the (v, e) domain.

4.1 Aim of the subdivision

The construction of the spinodal curve of the vapor side entails another way to subdivide the new tabulation in regions. In order to do not confuse the regions identified by IAPWS-IF97, listed using numbers, each region of the novel tabulation is named by letters. The way this subdivision is performed in different regions aims to fasten the research of the properties of thermodynamic state, giving the input couple (v, e).
However, it is important to keep in mind that the new tabulation should preserve the possibility to use the same steam-water tables for other models previously used such as HEM and HRM (see Chapter 6). The possibility to chose the utilization of one model rather than another one is done directly on EUROPLEXUS code. Anyway, this new subdivision took as a reference the one represented in figure 4.3, and elaborated in[33].
Therefore, whenever it was possible, the regions were not changed because not affected from the construction of the spinodal on the vapor side.

4.2 Subdivision of the grid in regions

In order to make clearer the subdivision executed, it is better to refer to the figures 4.1 and 4.2, illustrating respectively the subdivision of the (v, e) domain provided by[16] and the construction of the spinodal vapor curve with lower boundary imposed.
The first figure imposes the constraints in terms of range of applicability of the EoS provided by the IAPWS-IF97. While the second figure, clearly explicits the necessity to create another subdivision with respect to the previous one elaborated (see figure 4.3).
In fact, this one was able to handle just complete equilibrium states or metastable liquid conditions (see[33]). Therefore, due to the fact that in this work we take into account applications involving metastable vapor states, a new subdivision has been performed.

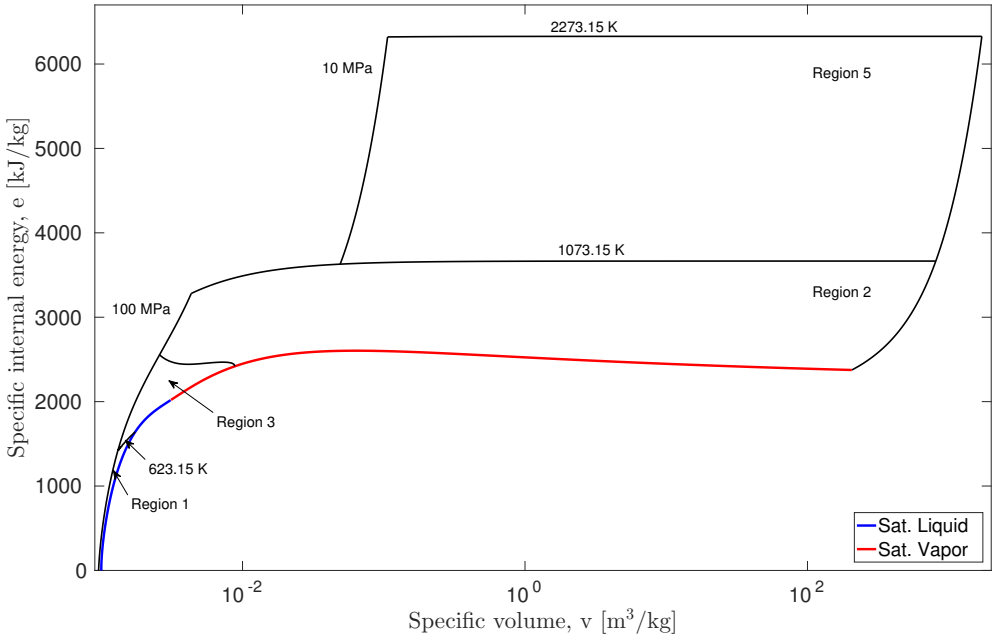

Figure 4.1: Figure taken by [18]. Regions subdivision according to IAPWS-IF97. Metastable vapor states are not considered here.

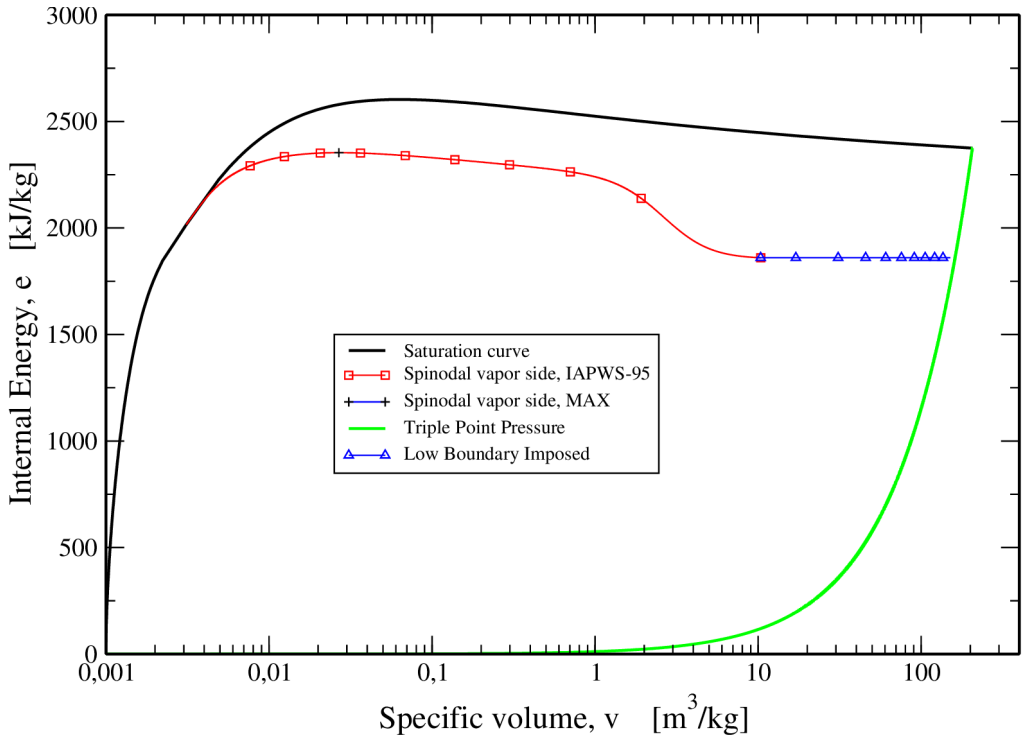

Figure 4.2: Spinodal curve of the vapor side in (v, e) domain. The blue horizontal line has been inserted in order to fix a physical and practical limit in terms of possible applications.

4.2.1 Low Region - LL

This region includes all the points belonging to the liquid phase. It is a region bounded as described below:

- on the left side by the border of the isobaric at $p = 100\,MPa$;
- on the right side by the spinodal curve, as long as the pressure is positive. Then, an isobaric $p = 0\,MPa$ has been imposed in order to consider only possible industrial applications (see [18]);
- on the bottom it is delimited by the horizontal line at $e = e_{trip_L} \approx 0\,\frac{kJ}{kg}$, while on the top the boundary is composed by the horizontal line $e = e_{crit} = 2019.03\,\frac{kJ}{kg}$.

To compute the points belonging to the LL region, the properties of the region 1 provided by IAPWS-IF97 have been used up to the temperature of $623\ K$. Over that temperature, the properties of region 3 have been used. The switch done, during the construction of the region, between the use of the properties of region 3 and region 1[16] leads to a small decrease of the accuracy on the points closed to the isothermal curve at $T = 623\ K$, as it will be shown in figure 5.10, in Chapter 5.

4.2.2 Left High Region - LH

The region Left High is one of the region that undergoes the inclusion of the new spinodal curve. This one influences the way the region is delimited, imposing the maximum of the same curve as one cardinal point in order to fix a boundary for the LH. The following key points characterize the region with respect to the same in the previous tabulation performed in [33]:

- top boundary fixed at specific internal energy e correspondent to the maximum of the spinodal curve, rather than the maximum of the saturation curve;
- right boundary fixed as the left part of the vapor spinodal curve, instead of the left part of the saturation curve.

The other two boundaries, which are the lower and the left one are respectively given by:

- horizontal line $e = e_{crit}$, coincident with the upper boundary of the LL region;
- isobaric curve at $p = 100\,MPa$.

Differently from the tables not including metastable vapor states[33], the construction of the LH region has been done using a switch between the properties of the region 2 and region 3 provided by IAPWS-IF97. If this switch is not performed, a discontinuity takes place as shown in figure 3.4.

4.2.3 Right Region - R

The Right region, as well as the LH one, undergoes the change applied on the tabulation due to the inclusion of the vapor spinodal curve. In this way, the lower-left boundary will be composed by the right part of the new introduced vapor spinodal curve. The upper boundary will be also modified, since the maximum of the spinodal curve replaces the function performed by the maximum of the saturation curve in figure 4.3. The other two boundaries are fixed as follows:

- right boundary imposed at $p = p_{trip}$, since there is no practical reason to go down to that limit in industrial cases, hence in nuclear applications;
- bottom boundary imposed fixing the FG horizontal line, as illustrated in figure 4.4.

The spinodal construction, as shown in Chapter 3, has been done imposing the constraint of the Eq. (3.1) at points of different temperatures, down to $273.16\ K$. This construction, has been stopped at the triple point temperature.
Consequently, a gap between the spinodal and the triple point pressure curves has been left. Since the region needs a boundary in order to be limited, it has been decided to insert a horizontal line correspondent to the internal energy of the right extreme of the spinodal (see figure 4.2).

4.2.4 Middle Temperature Region - MT

The MT region, as well as the previously described R and LH, is another region that is affected by the effects of the spinodal construction. In fact, this region has been properly created to cover the gap of the tabulation in terms of internal energy between the maximum of the spinodal and the maximum of the saturation curves. Having already mentioned the upper and the lower boundaries of this region, the other two boundaries are respectively:

- on the right side the triple point pressure curve $p = p_{trip}$;
- on the left side the isobaric curve at $p = 100\,MPa$.

4.2.5 High Temperature Region - HT

The last region, so called HT, contains all the points belonging to the supercritical vapor states. It has to be kept in mind that the tabulation must comply to the thresholds imposed by the IAPWS-IF97 in terms of pressure. In fact, at high temperatures the pressure limit corresponds to $10\ MPa$. However, this limitation imposed by IAPWS has been extended to $50\ MPa$ after few years.
Nevertheless, the limit imposed at $10\ MPa$ is widely enough to cover the range of industrial application concerning the supercritical vapor. The HT region, which is the one that completes the tabulated domain, presents these following boundaries:

- on the right side the triple point pressure curve;
- on the bottom the horizontal line for internal energy equal to the maximum of the saturation curve has been considered ($e = e_{max_{sat}}$);
- the upper boundary is composed by an isothermal curve at $T = 2273\ K$.
  In fact, at high temperatures the isothermal lines almost correspond to the iso-internal energy ones, since $\Delta e \approx c_v \Delta T$. Consequently, the upper boundary in terms of temperature can be slightly used as an internal energy boundary.
- Having identified the corner C (see the figure 4.4) as the corner where

$$\begin{aligned} p &= 100\,MPa, \\ T &= 1073\,K, \end{aligned} \tag{4.1}$$

and the corner D the point where

$$\begin{aligned} p &= 10\,MPa, \\ T &= 1073\,K, \end{aligned} \tag{4.2}$$

the left boundary can be finally divided in three parts:

- from the internal energy $e = e_{max_{sat}}$ (corner B) up to the so called corner C, the isobaric curve $p = 100\ MPa$;
- between the two corners C and D, the isothermal curve $T = 1073\ K$;
- the isobaric curve $p = 10\ MPa$ from the corner D up to the higher limit of the HT region.

The completed new steam-water tables, allowing the identification of the points belonging to the metastable regions, are finally represented in figure 4.4.

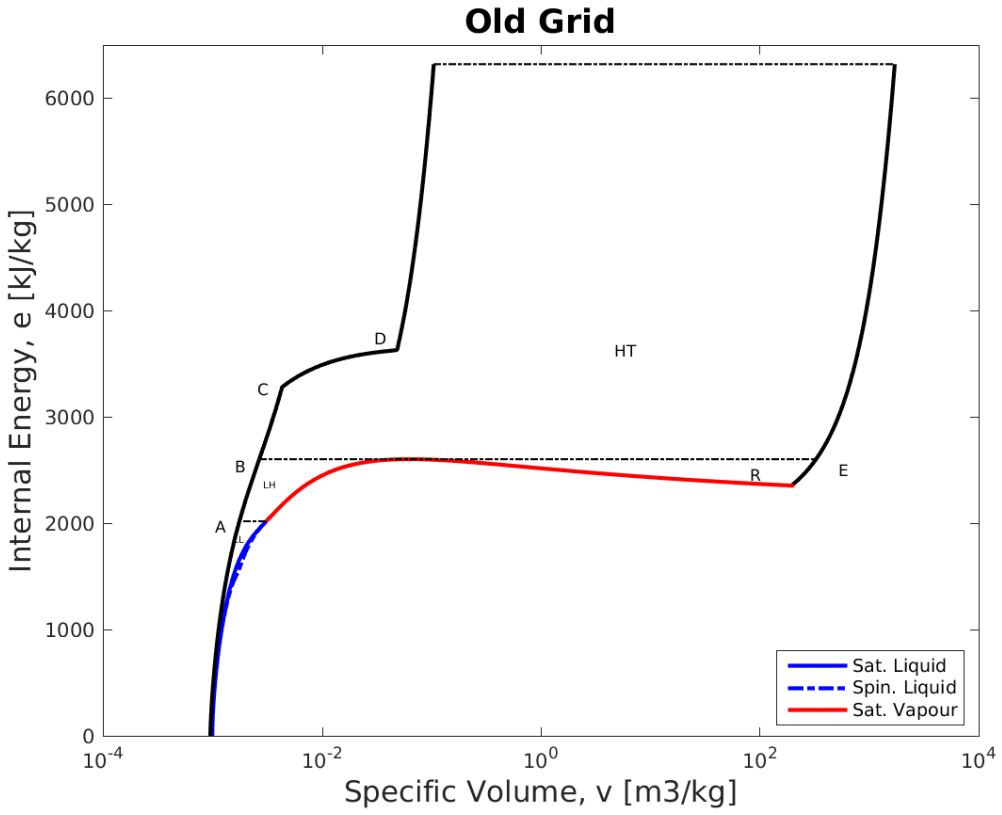

Figure 4.3: Picture showing the old grid of the tabulation on the (v, e) domain, performed in [33]. This tabulation can be used only coupled with HEM or HRM.

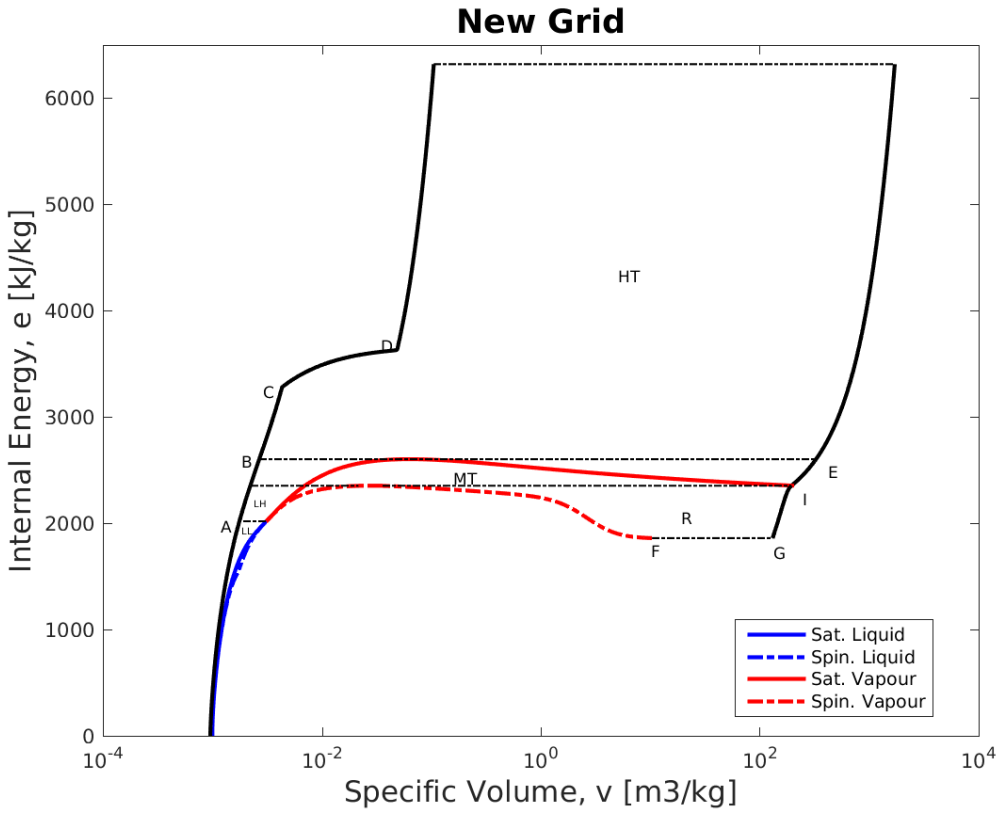

Figure 4.4: Picture showing the new grid of the tabulation on the (v, e) domain. The R region is completely belonging to the metastable vapor domain. This tabulation can be used coupled with Six-eq. model as well as HEM and HRM.

4.3 Research of the thermodynamic state

As we specified at the beginning of this Chapter, the aim of the creation of different regions for the tabulation is to facilitate the research of the thermodynamic state and its related properties through the algorithm.
Up to this moment what we know about the tabulation is that it is a set of points, where for each node corresponds a couple thermodynamic variables of the type (v, e). For all of these nodes we calculate the properties such as pressure, temperature and speed of sound, using the EoS. Now we explain how to find the properties of a random (v_0, e_0) couple entering the tabulation, for each mesh of the domain at each time-step.
This procedure is made up of several check performed, either on the e_0 and v_0. The first one of these checks involves the e_0 value. At the beginning we verify if the entry value is bounded by the maximum and minimum values of internal specific energy of the tabulation. If it is not bounded, the simulation is interrupted and an error occurs, otherwise another check on e_0 is performed in order to establish the region where the thermodynamic state lies.
Fixing the entry value of the internal specific energy e_0, a check on the specific volume v_0 is performed. In this step it is important to define the limit specific volumes belonging to the boundaries of

the region. To do that a spline-based method has been used, as the one described in [34].
The physical boundaries are accurately defined, using the coefficients of exact derivatives stocked during the implementation of the algorithm. In this way, for the entry value of e_0 we can calculate a v_{min} and a v_{max} for the limit minimum and maximum of the specific volumes bounding the value v_0. If v_0 is not bounded in any region, an error occurs and the simulation is interrupted, otherwise the true research of the point can be finally done.

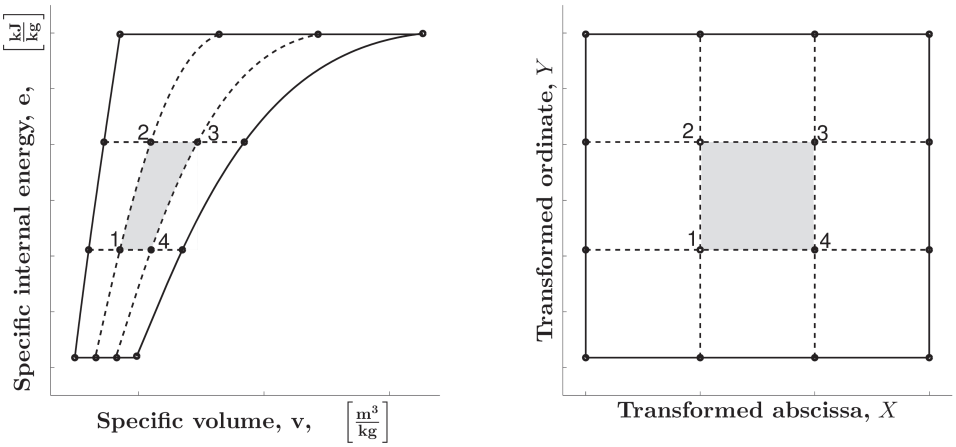

Figure 4.5: Figure taken from [18]. Picture illustrating the physical (v, e) domain on the left side and the squared transformed space on the right one. In the transformed space the abscissa X is bounded between 1 and 101, while the internal specific e energy lies on the ordinate axes Y.

To explain how the research is performed, it is necessary to precise that the (v, e) domain has been transposed in a regular, squared one (X, Y), as well as in figure 4.5. The specific internal energy e corresponds to the Y axes, while the specific volume v of the original domain has been squared and divided, for each Y, from the node $X_{min} = 1$ correspondent to the v_{min}, to the node 101 correspondent to the v_{max}.

Therefore, having defined a uniform ΔY and ΔX for the squared domain, getting the two entry coordinates (v_0, e_0), we can find the position of the concerned squared "cell" (j, i) as

$$j = int\left(\frac{X_0 - X_{min}}{\Delta X}\right), \qquad i = int\left(\frac{Y_0 - Y_{min}}{\Delta Y}\right). \tag{4.3}$$

So the exact coordinates (j, i) are well known, as well as the four thermodynamic nodes making up the cell. Then, the properties such as pressure, temperature and speed of sound can be derived through the bicubic interpolation, explained in details in [18] and [30].
This method of research of the thermodynamic state, which requires the transposition of the (v, e) domain in the (X, Y) one, is however necessary for two reasons:

- it improves the research of the thermodynamic state and its related properties, above all in the cases of stretched areas of the tabulation, which are very sensitive and where we could easily get wrong interpolations;
- it guarantees a higher accuracy, permitting the application of the bicubic interpolation and reduces the computational cost, avoiding further check operations.

Chapter 5

Steam Water Look-up table Maps

Since the tabulation has been completed, it is interesting to understand the range of applicability of the physical magnitudes in the elaborated domain. In order to satisfy this intent, this section provides a quantitative aspect of the analysis that has been theoretically explained in the previous chapters, showing some details in terms of the accuracy of the tabulation itself.

5.1 Thermodynamic properties

The plots illustrated in the following sections represent respectively pressure, temperature and speed of sound calculated for each thermodynamic state of the tabulated (v, e) domain. The calculation of these physical magnitudes is achieved by the inversion of the IAPWS-IF97 at each node, coupling it with a Newton-Raphson iterative algorithm, as in the case represented in Eq. (2.47).
Since that (p, T), or (ρ, T) for the states belonging to the region 3, have been found through the iterative algorithm, the other physical magnitudes, can be directly calculated using the polynomial provided by the IAPWS-IF97. According to the region where the states belongs to, a physical magnitude such as the speed of sound is found as follows

$$c = c_{EoS}(\rho, T) \qquad \text{for region 3}$$

$$c = c_{EoS}(p, T) \quad \text{for other regions.}$$

5.1.1 Pressure maps

In the plots in figures 5.1 and 5.2 the pressure range is represented respectively for HEM use and Six-equation one. In a (v, e) domain, it decreases from the left to the right going from 100 MPa, maximum allowable value according to IAPWS-IF97[16], to the triple point pressure $(6.12 * 10^{-4}$ $MPa)$ on the right border of the R region presented in section 4.2.
However, there are points where the pressure reaches the null value. This condition occurs only along the lower part of the spinodal curve of the liquid side, composed by an isobaric curve $p = 0\ MPa$.

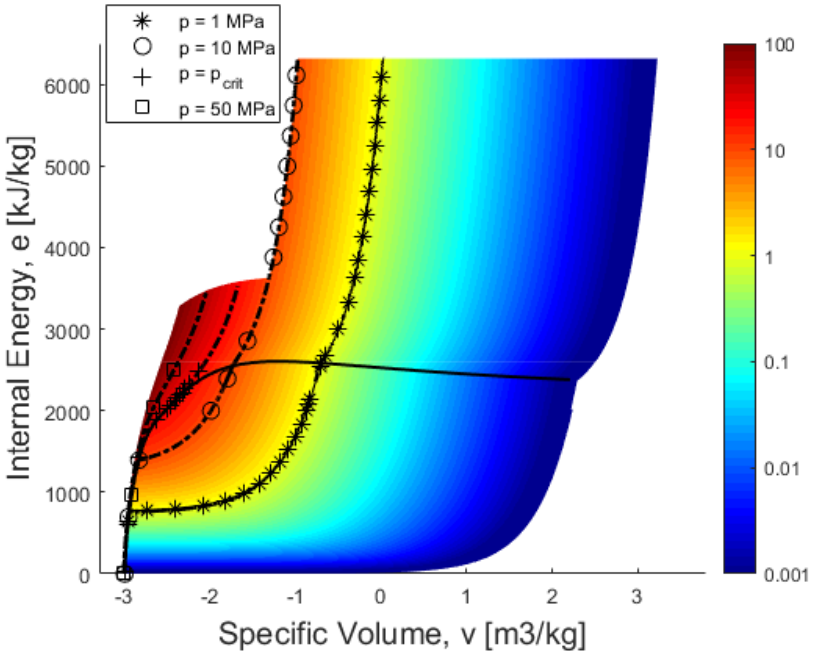

Figure 5.1: Pressure profile of the tabulated domain linked to the use of the HEM in a 2D plot. The pressure (in MPa) is represented in base 10. In black the saturation curve remarking the border between the mono-phase and the two-phase domain. Axis of specific volume, v is also in base 10. Pressure is calculated at saturation condition within the saturation curve.

5.1.2 Temperature map

The temperature field on the tabulated domain varies from $259\ K$, which corresponds to the point on the right low corner of the R region (point G in figure 4.4), to $2273\ K$, which is the top boundary in HT region of the tabulated domain (iso-internal energy and isothermal curves are almost coincident at high temperatures $\Delta e \approx c_v \Delta T$).

5.1.3 Speed of sound maps

The speed of sound is a physical magnitude which is directly calculated using the IAPWS-IF97, having already determined the couple (p, T), or (ρ, T). The importance of the speed of sound value during the calculation is not negligible. In fact, its value has a primary importance for the time step calculation, as it is explained in details in section 6.1.1.1.
In mono-phase states, the speed of sound has a higher value in a denser material, while for steam at very high temperatures its value increases with respect to a thermodinamic state at lower temperature. By the way, in a two-phase flow, according to the model used, a different value of speed of sound can be found. However, taking into account two points closed to the saturation curve, there is a difference of 1-2 orders of magnitude for the speed of sound value across the curve itself, as it is possible to see in figure 5.6.
This physical ascertainment leads obviously to a huge change of the time step value calculated.

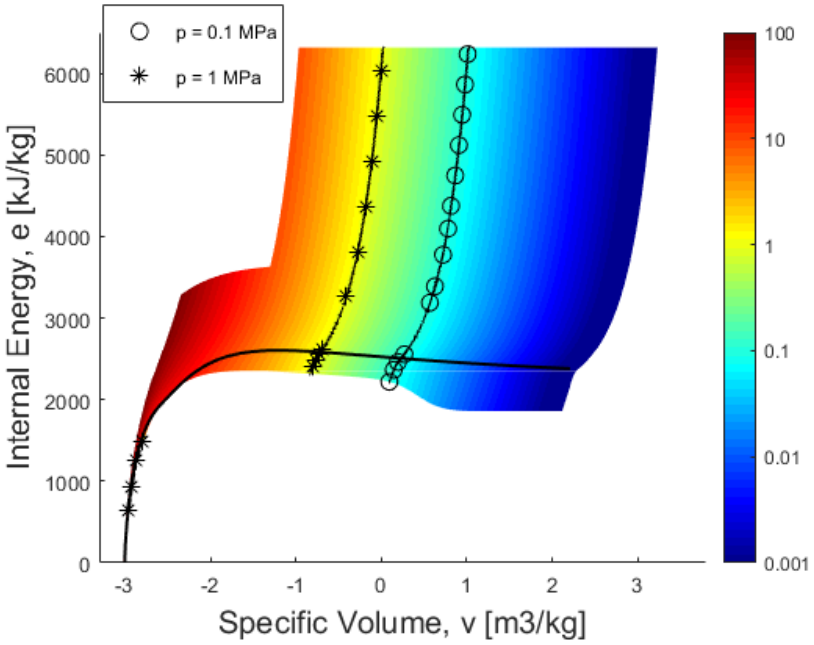

Figure 5.2: Pressure profile (Six-eq.) of the tabulated domain in a 2D plot. The pressure (in MPa) is represented in base 10. In black the saturation curve remarking the border between the stable and the metastable domain. Axis of specific volume, v is also in base 10. Pressure is calculated through region 2 or region 3 properties beyond the saturation curve.

5.2 Relative errors

Having built the tabulation, it is interesting to note its accuracy during the utilization. In order to do it, many couples of thermodynamic states (v, e) have been tested. Using the steam-water look-up tables, the properties such as pressure, temperature and speed of sound are calculated through an interpolation with the values of the neighbor cells, already tabulated.
The goal is to consider the physical magnitude of each "tested node" and compare it with the reference value given by the inversion of the EoS provided by IAPWS-97IF. To be clear on the procedure to apply, the original mesh of nodes has been taken into account. Then, this mesh has been refined, considering a number of rows multiplied by 5, as well as the number of columns.
In practice, if the mesh of one region is made up of $N \times M$ nodes, where N is the number of nodes in one column and M is the number of nodes in one row, the internal "tested node" number is

$$N_{tested\,nodes} = 5N \times 5M. \tag{5.1}$$

This general procedure has been applied for all the regions of the new grid, and for the two-phase in case of the equilibrium model. This part of the tabulation has a grid divided in three regions respectively of 200×200, 100×200 and 100×200 nodes.
Finally the table 5.1 summarizes what has been explained theoretically before. It is important to specify that all the nodes originally making part of the tabulation are not involved on the error calculation. In fact, these points are obtained by the inversion of the EoS, hence the error with respect to the nodes of the grid would be zero there.

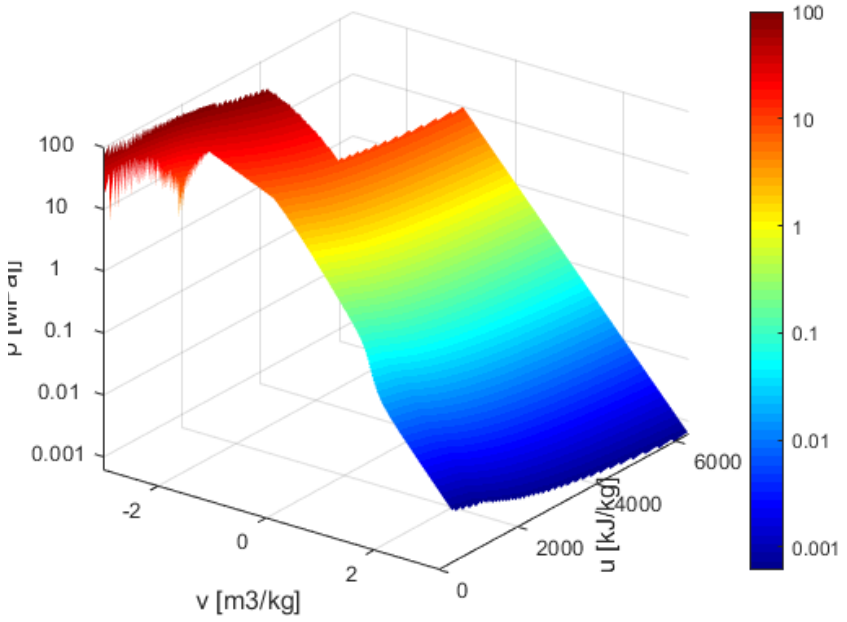

Figure 5.3: Pressure profile of the tabulated domain in a 3D plot. The pressure (in MPa) is represented as the exponent in base 10. Axis of specific volume, v is also in base 10. This figure represents the rapid pressure change in the liquid region, for small specific volume variation.

Furthermore, the error calculation has been performed for an hypothetical use of both HEM and Six-equation model for the points lying between the saturation and the spinodal curves.
The reason is due to the fact that in this work an equal attention has been devoted to perfect equilibrium model (HEM) applications, and to the complete disequilibrium ones (Six-equation model), for an employment in the next future.

Grid Region	Nodes in the Region	Tested Nodes in the Region
LL	200×200	1000000
LH	100×200	500000
R	100×200	500000
MT	100×300	750000
HT	200×200	1000000
Two Phase	–	1995000
Grid TOT-6eq.	–	3750000
Grid TOT-HEM	–	5745000

Table 5.1: Table of number of internal nodes (thermodynamic states) tested on the domain. Two different accuracy calculations have been done for HEM and Six-equation models.

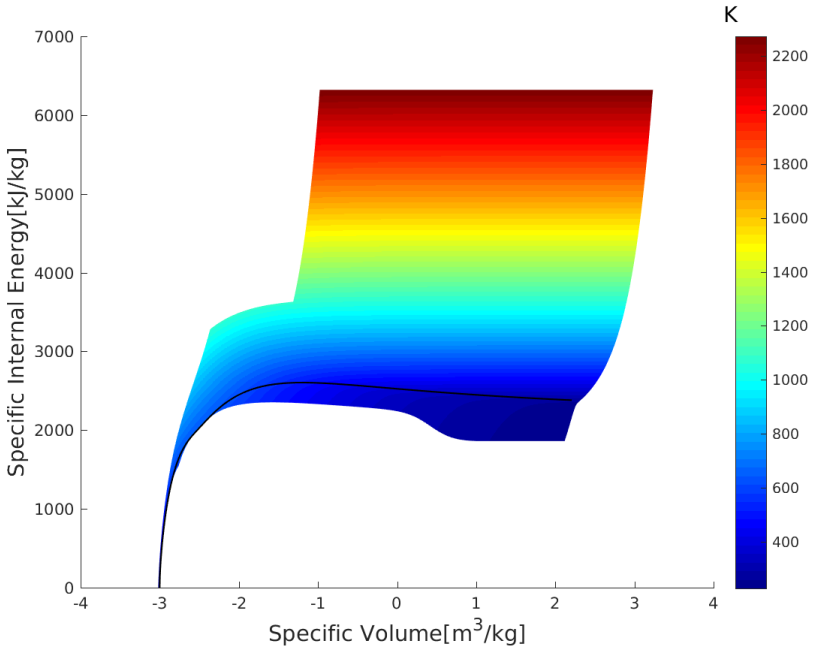

Figure 5.4: Temperature profile (in K) of the tabulated domain in a 2D plot. Axis of specific volume, v is in base 10. Temperature is calculated through region 2 or region 3 properties beyond the saturation.

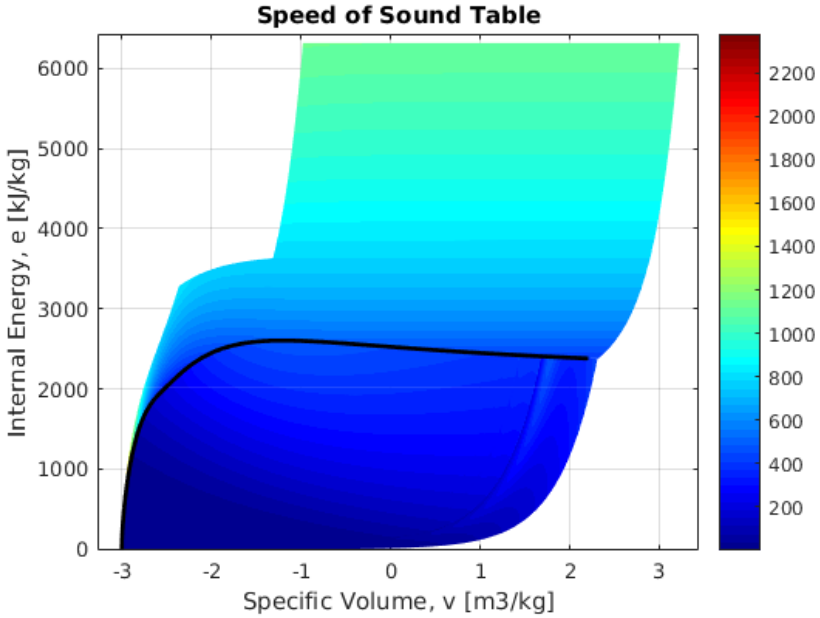

Figure 5.5: Speed of sound profile (in m/s) in a 2D plot of the tabulated domain with equilibrium conditions in the two-phase (HEM case). Axis of specific volume, v is in base 10.

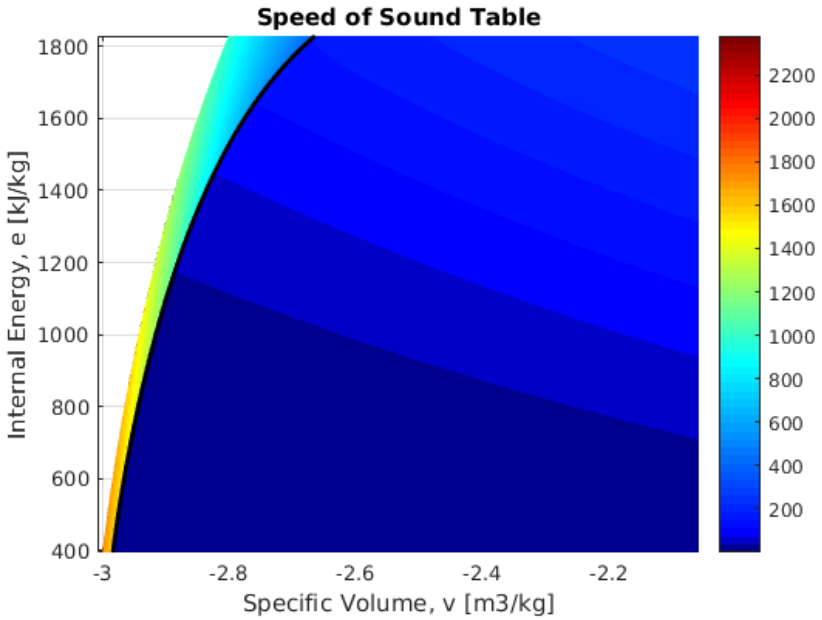

Figure 5.6: Zoom of speed of sound profile (in m/s) in a 2D plot of the LL region with equilibrium conditions in the two-phase. It is evident that across the saturation curve the value of the speed of sound drops down in the two-phase. This difference is more heightened for liquid states at higher densities. Axis of specific volume, v is in base 10.

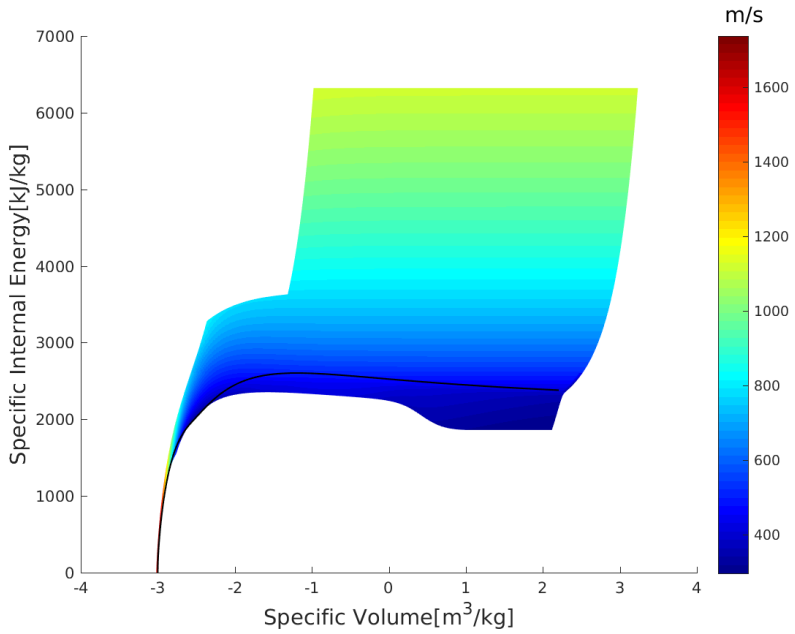

Figure 5.7: Speed of sound profile of the tabulated domain in a 2D plot where non equilibrium conditions occur (Six-eq. model case). Axis of specific volume, v is in base 10.

5.2.1 Pressure error maps

The physical magnitude chosen for the error calculation is the pressure for two main reasons:

- pressure is the magnitude with the strongest gradient in the (v, e) domain, hence, it undergoes a possible higher error in its calculation;
- this is also the variable of main interest during a calculation on EUROPLEXUS code. In fact, it is computed, while the other physical magnitudes such as temperature or speed of sound are calculated according to the pressure value.

It is important to remark that the pressure calculation in the tested nodes has been done using the bicubic interpolation (for further details see [18] and [30]). The pressure of the tested node is directly compared with the pressure resulting from the inverse equation of state, as in the Eq. (5.2)

$$Error = \left| \frac{\Delta p}{p} \right| = \left| \frac{p_{int} - p_{EoS}}{p_{EoS}} \right|. \tag{5.2}$$

The results for the pressure error are provided both for complete thermodinamic equilibrium conditions (HEM case) and also for disequilibrium conditions (Six-eq. model case), in order to guarantee the validity of the steam-water tables for the two models used.

Looking at the results, the error in pressure calculation differs according to the region considered but it has whenever quite acceptable values. In fact, even for the worst conditions, where discontinuities in properties calculation occur, it is maintained to low values as shown in figures 5.8 and 5.9. In these points, the error is included in a range between 10^{-4} and 10^{-3}.
For the rest of the domain, quite good results are achieved in terms of accuracy, while the two-phase region, tabulated only using the bilinear interpolation (less accurate method), presents an error in the range of 10^{-4} and 10^{-3}.
A peculiarity detail to remark is the magnified view of the LL and LH regions. The first one present a very low error between 10^{-6} and 10^{-8} compared with the reference pressure given by the inversion of the EoS. Only some points make an exception such as the ones beyond the saturation curve and the boundary between region 1 and 3 (accuracy around 10^{-6}).
Contrary to the LL, the LH region presents a lower level of accuracy. In fact, if in the stable vapor domain the results are quite satisfactory, the accuracy drops down for the metastable vapor states, where some points reaches the level of accuracy of 10^{-3}.
Wishing to achieve a higher performance, these results will be reviewed in order to improve the accuracy of this region.

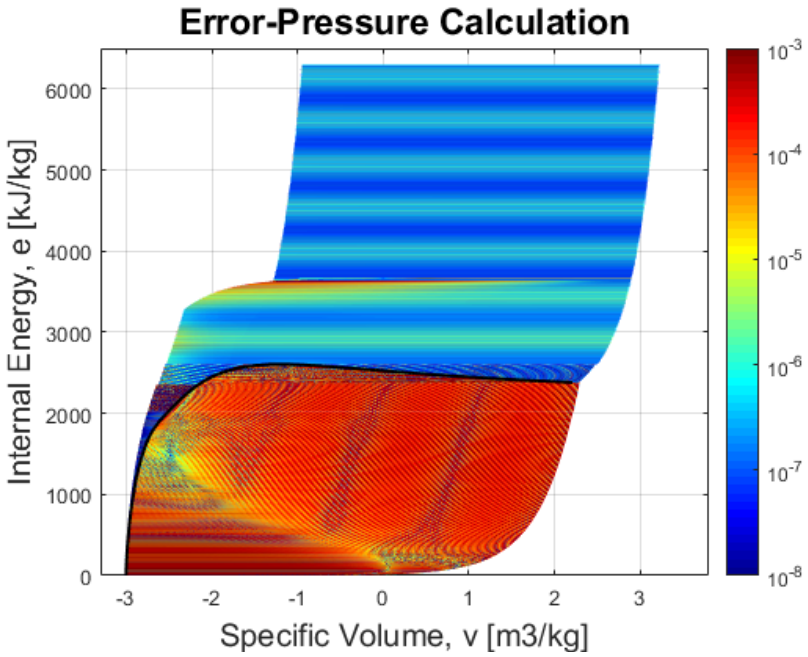

Figure 5.8: Error profile of the tabulated domain calculated with respect to the value provided by the EoS in a 2D plot (HEM case). Axis of specific volume, v is in base 10.

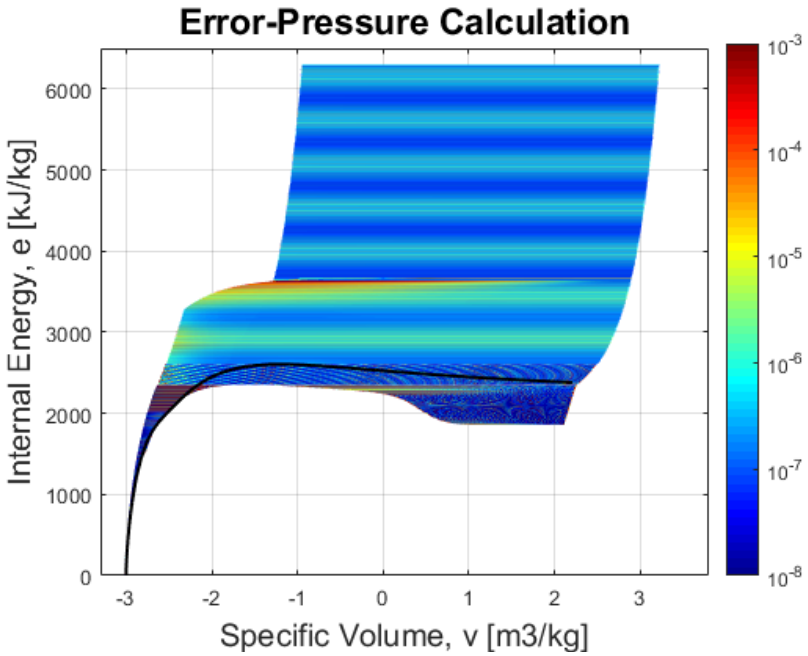

Figure 5.9: Error profile of the tabulated domain calculated with respect to the value provided by the EoS in a 2D plot (6-eq. case). Axis of specific volume, v is in base 10.

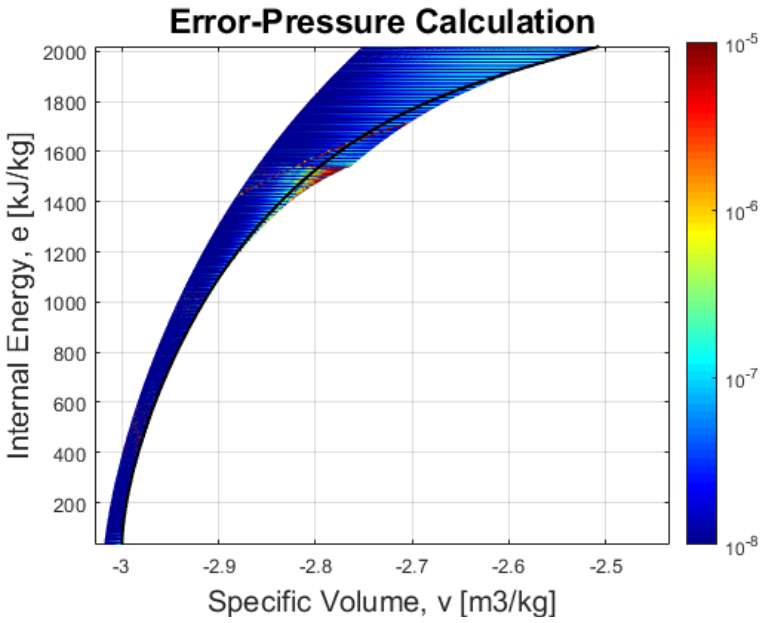

Figure 5.10: Zoom in LL region of the Error profile of the tabulated domain. The bicubic interpolation guarantees very performing results in a region widely considered for industrial applications. The highest error is in proximity of the point where the liquid spinodal and $p = 0\ MPa$ curves cross together. Axis of specific volume, v is in base 10.

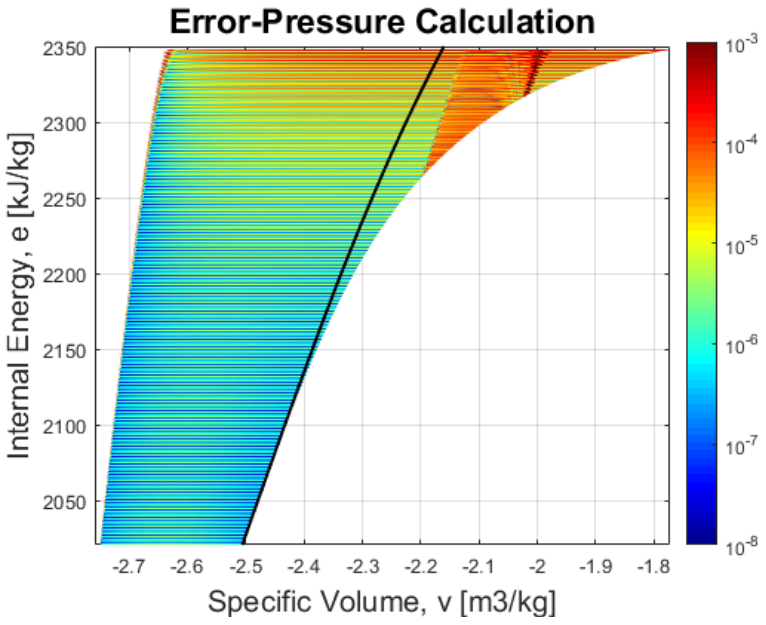

Figure 5.11: Zoom in LH region of the Error profile of the tabulated domain. The level of accuracy is lower than 10^{-4} in some points of the domain. The lower accuracy in these points is due to the discontinuity in properties calculation between region 2 and region 3. Axis of specific volume, v is in base 10.

Chapter 6

Numerical Simulation Tests

This Chapter is devoted to a use of the algorithm performed in order to study some industrial case presented at the beginning of this work. Moreover, different characteristics of the two-phase flow models already presented in section 2.3 will be shown, applying the models proposed in Chapter 2 for the simulations.
To do that, some significant test cases are analyzed using the EUROPLEXUS code, in order to validate the use of the novel steam-water look-up table.

6.1 Introduction to EUROPLEXUS code

EUROPLEXUS is a code derived by the merge of two other codes, CASTEM-PLEXUS, belonging to CEA (*Commissariat à l'énergie atomique et aux énergies alternatives*), and PLEXIS-3C, a software developed by CEA and JRC (Joint Research Center of European Commission). It is used to simulate fast transient phenomena of fluid-structure interaction, in nuclear and other industrial fields. In this code, several properties of solids and fluids are stocked within multiple libraries and used to simulate also phenomena of explosions, crashes and severe impacts. For further information, consult [2].

EUROPLEXUS code can be used for different purposes of diverse fields, from civil to military, or to simulate fluid fast dynamics phenomena for CFD, as done in this work. In this field, we focused only on two-phase flow models in 1D geometries, without taking care of interaction between fluid and structure. For this particular purpose, several models are available or under development inside the code.
Among the available models, only HEM and HRM have been used to simulate some industrial test cases. Both the models, as illustrated in sections 2.3.1 and 2.3.2, are coupled with a steam water look-up table algorithm, recently introduced on EUROPLEXUS code. However, the tabulation used during the simulation, is the one that will be used for the Six-equation single velocity model, soon available in the same code.
Therefore, the main goal was to prove that this new algorithm, as well as the old one, was adequate for the use of the coupling with HEM and HRM too.

6.1.1 Numerical method on EUROPLEXUS

The space discretization of the geometry in EUROPLEXUS is performed either in Finite Elements and Finite Volumes methods. Moreover, other formulations are under development. In this work, the adopted discretization scheme is a Finite Volume model, as the one illustrated in section 2.2.

The procedure used to solve the numerical scheme is different according to the model. For the HEM, the Euler equations in 1D geometry are discretized in their compact form as

$$\mathbf{U}_i^{n+1} = \mathbf{U}_i^n - \frac{\Delta t}{\Delta x}(\mathbf{F}_{i+\frac{1}{2}}^n - \mathbf{F}_{i-\frac{1}{2}}^n). \tag{6.1}$$

Setting the boundary conditions to the 1D domain and knowing the initial value of the $\mathbf{U}$ vector, the solution is linked to the one of a Riemann problem in order to find the fluxes at the interfaces of each cell, illustrated in section 2.2.1.

Unlike, the HRM is not a homogeneous model, and its compact vector form reads

$$\partial_t \mathbf{U} + \partial_z \mathbf{F}(\mathbf{U}) = \mathbf{b}. \tag{6.2}$$

Therefore, its solution is obtained using a fractional step procedure.

6.1.1.1 Fractional step procedure

As illustrated in section 2.3.1, HEM is a set of partial differential equations, hence, it does not need additional numerical techniques for its solution.
On the other hand, a fractional step technique is used to solve the system of equations for the HRM, due to the presence of the non conservative term $\Gamma_{l\to v}$, which is a source term for the formation of vapor from the liquid phase. It means that the numerical resolution of the PDE is split in two steps.
At each time step, first the homogeneous hyperbolic part of the system is solved, without considering the source terms. This step provides the non-equilibrium hydrodynamic field. Then, in the next separated step, the source term is activated when metastable liquid is detected (so called relaxation step).
The first step of the procedure represents the pure convection:

$$\partial_t \mathbf{U} + \partial_z \mathbf{F}(\mathbf{U}) = 0. \tag{6.3}$$

The definition of the $\mathbf{U}$ vector changes according to the model. In fact, for the HEM the vector of the conservative variables is $\mathbf{U}_{HEM} = (\rho, \rho u, \rho E)^T$, and the correspondent $\mathbf{F}(\mathbf{U})$ is $\mathbf{F}_{HEM} = (\rho u, \rho u^2 + p, u(\rho E + p))^T$.
In the case of the HRM, where the fractional step procedure is required, it is $\mathbf{U}_{HRM} = (\alpha_v \rho_v, \rho, \rho u, \rho E)^T$ and $\mathbf{F}_{HRM} = (\alpha_v \rho_v u, \rho u, \rho u^2 + p, u(\rho E + p))^T$. The problem, in its discretized form, is presented by the Eq (6.4),

$$\tilde{\mathbf{U}}_\mathbf{i} = L_{hyp}^{\Delta t}\, \mathbf{U}_i^n = \mathbf{U}_\mathbf{i}^\mathbf{n} - \frac{\Delta t}{\Delta x}(\mathbf{F}_{i+\frac{1}{2}}^n - \mathbf{F}_{i-\frac{1}{2}}^n). \tag{6.4}$$

In order to compute the approximate solution, an accurate Riemann solver has to be used, as explained in section 2.2.1. In our applications the HLLC has been chosen because of its good properties [10]. By using the HLLC-type Riemann solver, the solution of the fluxes through the cell left and right interfaces is computed over the time interval $[t^n, t^n + \Delta t]$ with given initial condition $\mathbf{U}_i^n$.

The approximate solution of Eq. (6.4), $\tilde{\mathbf{U}}_i$, will be the initial condition for the second step, i.e., the relaxation step. By solving the following ODE:

$$\frac{d\mathbf{U}}{dt} = \mathbf{b}, \tag{6.5}$$

an approximate solution $\mathbf{U}_i^{n+1}$ corresponding to the time level t^{n+1} is finally obtained, discretizing the Eq. (6.5)

$$\mathbf{U}_i^{n+1} = L_{source}^{\Delta t}\,\tilde{\mathbf{U}}_i = \tilde{\mathbf{U}}_i + \Delta t\,\mathbf{b} \tag{6.6}$$

The source term $\mathbf{b}$ in Eq. (6.5) could contain dissipative terms such as wall friction, body forces or injected energy. In the case of the HRM, the vector $\mathbf{b}$ contains just the mass transfer term, $\Gamma_{l\to v}$.

The relaxation step described for the HRM is a valid procedure that could be divided in several sub steps, according to the number of different source terms composing the vector $\mathbf{b}$, as in the case of an hypothetical use of the Six-eq. model, described in section 2.3.3. The way to proceed is the same as described before, but the initial condition of the next relaxation step will be the final solution of the previous one. This approach is summed up by

$$\mathbf{U}_i^{n+1} = L_{source}^{\Delta t}\,L_{hyp}^{\Delta t}\,\mathbf{U}_i^{n}, \tag{6.7}$$

where the terms L_{source} and L_{hyp} represent the application of the source and hyperbolic operators.

The time step calculation Δt, in Eq. (6.4), is thus provided by imposing the CFL number and considering the Δx fixed by the discretization of the mesh as follows,

$$\Delta t = CFL\frac{\Delta x}{c_{max}}, \tag{6.8}$$

where c_{max} is the maximum wave speed propagation throughout the domain at time level n as shown by the following Eq. (6.9)

$$c_{max} = \max(u - c, u, u + c), \tag{6.9}$$

while u is the velocity and c is the speed of sound of the fluid.
Therefore, according to the value of the speed of sound, the value of Δt can change of 1-2 orders of magnitude from one time step to another one.

If the initial condition is well known and the boundary conditions have been fixed, the Riemann problem is solved for all the time steps n and for all the cells of the 1D domain.

6.2 Steam Water Table Validation with model EAU

Before to start dealing with industrial test cases, it is useful to assess the use of the algorithm with another validated model for 1D calculation, still on EUROPLEXUS, the so called "model EAU".
The goal is to demonstrate that the coupling between HEM or HRM with the Steam Water Look-up Tables can guarantee the same results with another validated model, starting from the same physical hypothesis of complete thermodynamic equilibrium as

$$\begin{cases} \partial_t \rho + \partial_z(\rho u) = 0, \\ \partial_t(\rho u) + \partial_z(\rho u^2 + p) = 0, \\ \partial_t(\rho E) + \partial_z[(\rho E + p)u] = 0, \end{cases} \tag{6.10}$$

The only difference between the two approaches consist on a different EoS-type to close the system of equations: direct for the HEM, whereas the model EAU is strictly iterative.

6.2.1 Model EAU: main features

The model EAU is a two-phase flow model already available on EUROPLEXUS and still used for several nuclear calculations. It supposes, as well as the HEM model, the perfect equilibrium between the two phases.
Nevertheless, it does not use a direct look-up table procedure as well the HEM, but it employs an iterative method to find the pressure, given the input couple (v, e). The two main differences with respect to HEM are summed up as follows.

- The used EoS do not belong to IAPWS-IF97 but to the NBS/NRC[35], which is a more obsolete form with respect to the IAPWS-IF97 properties.
- The tabulation is created, but on a (p, T) domain. As a consequence, the research of the point is not direct, even for complete equilibrium states, with a consequent iterative procedure to apply.

Model	EoS	Type	Drawbacks
EAU	$\begin{cases} e = e(p,T) \\ v = v(p,T) \end{cases}$	ITERATIVE	Oscillating behavior Greater computational cost
HEM	$p = p(v, e)$	DIRECT	-

Table 6.1: Main features of EAU model in comparison with HEM. The Look-up Table avoids the iteration during the determination of the properties for an entry thermodynamic state in (v_0, e_0).

The inversion of the EoS provided by NBS/NRC does not always lead to the proper results, according to the guess value provided to the iterative procedure. Therefore, some oscillating behavior can be seen.
An important aspect to make clear is that the iterative procedure applied in EAU model is different with respect to the one used in HRM. Firstly, the iteration applied in EAU model is performed in a (p, T) tabulation, rather than the (v, e) as in the case of the HRM.
Secondly, the iterative procedure in EAU model is dictated by the research of a point that supposes a perfect equilibrium between the two phases. On the contrary, for HRM the iteration is due to the relaxed thermal equilibrium between the phases, which are in an initial condition of thermal non-equilibrium.

6.2.2 Cavitation test

In a cavitation test, chosen to validate the steam-water look-up table procedure, a 1D horizontal pipe is considered completely filled with water. Assuming to divide the pipe in two equal parts of $0.5\,m$ each, we consider as an initial condition a fluid going leftwards on the left part, while on the right one the fluid goes rightwards.

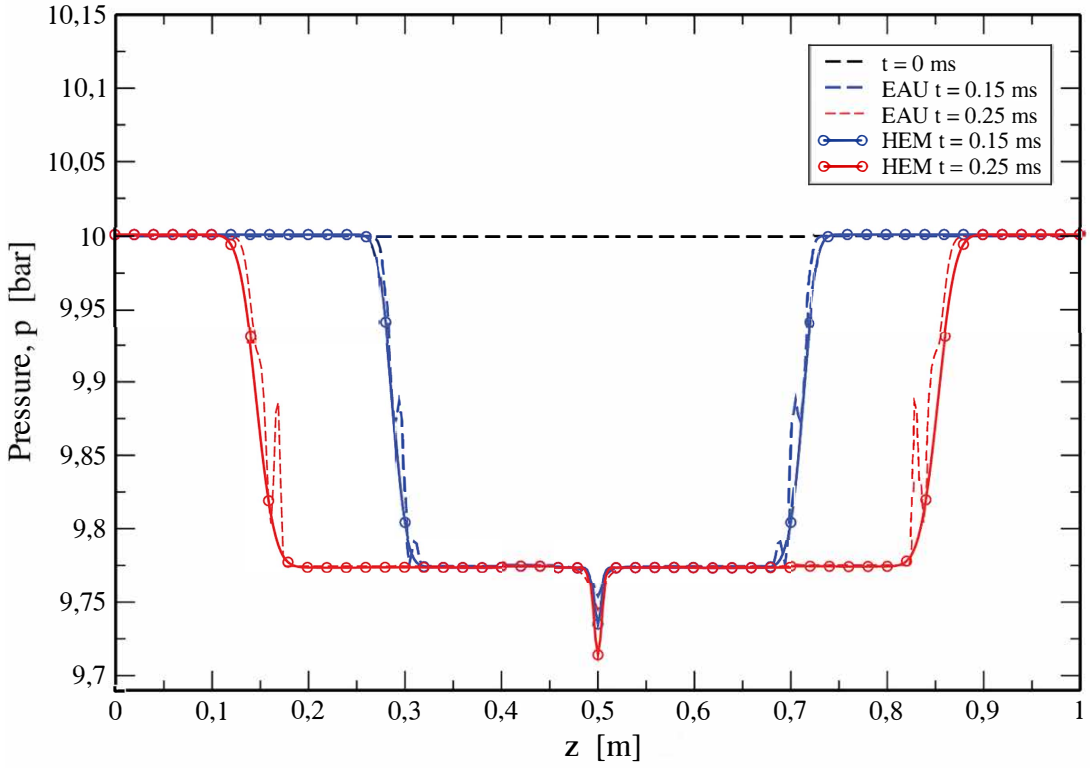

Figure 6.1: Pressure profile resulting from the two complete equilibrium models EAU and HEM. The results obtained by the EAU model present an oscillatory behavior due to the not really efficient iterative procedure.

This phenomena creates a discontinuity on the velocity field and a consequent Riemann problem to focus on. The main characteristics of the case are listed below, for what concerns the 1D geometry and the imposed initial conditions.

- Geometry
  - 1D horizontal pipe of $1\ m$ length;
  - Wall Boundary Conditions;
  - $CFL = 0.75$;
  - Mesh discretized in 400 cells.

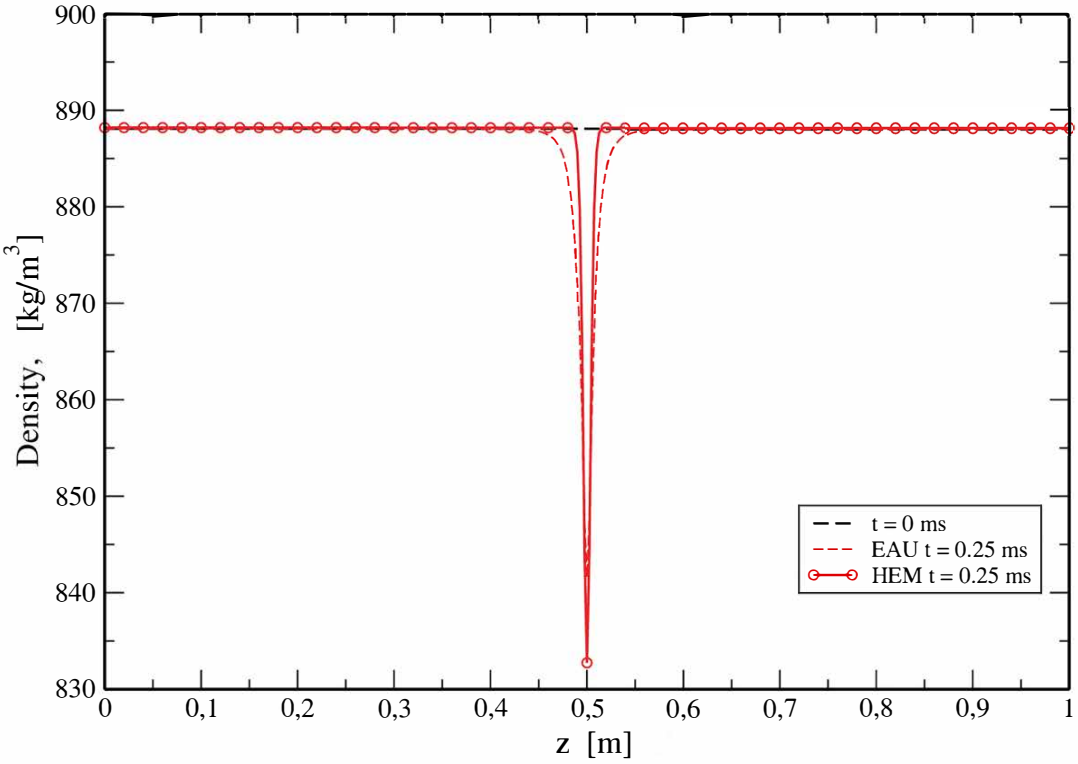

Figure 6.2: Density profile resulting from the two complete equilibrium models, EAU and HEM: the local depressurisation, corresponding to a decrease of the density, leads to an evaporation on the center part of the pipe.

The "wall" boundary condition establishes the physical equivalence between the two states of left and right with respect to the boundary. Only the velocity vector is specular with respect to the boundary, i.e.

$$\begin{aligned}(\vec{u}.\vec{n})_l &= -(\vec{u}.\vec{n})_r,\\ p_l &= p_r,\\ \rho_l &= \rho_r,\end{aligned}$$

where $\vec{n}$ is the vector normal to the surface.

Further details about boundary conditions for Finite Volumes Method on EUROPLEXUS are provided in [36].

- Initial conditions of left (L) and right (R) parts of the pipe
  - p_L = 10 bar , p_R = 10 bar;
  - T_L = 179 °C, T_R = 179 °C, T_{sat} = 179.88 °C;
  - u_L = -2 $\frac{m}{s}$, u_R = +2 $\frac{m}{s}$.

The results in figures 6.1 and 6.2 clearly show how the coupling with the tables is robust, compared with the same model that uses an iterative procedure. The HEM model, presenting almost the same trend of the results of the EAU model, is validated as an optimal and more performing model for two-phase flows, hence, as a possible usable tool for industrial applications.

6.3 Test cases and results with HEM and HRM

Since the HEM model has been tested and the look-up table procedure has been verified in section 6.2, it is now the moment to try to extend the use of this procedure to some industrial cases of interest. The goal is the one to understand if the look-up table algorithm, implemented on EUROPLEXUS code, could be employed for several kinds of industrial applications concerning two-phase fast transient flows.
Then, two main cases are proposed in this section in order to compare the different results obtained through the application of the HEM and HRM at the same tests.

6.3.1 Super Canon

During the past, Super Canon was a widely studied test case and some references are present in the literature, such as [37]. Some experimental measures are also available in order to test and validate different two-phase models with empirical data.
Super Canon is basically the test case which better recalls the acoustic phase of the LOCA accident in nuclear field. In this specific case, a pipe considered in 1D horizontal geometry, is completely filled with water at $150\ bar$ and 300 °C. Other data of the studied case are listed below:

- Geometry
  - 1D horizontal pipe of $4.389\ m$ length;
  - $CFL = 0.5$;
  - one Wall Boundary Condition in one side;
  - "Cavity" in correspondence to the breach;
  - Mesh discretized in 1000 cells.

  The condition of "Cavity", fixed at the left boundary is not a real boundary condition, because not truly imposed at the physical boundary of the domain. In fact, it is a condition forced to simulate the external environment.
  This ruse has been performed imposing the pressure of a huge external volume where the fluid outflows. This particular state, in fact, is conform with the accidental condition in a reactor building, where the reactor vessel and the primary circuit are located.

- Initial conditions
  - p = 150 bar;
  - T = 300 °C;
  - u = $0\ \frac{m}{s}$.

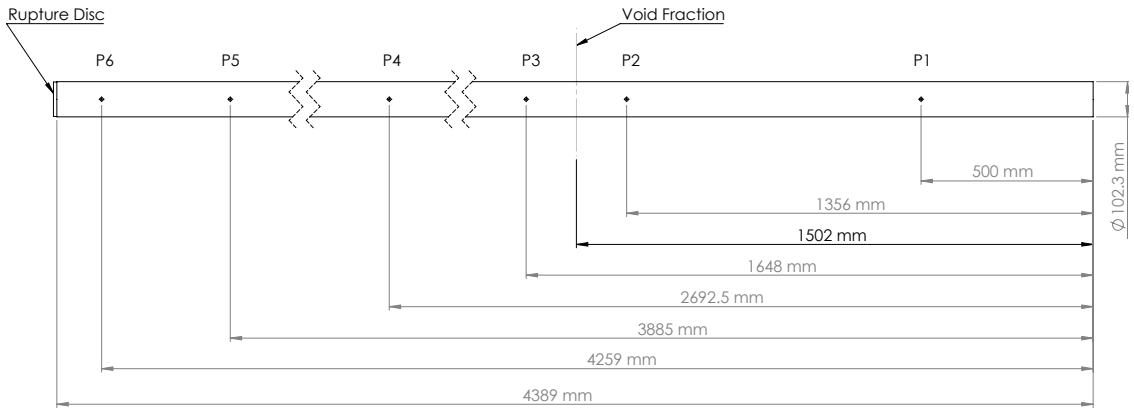

Figure 6.3: Figure taken by [18]. Super Canon 1D domain: several probes have been placed in order to study the evolution during the transient of the fluid in some single points.

At $t = 0\ s$, the sudden rupture of the left disk occurs and the fluid starts to move leftwards, getting out the pipe, that starts to be emptied. A fast depressurisation occurs, starting from the breach of the pipe on the left side, where the critical conditions are reached. A proof of that is represented by the fluid velocity that reaches the speed of sound value, as can be seen in figure 6.4.

The Mach number, which is equal to

$$Mach = \frac{u}{c}, \tag{6.11}$$

higher than one, in fact tells us that the fluid increases its velocity locally, close to the breach, avoiding the propagation of the physical information, traveling at the speed of sound. In fact, the pressure pulses propagating into the fluid, allows only the propagation in a restricted zone of action [38].
Consequently, the critical mass flow condition occurs at the breach of the pipe, where the pressure profile is getting stiffer. Other important peculiarities of the phenomenon can be remarked in the same figure 6.4. For example, the small vapor pocket that is generated on the right side of the pipe, where a local depressurisation occurs, and a pressure plateau along the center part of the pipe.
These interesting phenomena are predicted by both the models HEM and HRM, even if the pressure plateau during the phase transition is flatter in HRM profile.

Looking at different aspects and results provided by the two models, there are three main concepts to be remarked, listed as follows:

- a wider depressurisation occurs along the whole length of the pipe according to HRM with respect to the correspondent HEM results;

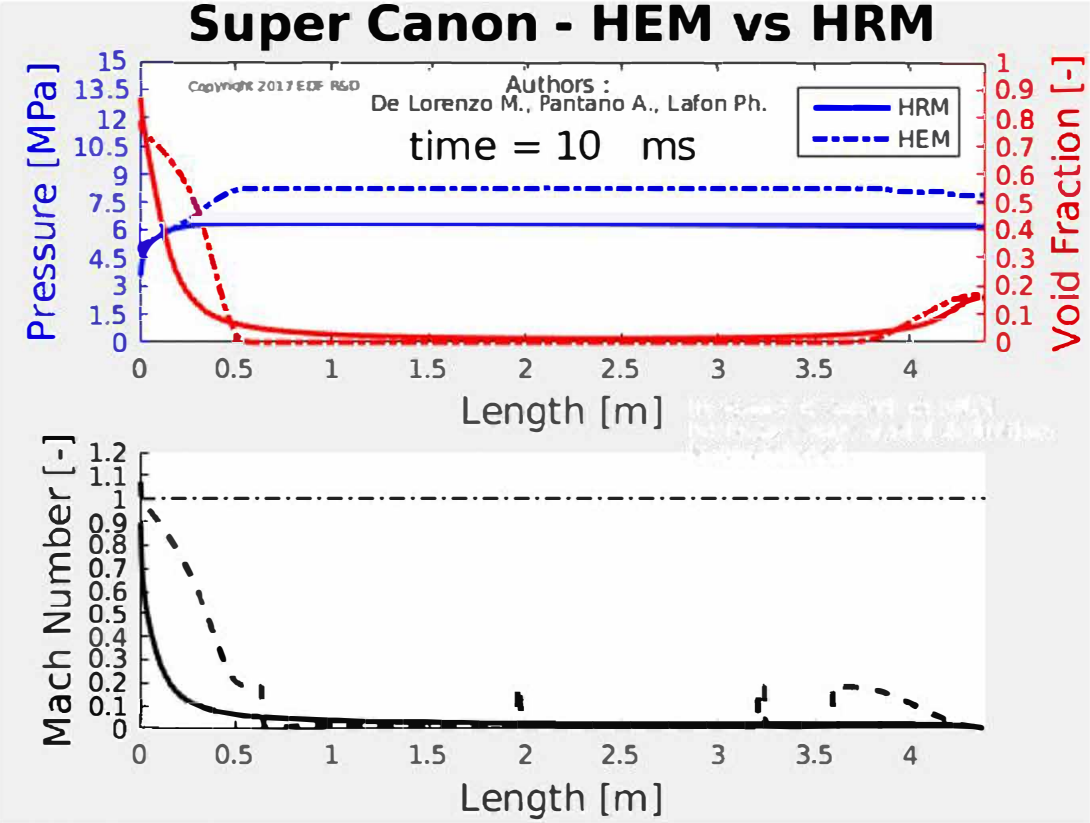

Figure 6.4: Snap at $t = 10\,ms$ of the Super Canon transient according to HEM and HRM. On the bottom of the figure a representation of the Mach number along the pipe. The critical velocity is reached at the breach of the pipe. It is important to specify that the homogeneous definition of speed of sound has been used also for the HRM.

- the vaporization occurring along the center part of the pipe is homogeneous in HRM, while according to HEM, it occurs when the left and the right waves match together;
- the speed of sound, in the two-phase domain, has two different definitions depending on the two-phase model. Furthermore, the HEM model presents two discontinuities in speed of sound definition, with visible consequences noted in the video A.3, as well as in the figure 6.4.
  For further details about speed of sound definitions in HEM and HRM consult [18].

6.3.1.1 Results in $(T - v)$ domain

In figure 6.5 the trend of one single point on the $(T - v)$ domain is shown. Let us imagine to be located on one probe, placed in this case on the point P1 of the pipe in figure 6.3 and to consider the time evolution of the fluid in this location.
At the beginning of the transient, at $t = 0\,s$ the fluid is purely liquid. Then, at the moment when the steam pocket is generated, a vaporization occurs, letting the fluid expand and the void fraction

$$\alpha_v = \frac{Volume_{vap}}{Volume_{mixture}},$$

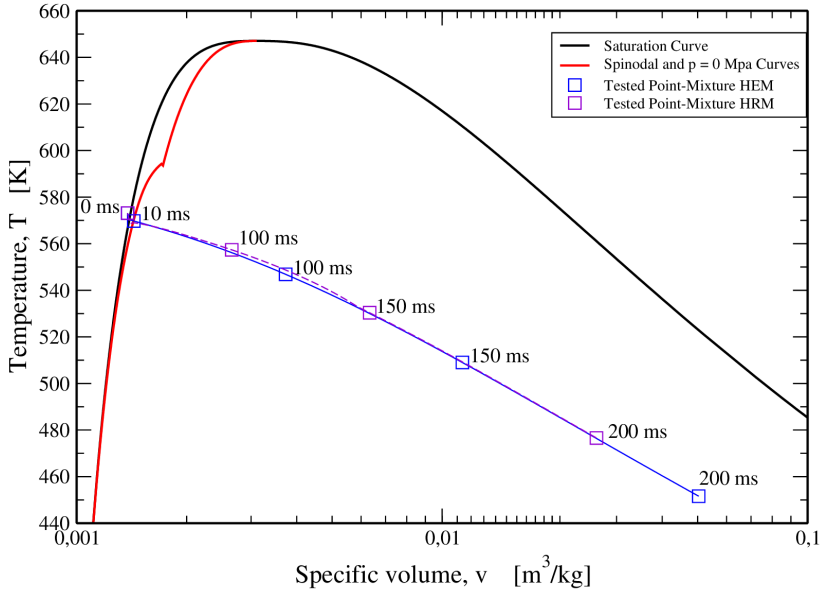

Figure 6.5: Time evolution in $(T - v)$ domain of the point located at p1 probe, according to the HEM and Homogeneous Relaxation Models.

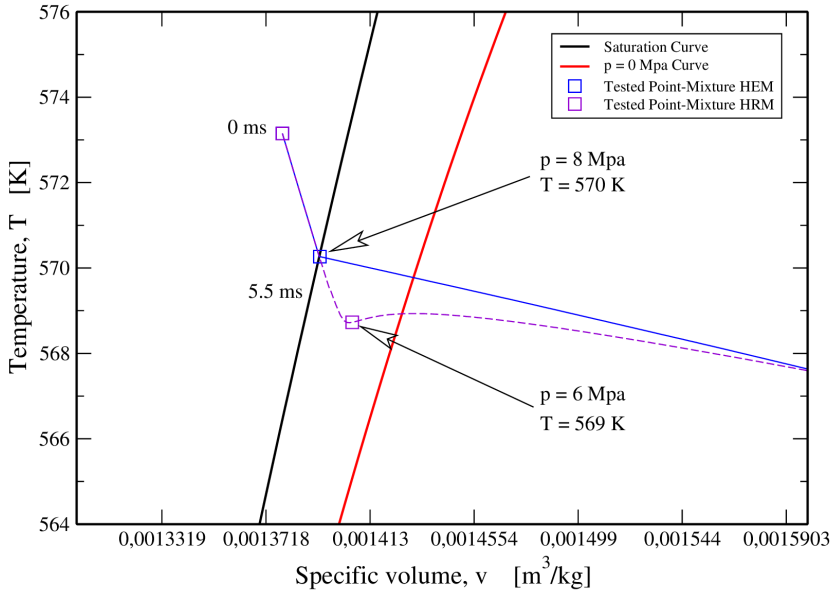

Figure 6.6: Zoom on $(T - v)$ of the first milliseconds of the depressurisation: a wider pressure drop occurs according to the HRM.

consequently increases. As it can be noted, the trends are quite similar between the predictions of the two models, even if the results of HEM are quite delayed on time with respect to the HRM ones. It is important to specify that the Θ used in HRM is the new one proposed in [18]

$$\Theta = 4 \cdot 10^{-5} \, \alpha_{v,eq}^{-0.25} \left(\frac{p_{sat} - p}{p_{crit} - p_{sat}} \right)^{-1.8} , \tag{6.12}$$

which is the most consistent with the empirical results, noticed in figure 6.8. Of course, having to deal with the same model but with another different Θ, the results will be slightly different, as can be seen in the video A.1. In fact, the degree of freedom introduced by the HRM has a wide importance in the evolution of the transient and on the timing to reach the equilibrium conditions.
A greater value of Θ means literally a slowdown on the achievement of the same equilibrium conditions. On the other hand a lower value of Θ, as can be practically observed for the results in figure 6.7, leads to have a HRM with a very closed behavior to HEM.

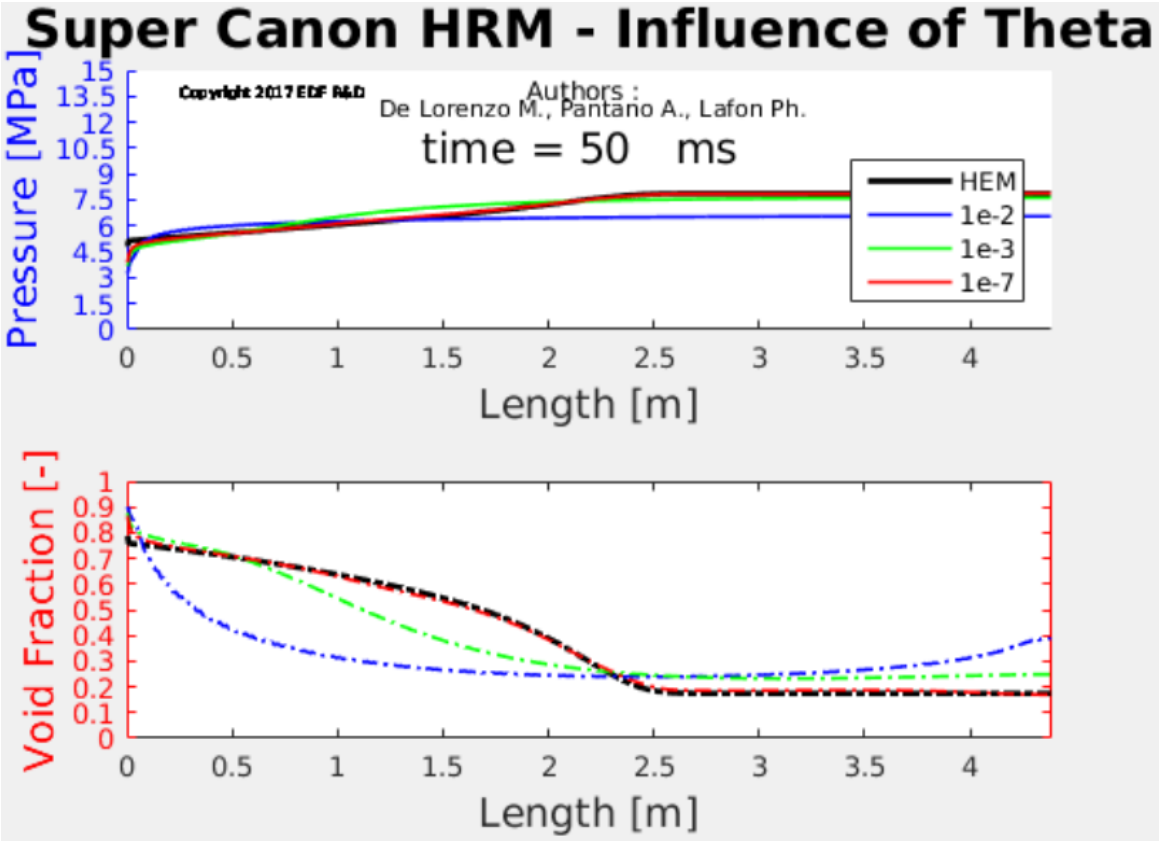

Figure 6.7: Snap at $t = 50\,ms$ of the Super Canon transient according to HEM and HRM. A small value of Θ leads the HRM to have similar results with respect to the HEM ones.

6.3.1.2 Results for pressure

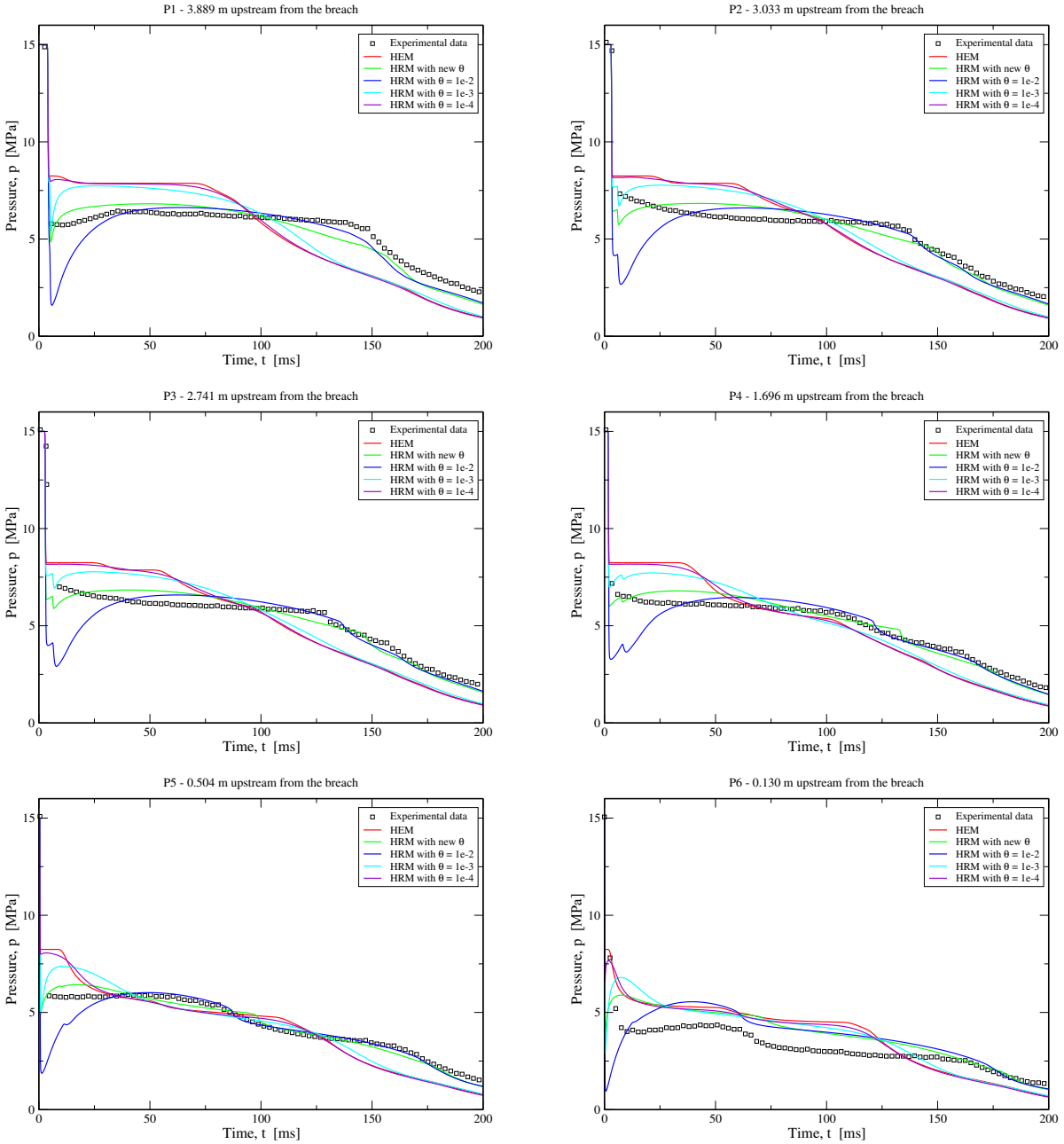

Figure 6.8: Pressure evolution during the transient according to HEM and HRM. The results given by the two models are compared with the empirical measurements, taken at the same points. Each figure represents the evolution on a point where a probe is located.

The pressure evolution results are represented in figures 6.8. In these figures, six points have been considered, each one correspondent to a different positions of the probes. The main goals are

- compare and validate the results of HEM and HRM with the experimental data;

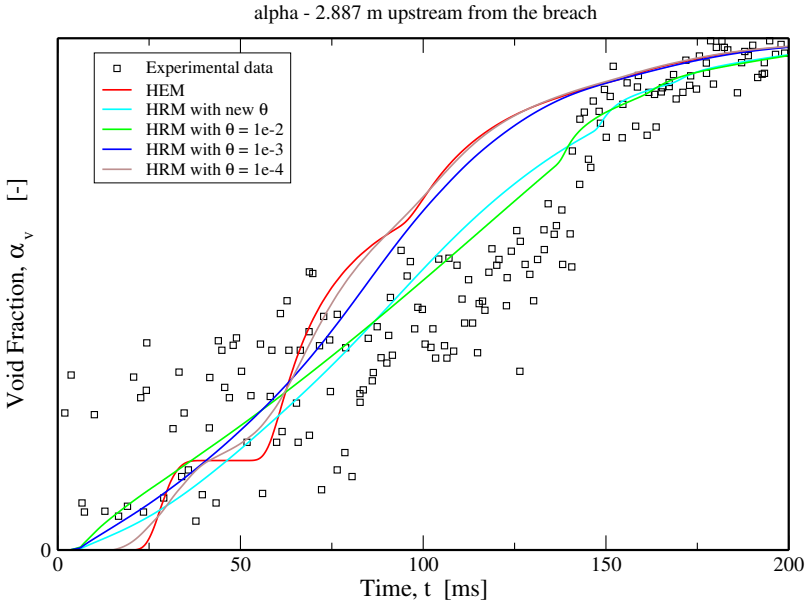

Figure 6.9: Time evolution of the void fraction in one point, where a probe is located. The results are then compared with the empirical measurements.

- observe how a HRM tends to a HEM if the Θ parameter tends to 0.

Even if the HEM provides satisfactory results, it is important to remark that the HRM shows a greater consistency with respect to the empirical ones. In fact, if just the first milliseconds are considered, the HRM with the Θ proposed in [18], is able to predict a lower depressurisation with respect to the HEM for points closed to the breach.
The same concept can be observed in more details in the video A.2, where it can be noted that a lower pressure leads to a higher vaporization, hence, to a higher α_v.

6.3.1.3 Results for α_v

Differently from the pressure, α_v is more difficult to measure. In fact, a neutron beam is used to detect the volume of steam in the two-phase mixture, with consequent complications and greater uncertainties on the experimental results obtained.

Furthermore, only one probe has been used to carry out the measurement of α_v, rather than the six points considered in case of the pressure measurement.
Even if the experimental data have a sparse trend, the results shown in figure 6.9 confirm the validation of the two HEM and HRM, and the importance of the choice of the Θ parameter in the determination of the results.

6.3.2 Steam explosion

The second case that we present in this section is not a depressurisation as the previous one, but a fast transient where a rapid and violent injection of energy occurs in few milliseconds. On the nuclear industry, this case can involve many safety concerns such as the RIA, which is an accident where a considerable amount of thermal energy is injected to the fluid at liquid state. This amount of energy generates a shock wave inside the fluid, causing wide damages to the surrounding structures.

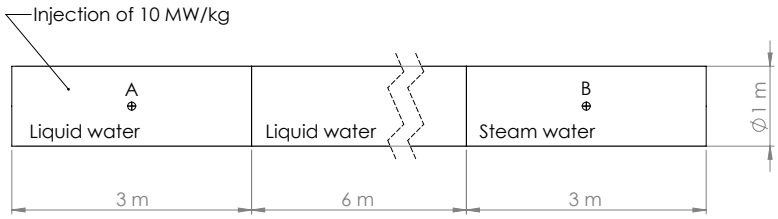

Figure 6.10: Figure taken from [18]. Picture illustrating the 1D domain of the steam explosion case.

In order to study this case, a 1D horizontal domain has been considered and divided in three parts, as illustrated in figure 6.10. The left one (3 m length), where only liquid water closed to the saturation condition is present, the center part (6 m length), where the conditions of the liquid part are the same as the left one, previously described. Finally, the right part (3 m length) is filled with pure steam in a thermodinamic state closed to the saturation.
Other data of the problem are given below:

Geometry

- 1D horizontal pipe of $12\ m$ length;
- $CFL_{HRM} = 0.1$;
- $CFL_{HEM} = 0.6$;
- two Wall boundary conditions imposed;
- Mesh discretized in 800 cells.

Initial thermodinamic conditions

Physical magnitude	Point A	Point B
Pressure[bar]	37.17	37.17
Temperature[K]	515.15	516.15
Saturation temperature[K]	516	516
Velocity[$\frac{m}{s}$]	0	0

Injected power density

- 10 $\frac{MW}{kg_{H2O}}$, $0.95\ GJ$ injected during the first 50 ms;

At time $t = 0\,s$, an amount of energy equal to $0.95\ GJ$ is injected only in the left side of the pipe, during the first $50\ ms$. After this time, there are no more energy sources in the system. Therefore, the liquid undergoes a consistent injection of energy, which leads it to the vaporization, as can be seen in the video A.6, as well as in the figure 6.11.

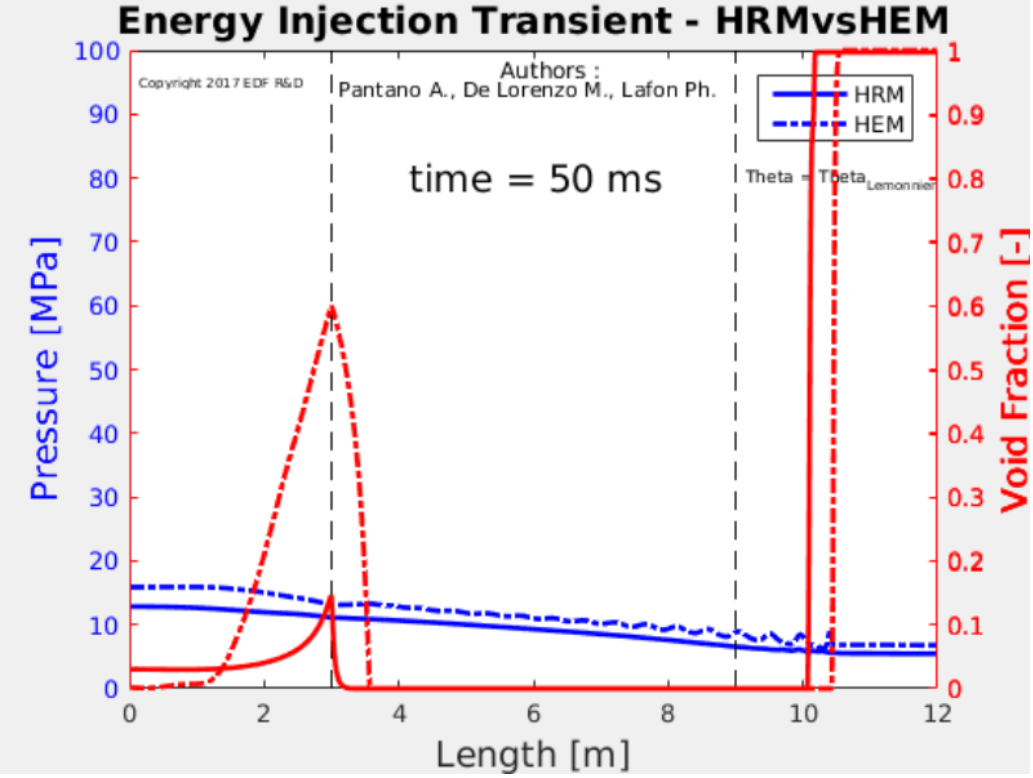

Figure 6.11: Snap at $t = 50\,ms$ of the Steam Explosion transient according to HEM and HRM. Different kinds of vaporizations are predicted by the two models.

The generated shock wave, propagates rightwards until it reaches the frontier between liquid and vapor. This frontier is like a barrier moving with the condensation front, and the wave can not propagate across it due to the difference of impedance between the two phases. In fact, having defined the acoustic impedance as

$$Z = c\rho, \tag{6.13}$$

if this magnitude undergoes a stiff change inside the media, the wave rebounds at the interface between the two phases. This one does not reach completely the final part of the back of the pipe, but a vapor layer persists, as when a piston compresses the fluid with the remaining dead space.
In the same video A.6, other important peculiarities should be remarked, such as

- a pressure drop after the beginning of the transient due to the starting movement of the fluid;
- a vaporization on the left side of the pipe, predicted in different ways according to HEM and HRM, with two peaks in HEM and just one in HRM;
- a pressure peak on the right side of the pipe, once the shock wave has completed its propagation rightwards.

6.3.2.1 Results in $(T - v)$ domain

In this subsection, two points are taken into account in the 1D domain and their physical state is reported in the (T, v) domain during the duration of the whole transient. Figure 6.12 describes the evolution of the fluid in point B.
Both the models predict the way the fluid, initially in a state of superheated steam, become liquid after the condensation front completes its propagation rightwards. So HEM and HRM are roughly able to describe the same phenomena, with the HRM results in delay with respect to the HEM ones.
Nevertheless, the phase transition from vapor to liquid is computed as instantaneous for both HEM and HRM. It is important to specify that the results shown in figure 6.12 are limited until the moment in time when the condensation front reaches the back of the pipe.
Similarly, in figure 6.13 the same results are shown for the point A, on the left side of the pipe. The fluid, initially at pure liquid conditions, undergoes the energy injection during the first 50 ms. The consequent movement of the fluid, which increases its velocity, leads to a depressurisation (see video A.6) and at the same time to the generation of vapor bubbles.
In a second moment (after 51 ms), the energy injected before, contributes to a wider vaporization of the liquid. When the shock wave comes back (respectively after 95 ms and 110 ms for HEM and HRM) a partial condensation occurs, leading the fluid to become liquid again according to the HEM results.

6.3.2.2 Influence of the discretization in HEM

This subsection has been done to test the influence of the mesh refinement on the solution, in order to get a mesh that could be performing in terms of computational costs, avoiding the numerical diffusivity.
This convergence study has been done especially for HEM, because in case of HRM some problems occur due to the iterative procedure of the model in the two-phase domain. In fact, the discontinuity of the derivatives provided by IAPWS-97IF does not ensure a result in some points of the two-phase domain.
Consequently, even if a refinement of the mesh could lead to an improvement on the accuracy of the solution, it can not be applied to the calculation for both the models due to the intrinsic problems of the HRM.
Finally, due to this constraint, the comparison between the results of the two models has been performed using a mesh discretized in 800 cells. Some interesting results are shown in figures 6.14 and 6.15, focusing on void fraction and pressure in point B of the 1D domain (see the figure 6.10).
It is important to remark, in figure 6.14, that for coarser meshes the vaporization does not occur anymore. On the other hand, considering the pressure trend with finer meshes, lower peaks are generated. Then, with these conditions, the greater the oscillating behavior the longer the time to reach the steady-state conditions.

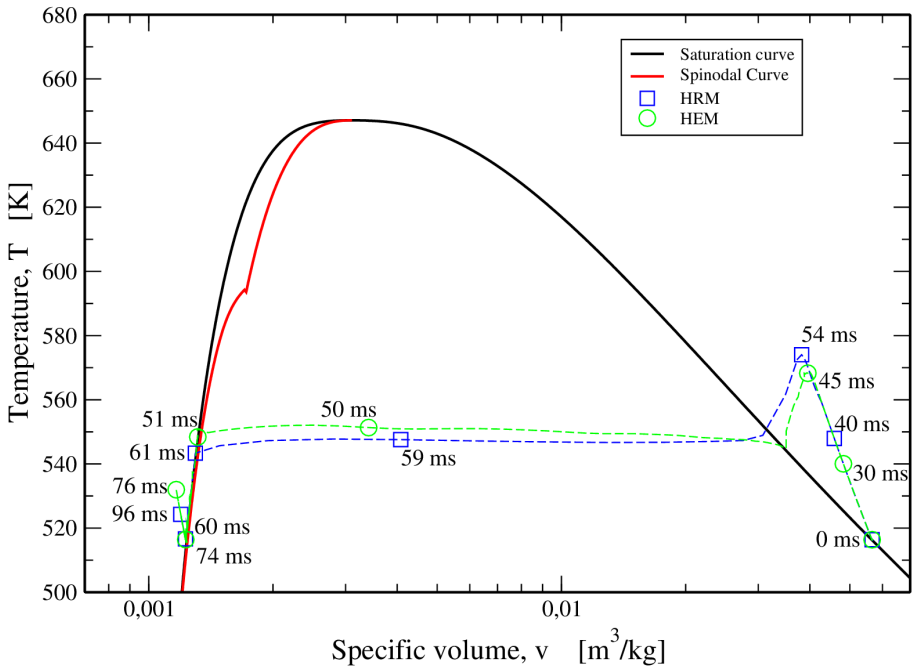

Figure 6.12: Time evolution in $(T - v)$ domain of the point located in correspondence of the back of the pipe (point B), according to HEM and HRM.

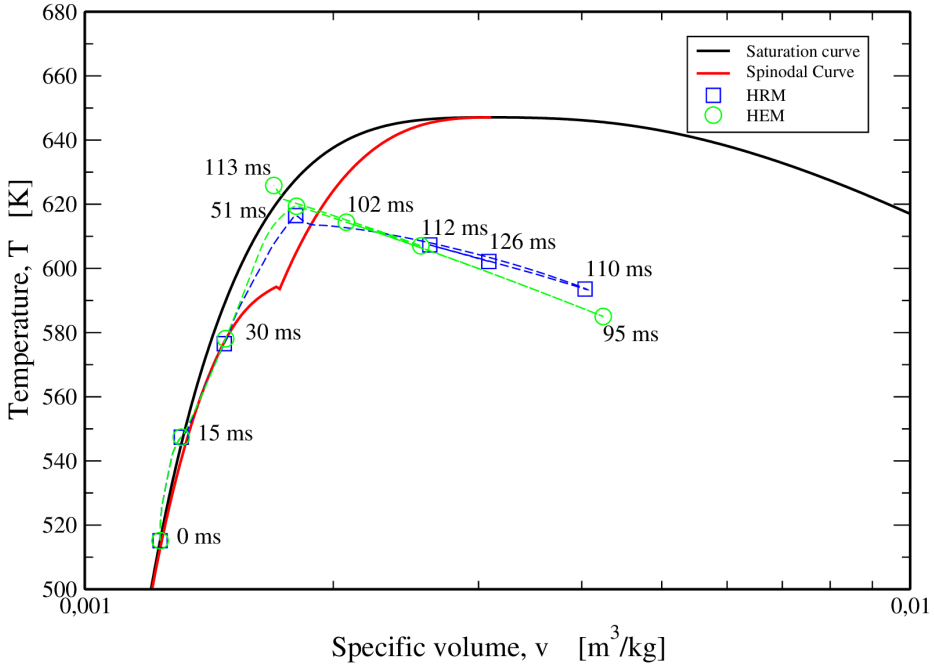

Figure 6.13: Time evolution in $(T - v)$ domain of the point located in correspondence of the left side of the pipe (point A), according to HEM and HRM.

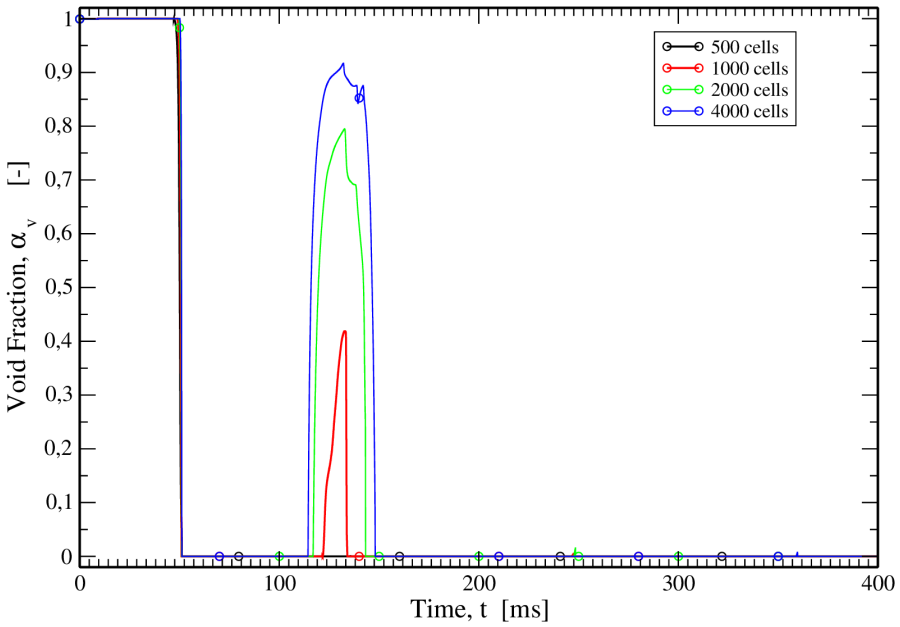

Figure 6.14: Mesh convergence for void fraction value in point B, according to HEM model. For a coarse mesh chosen, the void fraction is zero after the condensation. After the time $t = 150\,ms$ there is no more vapor presence in the fluid at that point.

6.3.2.3 Results for $\mathbf{T}, \alpha_\mathbf{v}, \mathbf{p}, \rho, \mathbf{u}$

In this subsection some results are shown to compare the two models. Differently from Super Canon in section 6.3.1, it is better to specify that there are not any empirical data to use as a reference for the computed results.
However, even if there could not be a validation procedure, the results are conform with the conditions imposed by the physical constraints. Due to some problems linked to the convergence of the iterative method, the results are compared with a mesh discretized in 800 cells, as mentioned in section 6.3.2.2, while the CFL number imposed is different for HEM and HRM.
The reason is mainly due to the high injection of energy on the left side of the pipe, which provokes the rapid transformation of the liquid that from the metastable conditions directly overcomes the spinodal curve, falling into a non-physical state.
This consequence is caused by the fact that, using the HRM, there is no other choice to take into account the effect of the source terms in the second step of the fractional step procedure (see section 6.1.1.1). Then, this splitting in two steps can cause a problem like that for not very low Δt.
Therefore, only for this particular case of steam explosion, the choice adopted is to reduce the CFL for the HRM, hence, the related Δt is proportionally reduced. Of course, we know that this constraint leads to an obvious increase of the computational cost, but this is the only strategy to circumvent the problem.

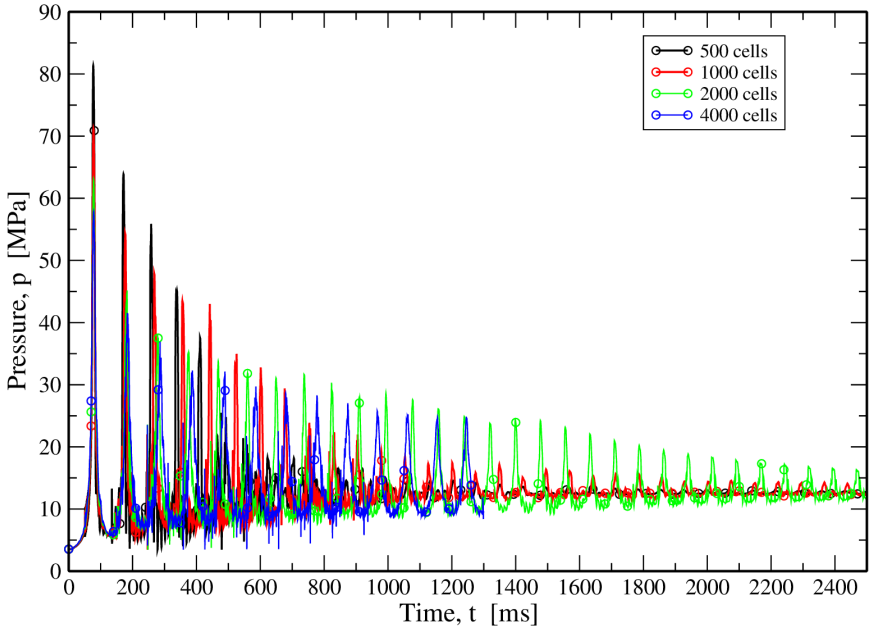

Figure 6.15: Mesh convergence for pressure value in point B, according to HEM model. Different pressure peak values are observed according to the discretization of the mesh. The calculation at 4000 cells has been stopped before due to its elevated computational time.

Then, the results on the two points are shown in figures 6.17 and 6.19 respectively for points A and B. As it has been mentioned, the rapid energy injection let the fluid move. Consequently, the pressure decreases at the beginning of the transient, as can be also noted in the video A.5.
On the other hand, in point B, when the condensation front arrives, it causes the pressure rise, which is computed in different ways by the two models.
Finally, as well as the Super Canon test, it is important to specify the Θ used for the application. In this case, the one proposed in Downar-Zapolski et al. [39] has been chosen

$$\Theta = 6.51 \cdot 10^{-4} \, \alpha_v^{-0.257} \left(\frac{p_{sat} - p}{p_{sat}} \right)^{-2.24} . \tag{6.14}$$

Of course, with different values of Θ, the results will be not the same, as it has been demonstrated in section 6.3.1 for Super Canon test. Furthermore, the effect of different constant values of Θ can be seen on the results for HRM, in the video A.4. The lower this parameter, the more the HRM tends to the HEM, hence the faster is the achievement of the thermodynamic equilibrium between the two phases.

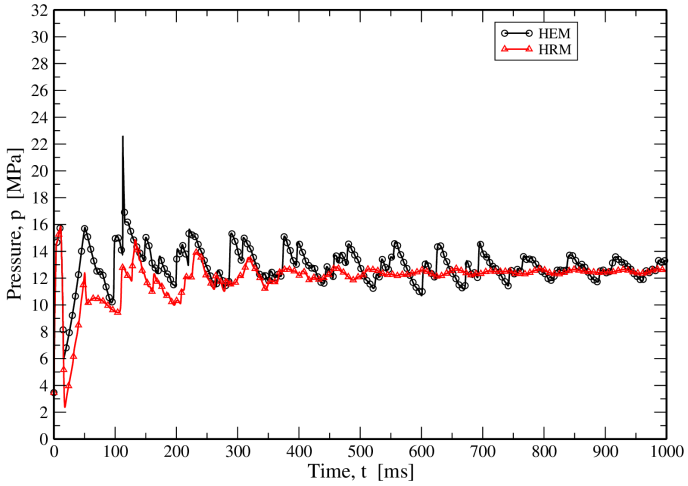

Figure 6.16: Steam Explosion phenomenon. Pressure evolution on the point A during the transient according to HEM and HRM. Mesh discretized in 800 cells.

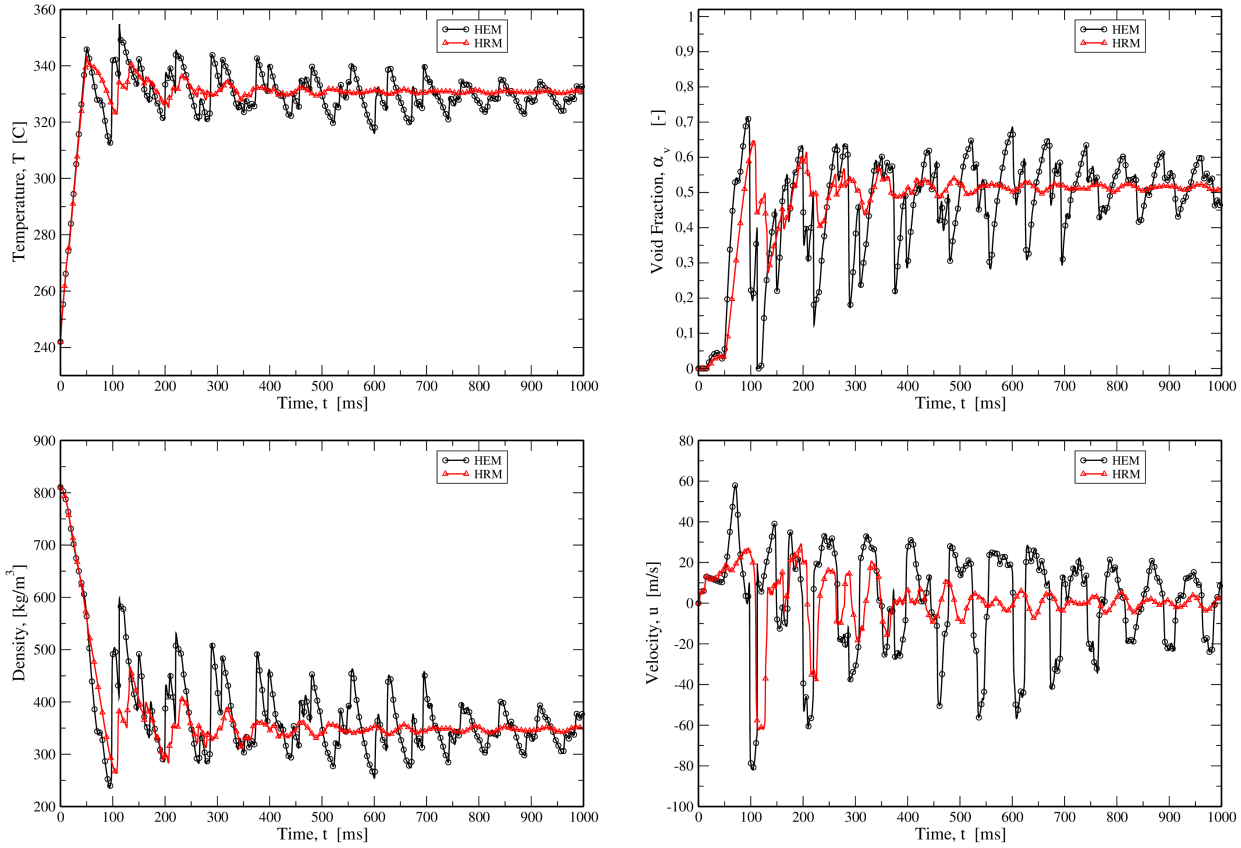

Figure 6.17: Physical magnitudes evolution during the transient according to HEM and HRM (point A). Mesh discretization in 800 cells.

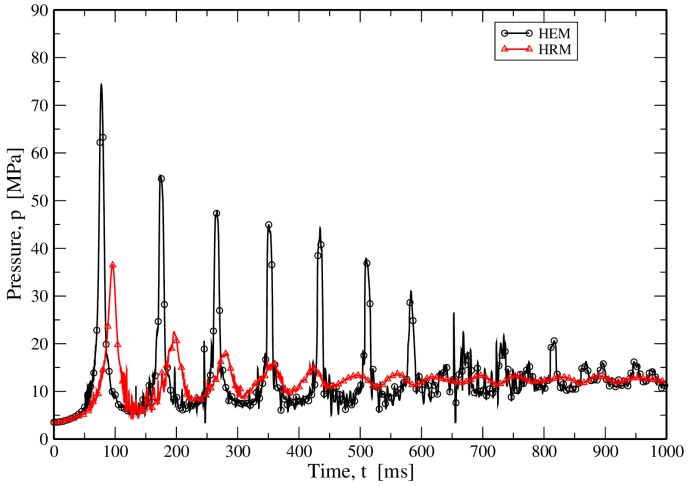

Figure 6.18: Steam Explosion phenomenon. Pressure evolution on the point B during the transient according to HEM and HRM. Mesh discretized in 800 cells.

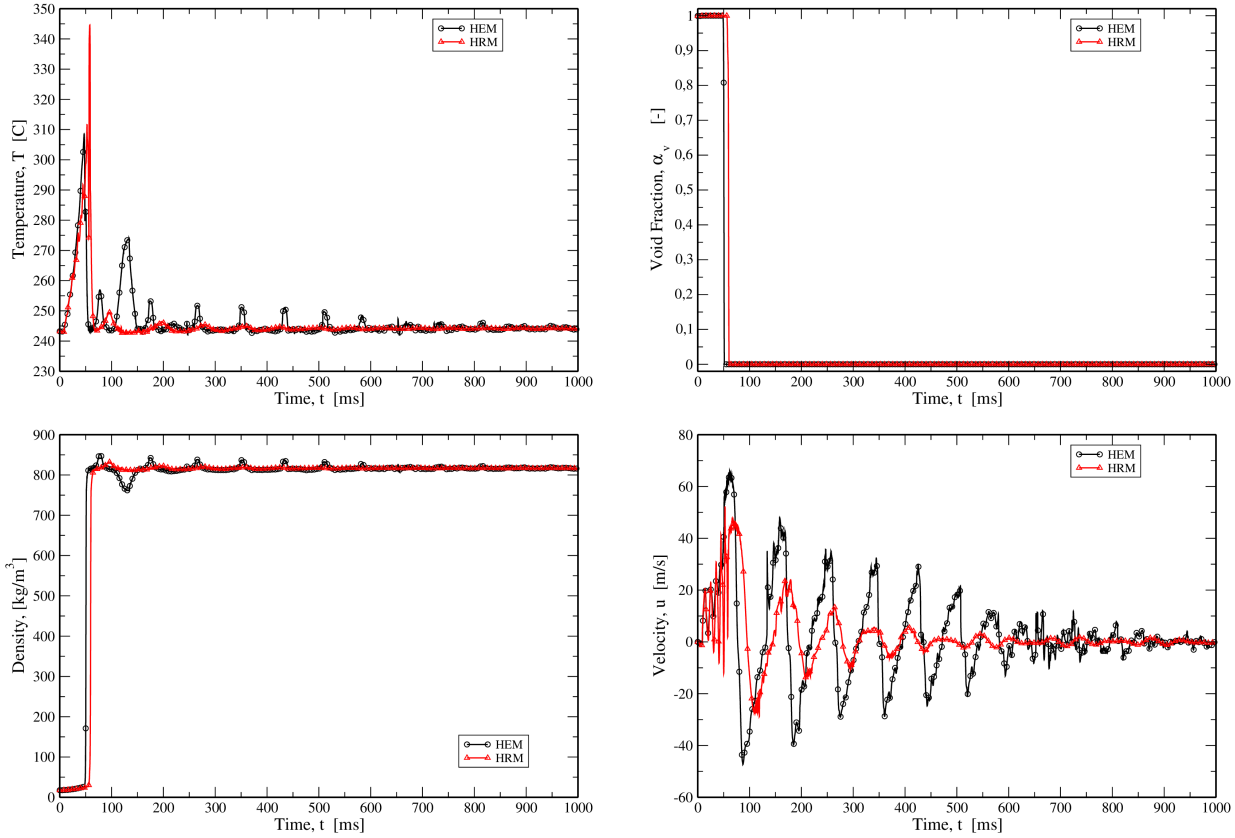

Figure 6.19: Physical magnitudes evolution during the transient according to HEM and HRM (point B). Mesh discretization in 800 cells.

Chapter 7

Conclusions and perspectives

The nuclear industry is one of the main fields which provides many interest for the research of new techniques and technologies. In this context, the present work has been carried out to better understand the differences between some two-phase models for fast transient flows.
The application of these models has been tested, describing first the main differences between them, and introducing the advantages and drawbacks of each one. It is important to precise that all of them, except for the "EAU model" rely on a Steam Water Look-up Table procedure, an algorithm coupled with the governing equations.

- The new HEM in EUROPLEXUS is a quite simple and robust model based on direct look-up table method. On the other hand, the perfect equilibrium conditions do not always ensure a complete understanding of the complexity of the physics when disequilibrium between the phases occurs.

- The new HRM in EUROPLEXUS is a model which takes into account the disequilibrium between the two phases.
  This model guarantees the advantage to consider the thermal disequilibrium in a two-phase flow. On the other hand it is computationally expensive and some troubles often occur due to the iterative procedure combined with the discontinuities of IAPWS-IF97 derivatives.

- Six-equation model considers the two phases in complete thermodynamic disequilibrium, using a look-up table procedure without any iteration, for each single phase.
  This model, can be also coupled with a direct look-up table method, avoiding the use of an iterative procedure. Therefore, it is finally introduced as the model that is able to handle in a more precise way the physics using a faster and direct scheme.

Aiming to use the Six-equation unique-velocity model as soon as possible, the tabulation on (v, e) has been performed considering new physical borders and dividing the domain in new regions, with respect to the ones in the old algorithm which did not included metastable states.
The first step was to construct the spinodal curve imposing its physical constraint. After this process, fixing all the boundaries of the domain, the tabulation has been reformulated in order to handle metastable conditions of liquid and vapor. Then, it has been used to test HEM and HRM, as it has been done in the recent past.
However, the main concern was to adapt it to the future use of the Six-equation model, in order to find directly $p_l = p_l(v_l, e_l)$ and $p_v = p_v(v_v, e_v)$ through the developed algorithm. The new Steam-Water

Tables, which guarantee a high accuracy with respect to the EoS, have been used in some test, coupled with HEM and HRM in EUROPLEXUS code, showing interesting and performing results in cases involving nuclear safety topics. Therefore, the results have provided an improvement on the study of some nuclear safety concerns, such as LOCA and RIA.

If some interesting contributions have been presented in this report, on the other hand, other important aspects have to be reviewed in order to boost the performance and the accuracy of the steam-water look-up tables in some regions.
Moreover, for what concerns the application, the steam-water tables can be used to perform other test cases, not only limiting them strictly to the nuclear field. In fact, they can be used in all the industrial applications concerning the water.
Furthermore, the improvement of the Six-equation unique-velocity model and its relative source terms, could provide a more performing, direct, and faster method to be used in two-phase flow cases during the next future.

This work improved and widened the research on fast transient phenomena, giving a good contribution to EDF R&D in the research devoted to the project FAST. In particular, this specific brench of study, related to the Steam-Water Look-up Tables, was started by my colleague Michele Di Matteo (s211191) [30] from Politecnico di Torino, widened through this work, and completed this year.
This thesis, and its work of research behind, contributed to extend the knowledge on the two-phase flow models. Within this work, the importance of the coupling with a Steam-Water Look-up Table has been remarked for the calculation of the properties, in particular for to the forthcoming Six-equation model.

Appendices

Appendix A

List of video in attachment

A.1 SUPER CANON HRM vs HEM p alpha DIFFERENT THETA

Video showing the evolution in time of pressure along the whole domain (half screen on the top) and void fraction (half screen on the bottom). In case of HRM, the different trends are related to different values of Θ used.

A.2 SUPER CANON HRM vs HEM p alpha ONLY

Video showing the evolution in time of pressure along the whole domain (scale on the left side) and void fraction (scale on the right side).

A.3 SUPER CANON HRM vs HEM p alpha MACH

Video showing the evolution in time of pressure along the whole domain (scale on the left side) and void fraction (scale on the right side), according to HEM and HRM. These two magnitudes are both represented on the half screen on the top. The half screen on the bottom illustrates the evolution in time of the Mach number along the whole domain. The speed of sound of HRM is the one of the homogeneous model, which does not take into account the effect of the source terms.

A.4 STEAM EXPLOSION HEM DIFFERENT THETA

Video showing the evolution in time of pressure along the whole domain (half screen on the top) and void fraction (half screen on the bottom). In case of HRM, the different trends are related to different values of Θ used.

A.5 STEAM EXPLOSION HEM p alpha T-Tsat vel

Video showing the evolution in time of pressure along the whole domain (scale on the left side) and void fraction (scale on the right side), according to HEM model. These two magnitudes are both

represented on the half screen on the top. Moreover, on the bottom one, the difference between the temperature and the saturation value is presented (scale on the left side), while the velocity evolution is shown with its scale on the right side.
When the pressure is higher than the critical value, there is no more possibility to have saturation conditions. Therefore the line of the $(T - T_{sat})$ is no more represented.

A.6 STEAM EXPLOSION HEM vs HRM

Video showing the evolution in time of pressure along the whole domain (scale on the left side) and void fraction (scale on the right side).

Appendix B

Definition of speed of sound on spinodal curve

This paragraph is a support tool for the speed of sound calculation on the spinodal curve. The speed of sound has been determined by its mathematical definition, obtaining the same results as the one given by IAPWS-95 Formulation. This physical magnitude has to be written, using its definition such as

$$c_s = \sqrt{\left(\frac{\partial p}{\partial \rho}\right)_s}.$$

Making some manipulation on the first order derivative $\left(\frac{\partial p}{\partial \rho}\right)_s$, we can rewrite it as

$$\left(\frac{\partial p}{\partial \rho}\right)_s = -v^2 \left[\left(\frac{\partial v}{\partial p}\right)_s\right]^{-1} = -\rho^{-2} \left(\frac{\partial p}{\partial v}\right)_s. \tag{B.1}$$

Using the relation

$$\left(\frac{\partial p}{\partial v}\right)_s = \left(\frac{\partial p}{\partial v}\right)_T - \left(\frac{\partial p}{\partial T}\right)_v \left(\frac{\partial s}{\partial v}\right)_T \left(\frac{\partial s}{\partial T}\right)_v^{-1}$$

in Eq. (B.1), and considering the spinodal as the curve where

$$\left(\frac{\partial p}{\partial v}\right)_T = 0,$$

we obtain the speed of sound definition as a function of the following first derivatives

$$c_s = \sqrt{\rho^{-2} \left[\left(\frac{\partial p}{\partial T}\right)_v \left(\frac{\partial s}{\partial v}\right)_T \left(\frac{\partial s}{\partial T}\right)_v^{-1}\right]}. \tag{B.2}$$

Then, considering the following Maxwell relation

$$\left(\frac{\partial s}{\partial v}\right)_T = \left(\frac{\partial p}{\partial T}\right)_v$$

and replacing it in Eq. (B.2), we finally get the following definition of speed of sound

$$c_s = \sqrt{\rho^{-2}\left[\left(\frac{\partial p}{\partial T}\right)_v^2 \left(\frac{\partial T}{\partial s}\right)_v\right]}. \tag{B.3}$$

Then, wanting to express the first derivative $\left(\frac{\partial T}{\partial s}\right)_v$ as a function of other well known physical magnitudes, we consider the differential entropy definition

$$ds = \frac{1}{T}\,de + \frac{p}{T}\,dv.$$

Manipulating it, we can furthermore consider

$$\left(\frac{\partial s}{\partial T}\right)_v = \left(\frac{\partial(\frac{de}{T})}{\partial T}\right)_v + \left(\frac{\partial(\frac{p\,dv}{T})}{\partial T}\right)_v, \tag{B.4}$$

where the first component of Eq. (B.4) can be finally evaluated as

$$\left(\frac{\partial(\frac{de}{T})}{\partial T}\right)_v = \frac{1}{T}\left(\frac{\partial e}{\partial T}\right)_v,$$

while the second one is trivially

$$\left(\frac{\partial(\frac{p\,dv}{T})}{\partial T}\right)_v = 0.$$

Taking into account the definition of the specific heat capacity at constant volume

$$C_v = \left(\frac{\partial e}{\partial T}\right)_v,$$

the Eq. (B.4) can we rewritten as

$$\left(\frac{\partial s}{\partial T}\right)_v = \frac{C_v}{T}. \tag{B.5}$$

Using the Eq. (B.5) in Eq. (B.3), the speed of sound can finally calculated as

$$c_s = \sqrt{\rho^{-2}\left[\frac{T}{C_v}\left(\frac{\partial p}{\partial T}\right)_v^2\right]}. \tag{B.6}$$

The first order derivative in Eq. (B.6) $\left(\frac{\partial p}{\partial T}\right)_v$, as well as the C_v, are properties determined using the IAPWS-95 Formulation. Therefore, for a point belonging to the spinodal at given temperature and density, the speed of sound can be calculated.

Bibliography

[1] EDF Energy (2018), EDF Energy Fuel Mix, www.edfenergy.com, extracted at 18/04/2018 from www.edfenergy.com/fuel-mix.

[2] Commissariat à l'énergie atomique, 2017, EUROPLEXUS A Computer Program for the Finite Element Simulation of Fluid-Structure Systems under Transient Dynamic Loading, USER'S MANUAL.

[3] Journeau C. et al. , 2017, Safest Roadmap for Corium Experimental Research in Europe, ASME J. Risk Uncertainty Part B 4(3), 030901.

[4] Tijselling A.S, Anderson A.,2006, The Joukowsky equation for fluids and solids. TUE Conference Proceedings, Eindhoven.

[5] Morrison D. , 2007, Eliminating water hammer, Fine Homebuilding, Issue 190.

[6] Becht C.V. , 2016 Introduction to LOCA Blowdown Loads on Reactor Internals and Fluid-Structure Interaction, Becht Engineering.

[7] Bianchini S., Bressan A., 2005, Vanishing viscosity solutions of nonlinear hyperbolic systems. Ann. of Math., Vol. 161, 223-342.

[8] Toro E., Riemann Solvers and Numerical Methods for Fluid Dynamic, Third Edition, 2009, Springer.

[9] Ferziger H., Perić M., 2002, Computational Methods for Fluid Dynamics, Springer, third edition.

[10] De Lorenzo M., Pelanti M., Lafon Ph., 2018, HLLC-type and path-conservative schemes for a single-velocity six-equation two-phase flow model: a comparative study. Applied Mathematics and Computation, Vol. 333, 95-117.

[11] Davis S.F., 1988, Simplified second-order Godunov-type methods. SIAM J. Sci. Stat. Comput., Vol. 9, 445-73.

[12] Pinto del Corral N., 2014, Analysis of Two-Phase Flow Pattern Maps, Master Thesis, Brno University of Technology.

[13] Clerc S., 2000, Numerical Simulation of the Homogeneous Equilibrium Model for Two-Phase Flows, Journal of Computational Physics Vol. 161, 354-75.

[14] Holzapfel, W. B. (2004). "Equations of state and thermophysical properties of solids under pressure" in "High-Pressure Crystallography" ed. A. Katrusiak and P. McMillan. Netherlands: Kluver Academic. pp. 217-236.

[15] Soave, G. Equilibrium Constants from a Modified Redlich-Kwong Equation of State, Chem. Eng. Sci.,1972, Vol. 27, 1197-1203.

[16] International Association for the Properties of Water and Steam, August 2007 Revised Release on the IAPWS Industrial Formulation 1997 for the Thermodynamic Properties of Water and Steam.

[17] Bartak J., 1990, A study of the rapid depressurisation of hot water and the dynamics of vapor bubble generation in superheated water., Int. Journal Multiphase Flow, Vol. 16, 789-98.

[18] De Lorenzo M., Lafon Ph., Di Matteo M., Pelanti M., Seynhaeve J.-M, Bartosiewicz Y., 2017, Homogeneous Two-Phase Flow Models and Accurate Steam-Water Table Look-up Method for Fast Transient Simulations, EDF, UCL, ENSTA, Politecnico di Torino, International Journal of Multiphase Flow, Vol. 95, 199-219.

[19] De Lorenzo M., 2018, Modelling and Numerical Simulation of Metastable Two-Phase Flows, PhD Thesis, Université Paris-Saclay, Paris, France.

[20] Pelanti M., Keh-Ming Shyue K.-M., A mixture-energy-consistent six-equation two-phase numerical model for fluids with interfaces, cavitation and evaporation waves, J. Comput. Phys., Vol. 259, 331-57.

[21] Kapila A.K., Menikoff R., Bdzil J.B., Son S.F., Stewart D.S., 2001, Two-phase modeling of deflagration-to-detonation transition in granular materials: reduced equations, Physics of Fluids, Vol. 13, 3002-25.

[22] Baer M.R., Nunziato J.W., 1986, A two-phase mixture theory for the deflagration-to-detonation transition (ddt) in reactive granular materials. Int. J. Multiphase Flow, Vol. 12, 861-889.

[23] Porsching T.A., 1977, A Finite Difference Method for Thermally Expandable Fluid Transient. Nucl. Sci Eng. Vol. 64, 177.

[24] Flåtten T., Lund H., 2011, On solution to equilibrium problems for systems of stiffened gases, Applied Math., Vol. 71, No. 1, pp. 41-67.

[25] Saurel R., Abgrall R., 1999, A Multiphase Godunov Method for Compressible Multi uid and Multiphase Flows. J. Comput. Phys. Vol. 150, 425-467.

[26] Kretzschmar H.-J. et al., 2007, Supplementary Backward Equations p(h,s) for the Critical and Supercritical Regions (Region 3), and Equations for the Two-Phase Region and Region Boundaries of the IAPWS Industrial Formulation 1997 for the Thermodynamic Properties of Water and Steam, Journal of Engineering for Gas Turbines and Power, Vol. 129, Issue 4, 1125-1137.

[27] Haar, Gallagher, Kell, NBS/NRC Steam Tables, Hemisphere Publishing Corporation, 1984, NBS/NRC Wasserdampftafeln, Springer Verlag, 1988.

[28] Wagner W., Pruss A., The IAPWS Formulation 1995 for the Thermodynamic Properties of Ordinary Water Substance for General and Scientific Use, 2002, j. Phys. Chem. Ref. Data, Vol 31, 388-535.

[29] Kunick M. et al., 2015, CFD Analysis of Steam Turbines with the IAPWS Standard on the Spline Based Table Look-Up Method(SBTL) for the Fast Calculation of Real Fluid Propertie, Turbine Technical Conference and Exposition : Proceedings of ASME Turbo Expo 2015, Vol.8.

[30] Di Matteo M., 2017 Development of an accurate steam-water table look-up method to be coupled to homogeneous two-phase flow models for fast transient simulations, Master Thesis, Politecnico di Torino, Turin, Italy.

[31] Kunick M., Berry R. A., Martineau R. C., Kretzschmar H.-J. and Gampe U. , 2017, Application of the new IAPWS Guideline on the fast and accurate calculation of steam and water properties with the Spline-Based Table Look-Up Method (SBTL) in RELAP-7.kerntechnik Vol. 82, Issue 3.

[32] Kiefer J., 1953, Sequential minimax search for a maximum, Proceedings of the American Mathematical Society, 4 (3): 502–506.

[33] Di Matteo M., 2016, Development of new steam-water tables to be used in the EUROPLEXUS code. Internship report, EDF R&D - AMA Department.

[34] International Association for the Properties of Water and Steam, 2015, Guideline on the Fast Calculation of Steam and Water Properties with the Spline-Based Table Look-Up Method (SBTL).

[35] Haar L., Gallagher J. S., Kell G. S. , NBS/NRC steam tables : thermodynamic and transport properties and computer program for vapor and liquid states of water in SI units, Third Edition, 1984, Washington D.C. : Hemisphere Pub. Corp.

[36] P. Galon, S. Potapov Méthode des volumes finis pour les écoulements compressibles - Analyse bibliographique. Rapport DEN/DM2S/ SEMT/DYN/ RT/03.013/A.

[37] Reocreux, M.; Katz, G. (eds.); CEA Centre d'Etudes Nucleaires de Fontenay-aux-Roses, 92 (France). Dept. de Surete Nucleaire; Nuclear Energy Agency, 75 - Paris (France), Feb 1981; v. 2 p. 667-686; Commissariat a l'Energie Atomique; Paris, France.

[38] Munson B. R., Okiishi T. H., Huebsch W. W., Rothmayer A. P., 2013, Fluid Mechanics, Wiley, seventh edition.

[39] Downar-Zapolski P., Bilicki Z., Bolle L., Franco J., 1996, The non-equilibrium relaxation model for one-dimensional flashing liquid flow. Int. J. Multiphase Flow, Vol. 22, 473-83.

[40] Saurel R., Petitpas F., Abgrall R., 2008, Modelling phase transition in metastable liquids. Application to cavitating and flashing flows. J. Fluid Mech., Vol. 607, 313-50.

[41] Flåtten T., Lund H., 2012, Relaxation two-phase flow models and the subcharacteristic conditions. Math. Models Methods Appl. Sci., Vol. 21, 2374-2407.

[42] Zein A. et al., 2010, Modeling Phase Transition for Compressible Two-Phase Flows Applied to Metastable Liquid, Journal of Computational Physics, Vol. 229, 2964-2998.

[43] Bilicki J., Kestin J., 1990, Physical Aspects of the Relaxation Model in Two-Phase Flow, Proceedings of the Royal Society A, Math. Phy. Sciences, Vol. 428, 379-97.

[44] Bilicki Z., Kestin J., 1990, Physical aspects of the relaxation model in two-phase flow, Proceedings of the Royal Society A, Math. Phy. Sciences, Vol. 428, 379-97.

[45] Daude F., Galon P., Gao Z., Blaud E., 2014, Numerical experiments using a HLLC-type scheme with ALE formulation for compressible two-phase flows five-equation models with phase transition. Comput. Fluids, Vol. 94, 112-38.